DEVELOPMENT OF SOFC ANODES RESISTANT TO SULFUR POISONING AND CARBON DEPOSITION

A Thesis
Presented to
The Academic Faculty

by

Song Ho Choi

In Partial Fulfillment
of the Requirements for the Degree
Doctor of Philosophy in the
School of Materials Science & Engineering

Georgia Institute of Technology
December 2007

DEVELOPMENT OF SOFC ANODES RESISTANT TO SULFUR POISONING AND CARBON DEPOSITION

Approved by:

Dr. Meilin Liu, Advisor
School of Materials Science and Engineering
Georgia Institute of Technology

Dr. Tom Fuller
School of Chemical and Biomolecular Engineering
Georgia Institute of Technology

Dr. Arun Gokhale
School of Materials Science and Engineering
Georgia Institute of Technology

Dr. Preet Singh
School of Materials Science and Engineering
Georgia Institute of Technology

Dr. Christoper Summers
School of Materials Science and Engineering
Georgia Institute of Technology

Date Approved: Nov. 8, 2007

ACKNOWLEDGEMENTS

I would like to thank my advisor, Dr. Meilin Liu, for his exceptional guidance and valuable support throughout my years here, and all members of my committee, Dr. Arun Gokhale, Dr. Preet Singh, Dr.Christoper Summers, and Dr. Tom Fuller for their useful discussions and advices throughout this process.

I would like to particularly thank my boss, Sun-Kyu Jeon who is the president of KoMiCo, and other co-workers, whose valuable financial support, guidance, and encouragement helped me complete my degree.

I am thankful to Dr. YonMan Choi, Dr. Jenghan Wang, Dr. Charles Compson, Dr. Namtae Choi, Harry Abernathy, Zhe Cheng for their efforts and discussions throughout the completion of this research. I have had the great pleasure of working with other group members through useful discussions and the collaborations.

Finally, I would like to express my gratitude to my parents, Bansok Choi and Youngae Choi, for the years of support and encouragement. I would like to thank my wife, Yunjung Kim, for her support and understanding and my lovely daughter, Ellie, for her beautiful smile that makes me always happy.

TABLE OF CONTENTS

LIST OF TABLES

LIST OF FIGURES

LIST OF SYMBOLS AND ABBREVIATIONS

AC	Alternative Current
CTE	Coefficient of Thermal Expansion
DC	Direct Current
DOS	Density of States
EDS	Energy dispersive X-ray Spectroscopy
OCV	Open Circuit Voltage
SEM	Scanning Electron Microscopy
SOFC	Solid Oxide Fuel Cell
XRD	X-ray Diffraction
YSZ	Yittria-stabilized Zirconia

SUMMARY

The advantages of solid oxide fuel cells (SOFCs) over other types of fuel cells include high energy efficiency and excellent fuel flexibility. In particular, the possibility of direct utilization of fossil fuels and renewable fuels (e.g., bio-fuels) may significantly reduce the cost of SOFC technologies. However, it is known that these types of fuels contain many contaminants that may be detrimental to SOFC performance.

Among the contaminants commonly encountered in readily available fuels, sulfur-containing compounds could dramatically reduce the catalytic activity of Ni-based anodes under SOFC operating conditions. While various desulphurization processes have been developed for the removal of sulfur species to different levels, the process becomes another source of high cost and system complexity in order to achieve low concentration of sulfur species. Thus, the design of sulfur tolerant anode materials is essential to durability and commercialization of SOFCs. Another technical challenge to overcome for direct utilization of hydrocarbon fuels is carbon deposition. Carbon formation on Ni significantly degrades fuel cell performance by covering the electrochemically active sites at the anode. Therefore, the prevention of the carbon deposition is a key technical issue for the direct use of hydrocarbon fuels in a SOFC.

In this research, the surface of a dense Ni-YSZ anode was modified with a thin-film coating of niobium oxide (Nb_2O_5) in order to understand the mechanism of sulfur tolerance and the behavior of carbon deposition. Results suggest that the niobium oxide was reduced to NbO_2 under operating conditions, which has high electrical conductivity. The NbO_x coated dense Ni-YSZ showed sulfur tolerance when exposed to 50 ppm H_2S at

700°C over 12 h. Raman spectroscopy and XRD analysis suggest that different phases of NbS_x formed on the surface. Further, the DOS (density of state) analysis of NbO_2, NbS, and NbS_2 indicates that niobium sulfides can be considered as active surface phases in the H_2S containing fuels. It was demonstrated that carbon formation was also suppressed with niobium oxide coating on dense Ni-YSZ in humidified CH_4 (3% H_2O) at 850ºC. In particular, under active operating conditions (a current is passing through the cell), there was no observable surface carbon as revealed using Raman spectroscopy due probably to electrochemical oxidation of carbon. Stable performances of functional cells consisting of Pt/YSZ/Nb_2O_5 coated dense Ni-YSZ in the fuel were achieved; there was no observable degradation in performance due to carbon formation. The results suggest that a niobium oxide coating has prevented carbon from formation on the surface probably by electrochemically oxidation of carbon on niobium oxide coated Ni-YSZ.

On the other hand, computational results suggest that, among the metals studied, Mo seems to be a good candidate for Ni surface modification. Ni-based anodes were modified with Mo using wet-impregnation techniques, and tested in 50 ppm H_2S-contaminated fuels. It was found that the Ni-Mo/CeO_2 anodes have better sulfur tolerance than Ni, showing a current transient with slow recovery rather than slow degradation in 50 ppm H_2S balanced with H_2 at 700°C.

CHAPTER 1

INTRODUCTION

1.1. Significance of this research

Solid oxide fuel cells (SOFCs) convert a gaseous fuel to electricity through electrochemical reactions, with higher conversion efficiency than other energy conversion devices. Furthermore, several advantages of fuel cells such as environmental compatibility and fuel flexibility become important reasons for researchers to have great interest in them.[1]

In the operation of an SOFC, the two major electrode reactions are fuel oxidation at the anode and oxygen reduction at the cathode. While pure hydrogen is a preferred fuel for fuel cells, there are various practical barriers to the direct use of pure hydrogen due to high cost of the hydrogen production and storage. Instead, reformed gases produced from fossil fuels (e.g., methane, propane and butane) at elevated temperatures for SOFC operation, have been considered as practical fuels.[2]

However, using reformed gases or hydrocarbon-containing fuels for SOFCs brings technical challenges to overcome: sulfur poisoning and carbon coking.[3] Currently, Ni-YSZ (Y_2O_3 doped ZrO_2) cermets are being widely used as the anode materials.[4] In spite of the good catalytic activity of Ni for reforming of hydrocarbon fuels and for hydrogen oxidation, it is known that the electrochemical performance of the Ni-YSZ

anode is severely degraded by the sulfur contaminants. The degradation in performance of a fuel cell can not fully be regenerated when the concentration of sulfur is sufficiently high. Furthermore Ni is an excellent catalyst for carbon formation, when exposed to a hydrocarbon fuel.[5] The carbon formation on Ni remarkably degrades the electrochemical performance of the cell by covering the active reaction sites, such as the triple phase boundaries (TPBs) at the intersection between metal (Ni), electrolyte (YSZ), and fuel (hydrogen). Therefore, the prevention of sulfur poisoning and carbon formation on the anode is the key technical challenges for the direct use of sulfur-containing reformed gases and hydrocarbon fuels in SOFCs.[6]

To date, the detailed mechanism for sulfur poisoning of Ni-YSZ anode is still lacking, and there are no clear guidelines for selection of sulfur-tolerant anode materials. Various candidate materials have been studied as alternative anodes to replace Ni-YSZ, including LST($La_{1-x}Sr_xTiO_3$),[7] LSCM($La_{1-x}Sr_xCr_{1-x}Mn_xO_3$),[8] and $Cu/CeO_2/YSZ$.[9] While each candidate has its advantages to overcome sulfur poisoning and carbon coking, none of these materials can satisfy all the practical requirements for SOFCs. For example, reasonable sulfur tolerance at low concentration of H_2S was observed with LST but its electrochemical performance was not acceptable. It was reported that the performance of LSCM was acceptable compared to that of Ni-YSZ and no carbon formation was observed. However, sulfur poisoning was observed in LSCM. In the case of $Cu/CeO_2/YSZ$, tolerance to sulfur poisoning and coking was observed up to the certain concentration of H_2S, however, ion impregnation must be used in the fabrication of the anode (not cost effective).

1.2. Research objectives

The main objective of this research is to modify the surface of Ni-YSZ anodes for tolerance to sulfur poisoning and carbon deposition.

In particular, the technical objectives can be described as follows.

- **To develop an effective method for evaluation of sulfur tolerance with minimum experimental uncertainties.**

- **To systematically modify the surface of conventional Ni-YSZ for sulfur tolerance using a thin-film deposition process such as sputtering, in order to improve the sulfur tolerance of Ni-YSZ without sacrificing the electrochemical performance.**

- **To understand the mechanism of sulfur-anode interactions under typical fuel operating conditions using various characterization techniques, including SEM/EDS, XRD, and Raman spectroscopy in order to provide some general guidance for the design of better anode materials.**

- **To explore the carbon tolerance of the sulfur tolerant materials using Raman-spectroscopy for the extension to practical applications of the sulfur tolerant anode.**

1.3. References

1. N.Q. Minh, and T. Takahashi, in Science and Technology of ceramic fuel cells, Elsevier Science, Amsterdam, The Netherlands, 1995.

2. B.C.H. Steele, and A. Heinzel, Nature, **414**, 345 (2001).

3. B.C.H. Steele, Nature, **400**, 619 (1999).

4. M. Ihara, T. Kusano, and C. Yokoyama, J. Electrochem. Soc., **148**, A209 (2001).

5. H. Kim, C. Lu, W.L. Worrell, J.M. Vohs, and R.J. Gorte, J. Electrochem. Soc., **149,** A247 (2002).

6. R.J. Gorte, and J.M. Vohs, J. Catalysis, **216**, 477 (2003).

7. O.A. Marina, and L.R. Pederson, *Proceedings of 5th European Solid Oxide Fuel Cell Forum* 481 (2002).

8. S. Tao, and J.T.S. Irvine, Nature Letters, **2**, 320 (2003).

9. H. Kim, S. Park, J.M. Vohs, and R.J. Gorte, J. Electrochem. Soc., **148**, A693 (2001).

CHAPTER 2

BACKGROUND

2.1. Fundamentals of SOFCs

A solid oxide fuel cell consists of a cathode, an electrolyte and an anode as schematically shown in Figure 2.1. Mostly, LSM($La_{1-x}Sr_xMnO_3$), YSZ and Ni-YSZ are used for cathode, electrolyte and anode in SOFCs, respectively, as described in Table 1.1. The operation of SOFCs includes the reduction of oxygen (oxidant) at the cathode and the oxidation of hydrogen (fuel) at the anode. Oxygen at the cathode is reduced to O^{2-} which will combine with an $V_O^{\cdot\cdot}$ to form O_O^X. At the same time, electrons are released from the anode which travels through the external circuit to the cathode. The cathodic reaction can be described as

$$\tfrac{1}{2}\,O_2\ (\text{gas}) \ + \ V_O^{\cdot\cdot} \ + \ 2e' \ = \ O_O^X \qquad (1)$$

The oxygen ions are transported through the electrolyte to the anode where they react with hydrogen to produce water and electrons. The anodic process is represented by the following reaction:

$$H_2 + O_O^X \ = H_2O + 2e' \ + \ V_O^{\cdot\cdot} \qquad (2)$$

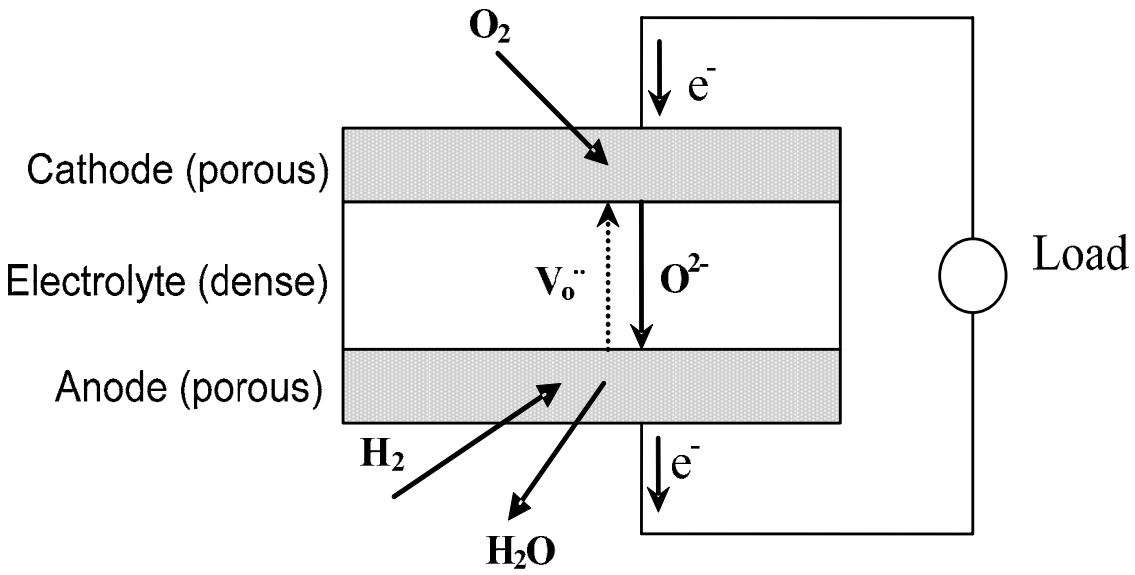

Figure 2. 1. Schematic of solid oxide fuel cell operation

Table 2. 1. SOFC materials

	ZrO_2 based	CeO_2 based
Cathode	$La_{1-x}Sr_xMnO_3$ (LSM)	$Sm_{1-x}Sr_xCoO_3$ (SSC)
Electrolyte	Y_2O_3 doped ZrO_2 (YSZ)	Gd_2O_3 doped CeO_2 (GDC)
Anode	**Ni + YSZ**	**Ni + GDC**

Thus, the overall cell reaction is,

$$H_2 + \tfrac{1}{2} O_2 = H_2O \qquad (3)$$

The Nernst potential across the cell, E_N, is given by

$$E_N = E^0 + \frac{RT}{4F} \ln P_{O2} + \frac{RT}{2F} \ln \frac{P_{H2}}{P_{H2O}} \qquad (4)$$

E_0 : standard cell voltage

At standard state E_N is equal to E^0 and some E^0 values are shown in table 1.2 for different fuels.

Table 2. 2. Standard cell voltages in several fuels

Reaction	E_0 (V) at 1000ºK
$H_2 + \frac{1}{2} O_2 = H_2O$	0.997
$CO + \frac{1}{2} O_2 = CO_2$	1.013
$CH_4 + 2O_2 = CO_2 + 2H_2O$	1.039
$C + O_2 = CO_2$	1.027

The open circuit voltage of an SOFC can be equal or lower than the Nernst potential, which can be calculated theoretically under an operating condition. The actual cell voltage is given by

$$V = E_N - IR_i - (\eta_a + \eta_c) \quad (5)$$

where IR_i is the ohmic loss, η_a is the anode polarization and η_c is the cathode polarization.[1] In order to achieve high performance of the cell, the ohmic loss originated from the cell materials and the losses due to electrode polarization must be minimized. The electrode polarization is related to the electrochemical reactions at the cathode and anode. The kinetics of the hydrogen oxidation and the reduction of oxygen are critical to determine the electrode polarization.[1]

2.2. Electrochemical degradation of fuel cell performance

Even though pure hydrogen is a preferred fuel for fuel cells, hydrocarbon fuels, reformed coal gas (syngas), and bio-derived fuels have attracted much attention due to the high cost of hydrogen production and the difficulty of hydrogen storage. In particular, hydrocarbon fuels can be directly used for the operation of SOFCs because the reformation of hydrocarbon fuels can take place at the high operating temperature, producing H_2 and CO. However, reformed gases from coal and hydrocarbon fuels such as methane, butane, propane, and gasoline contain various contaminants, especially H_2S

(upon reforming, most sulfur compounds are converted to H_2S). It is known that small amounts of H_2S could significantly degrade the performance of Ni-YSZ anodes.

The carbon formation, which is also called, coking, on the anodes severely deactivates the electrochemical performance of SOFCs. Steam reforming can be applied in order to avoid carbon deposition but the ratio of steam to carbon should be over 3. The addition of steam significantly reduces the energy efficiency. Therefore, developing novel anode materials or structures with tolerance to sulfur poisoning and carbon formation is a critical challenge to commercializing SOFCs.

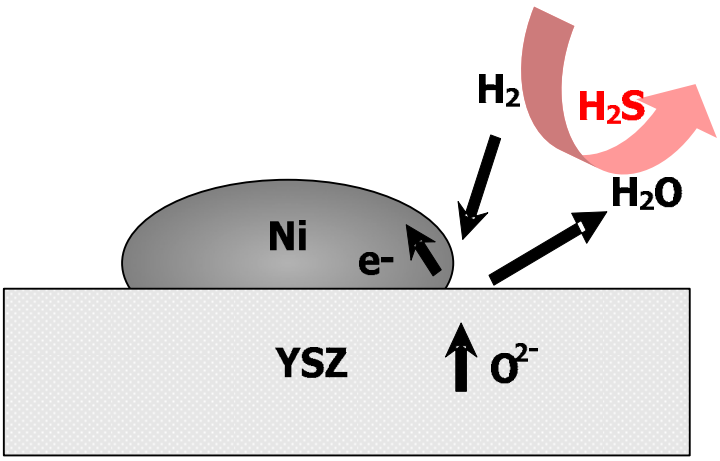

Figure 2. 2. Schematic of electrochemical reactions in anode

2.2.1. Sulfur poisoning

Based on Figure 2.2, the severe degradation of anode functionality due to sulfur-containing fuels can be attributed to adsorption of sulfur at surface active sites and to sulfidation of anode materials due to the reaction with sulfur, followed by the loss of catalytic activity, conductivity and stability at the anode. It has been reported that the degree of degradation varies with the operating temperatures, loading current, and the concentration of sulfur in the fuel, but the mechanism of sulfur poisoning is yet to be identified.

Listed below are two possibilities for electrochemical oxidation of H_2S at 1000ºK,[2]

$$H_2S + 3O^{2-} \leftrightarrow H_2O + SO_2 + 6e^- \quad (6)$$

$$H_2S + O^{2-} \leftrightarrow H_2O + 1/2\ S_2 + 2e^- \quad (7)$$

Additionally, thermal decomposition of H_2S is also known to occur as follows

$$H_2S \leftrightarrow H_2 + \tfrac{1}{2}\ S_2 \quad (8)$$

The sulfur formed by reactions (7) and (8) can be electrochemically oxidized by the following reaction

$$\tfrac{1}{2}\ S_2 + 2O^{2-} \leftrightarrow SO_2 + 4e^- \quad (9)$$

In the case of Ni-YSZ anode, it is known that surface sulfur adsorption or sulfidation of anode materials[3, 4] results in decrease in fuel cell performance. The elementary steps involved in sulfur poisoning can be described as follows.

$$H_2S\,(g) \leftrightarrow HS_{ads} + H\,(g/ads) \leftrightarrow S_{ads} + H_2\,(g/ads) \quad (10)$$

$$Ni + H_2S \leftrightarrow NiS + H_2 \quad (11)$$

However, detailed mechanisms of sulfur poisoning are yet to be determined. Thus more fundamental study on the mechanism of sulfur poisoning is necessary to provide effective guidance for the development of sulfur tolerant anode materials.

2.2.2. Carbon deposition

Hydrocarbon fuels can be directly used for the operation of a fuel cell because the reformation of hydrocarbon fuels can take place at the high operating temperature, producing H_2 and CO. For example, the steam reforming of methane can be described as,

$$CH_4\,(\text{or hydrocarbon fuels}) + H_2O = CO + 3H_2 \quad (12)$$

When hydrogen is used as a fuel, the anode polarization is much less important than the cathode polarization. When a hydrocarbon fuel is used, however, the anode polarization becomes a major factor in determining the cell performance, due to the slow

electrochemical oxidation of CO produced by the reformation of the hydrocarbon fuel and carbon deposition described by the following reactions:

$$2CO = CO_2 + C \quad (13)$$

$$CH_4 \text{ (or hydrocarbon fuels)} = 2H_2 + C \quad (14)$$

2.3. Criteria for selection of anode materials

A viable anode material should have the following desirable properties:

(1) Adequate chemical and electrochemical stability under fuel cell operating conditions (exposed to sulfur containing fuels at high temperature);

(2) Sufficient electronic conductivity for current collection to minimize in-plan sheet resistance and ohmic loss;

(3) Good catalytic activity for oxidation of fuels (hydrogen, CO, and hydrocarbons) to minimize the electrode polarization losses

The candidate materials should have high electrical conductivity. The electrical conductivity of Ni is 2×10^5 Scm^{-1} while that of porous Ni-YSZ is in the range of 10^2-10^4 Scm^{-1} at 1000°C. Thus, the electrical conductivity of candidate materials should be at

least close to 100 Scm^{-1} in order to replace Ni-YSZ.[5] For a thin-film coating on Ni-YSZ, however, the required conductivity can be as low as 1 Scm^{-1}.

Materials should be chemically stable under operating conditions because the anode materials are always exposed to reducing atmosphere with fuels at elevated temperature (600-1000°C). Sufficient resistance to oxidation is required due to the presence of H_2O and other oxidizing gases (CO_2, CO…) in the fuel. Candidate materials should not have any undesirable reactions with other cell materials during the operation or fabrication process.

The catalytic activity for electrochemical oxidation of various fuels is necessary to minimize the interface polarization at the anode. Normally, the interfacial resistance of Ni-YSZ is about 0.2cm^2 in the range of 950 -1000°C. Thus the interfacial polarization resistance of candidate materials should be comparable to that of Ni-YSZ.

Thermal compatibility with other cell materials is important because SOFCs are operated in the temperature range of 600-1000°C. Thus, new materials should have similar CTE (coefficient of thermal expansion) with that of YSZ. Because CTE of YSZ is about 10.8×10^{-6} K^{-1}, the marginal CTE of candidate materials should be in $10\text{-}12\times10^{-6}$ K^{-1}.

The properties described above are essential requirements that must be considered in the development of new anode materials. In addition, it should be pointed out that the candidate materials should have sulfur tolerance when H_2S containing fuels are used.

2.4. Literature reviews for sulfur poisoning in SOFCs

2.4.1. Sulfur poisoning of conventional Ni-YSZ

The Ni-YSZ cermet has been the best option of anode materials over 30 years because Ni is a good catalyst for hydrogen oxidation and electrical current collector in reducing atmosphere. However, for practical applications of SOFCs, sulfur poisoning and carbon coking became significant problems to be solved.[6] Dees *et al.*[7] revealed that sulfur poisoning increased anode interfacial resistance, while the bulk resistance remained unchanged. Geyer *et al*.[8] reported the interfacial resistance increased 33% by only 5 ppm H_2S at 950°C in 97%H_2/3%H_2O. The poisoning effect dependence on operating temperature and concentration of H_2S was investigated by Matsuzaki *et al*.[9] Sasaki *et al*.[10] observed the degradation of the cell voltage of 6.3, 15.2 and 22.8% when the concentration of H_2S was 1, 3 and 5ppm respectively. The cell voltage degradation of 20, 27 and 81% at 1000, 900 and 850°C was also observed respectively in 5ppm H_2S. The results indicated that the sulfur tolerance increased with the increase of the temperature. S. J. Xia *et al*.[11] reported that Ni-YSZ composite anode operated in humidified H_2 with 10ppm H_2S at 880°C showed the increase of the polarization resistance from ~1.6 Ωcm^2 to ~ 8.2 Ωcm^2 and the degradation of the performance were accelerated under a load and higher current density. They also concluded that the active Ni-YSZ sites are blocked with adsorbed sulfur or H_2S in case of the reversible process, and with the formation of a Ni-S compound in case of the irreversible process during sulfur poisoning. In spite of extensive work on the sulfur poisoning of Ni-YSZ, the understanding of performance

degradation by sulfur poisoning was not elucidate due to the complexity of gas-solid reaction and limited experimental data to verify the poisoning mechanism.

2.4.2. Alternative anode materials for sulfur tolerant anodes

For developing an alternative to Ni as the anode material, recently Cu has been studied because Cu is inactive not only to carbon formation but also to sulfur poisoning. It was reported that Cu can be used as an anode material without carbon deposition when CH_4 is used as a fuel.[12] On the other hand, a SOFC with $Cu/CeO_2/YSZ$ anode with a hydrogen fuel containing H_2S showed no sulfur poisoning effect up to 450ppm H_2S at 800°C.[13] They also claimed that sulfur poisoning above 450ppm H_2S was caused due to the formation of Ce_2O_2S from the reaction between CeO_2 and H_2S. In addition, hydrocarbon fuels containing high concentration of sulfur species (5000ppm) was applied to investigate the sulfur poisoning of the $Cu/CeO_2/YSZ$ anode.[14] The result showed that stable performance can be achieved in the fuel.

However, because the melting temperature of Cu or CuO is much lower than that of Ni, the conventional ceramic processing such as sintering can not be applied. Usually, the Ni-YSZ cermet should be fabricated at over 1200°C to achieve sufficient electrical contact, but Cu or CuO starts to melt at the temperature. To overcome the problem, a new fabrication method for the Cu application was demonstrated by wet impregnation.[15] To compare the effect of the fabrication process on the performance of the cell, NiO was also impregnated into a porous matrix of GDC (Gd_2O_3 doped CeO_2), and the cell was compared to the Ni-YSZ anode fabricated by the conventional sintering process. It was

found that the cell fabricated by the wet impregnation lowered the cell performance.[16] In addition, C. Lu *et al*.[17] found out that Cu has no catalytic effect and just plays a role as a current collector, through the wet impregnation of Au into YSZ matrix instead of Cu.

K. Sasaki *et al.*[10] reported that the sulfur tolerance can be improved by using Sc_2O_3-doped ZrO_2 instead of YSZ. Besides, with the impregnation of various additives such as CeO_2, Y_2O_3 and MgO into the Ni-YSZ anode, they showed that sulfur poising can be reduced through the surface modification.

MoS_2 and other composite metal sulfides such as M-Mo-S (M=Fe, Co or Ni) were investigated by Liu *et al.,*[18] showing a reasonable performance with Co-Mo-S mixed with up to 10% Ag powder when H_2S was used as fuel. Yates *et al*.[19] also studied CoS_2, WS_2 and $LiCoS_2$ for the utilization of H_2S as fuel. However, they showed low current density of 20mA/cm^2 with 25% H_2S and phase instability. Smith *et al.* [20] applied Mo into the Ni-YSZ anode by Mo salt impregnation. While failure was observed in the anode without Mo impregnation, the anode with Mo impregnation showed better stability when the anode was exposed to sulfur in fuel.

As the alternative of the Ni-YSZ, titanium oxide based materials have been also extensively studied. Mukundan *et al.*[21] compared the sulfur poisoning of various anode candidates such as LSCM, LSC and LST at 10ppm and 1000ppm. Among these anode materials, LST anode showed no degradation when up to 5000ppm of H_2S in a hydrogen fuel, indicating the LST has better sulfur tolerance than other anode materials.

LSCM was synthesized by Tao *et al*.[22] as an alternative anode of Ni-YSZ. LSCM is comparable to that of Ni-YSZ anode in terms of electrochemical performance, showing the anode polarization of 0.2Ωcm^2 at 900°C in 97% H_2/3% H_2O. However, Zha *et al*.[23]

revealed that the resistance to sulfur poisoning of LSCM was not acceptable in fuels containing 10% H_2S even though LSCM has a good redox stability and electrochemical performance. LSV was investigated by Aguilar *et al.*[24] and they observed an enhancement of the cell current of about 175% when 5% H_2S was introduced to humidified H_2. They concluded that the sulfur enhancement was caused by the formation of the active phase SrS and the removal of insulation phase ($Sr_3V_2O_8$).

Niobia based anode materials were also studied to substitute the conventional Ni-YSZ.[25] If Nb_2O_5 is reduced, it is known that its electrical conductivity increases up to 200 Scm^{-1}. Thus they are regarded as good candidates for the replacement of Ni in Ni-YSZ anode. Reich *et al*.[26] studied Nb_2TiO_7 which showed a good electrical conductivity. However, several problems for substituting Ni-YSZ were confirmed such as low coefficient of thermal expansion (CTE) and poor ionic conductivity compared to those of Ni-YSZ.[27]

2.5. Literature reviews for carbon deposition in SOFCs

2.5.1. Cu as alternative material

For developing an alternative to Ni as the anode material, recently Cu has been focused as a candidate because Cu is inactive to carbon deposition during the reformation of hydrocarbon fuels. Thus, Cu was reported as new anode material for utilization of CH_4 without carbon deposition.[14] However, due to low melting temperature of Cu comparing

to Ni, sintering process at high temperature can not be applied. Therefore, a new fabrication method for the Cu application was proposed by wet impregnation.[12,14,15] In spite of some drawbacks of Cu application, Cu has been paid attention for the substitution of Ni in the anode because it prevents the carbon formation which is a critical issue when hydrocarbon-containing fuels are used. Therefore, it is worth putting more efforts on improving the cell performance using Cu as the alternative anode material for the application of hydrocarbon fuels.

2.5.2. Catalytic Effect of CeO_2

CeO_2 has been known as a catalyst for the direct oxidation of hydrocarbons and its catalytic behavior has been reported through many experiments using CeO_2 in the anode. B.C. Steele *et al.*[28] showed that the electrochemical oxidation of CH_4 at 990°C can be accomplished by applying CeO_{2-X} to the anode. In addition, the criteria of an anode material for the oxidation of hydrocarbons were proposed: i) good electronic conductivity ii) enhancement of oxygen diffusion coefficients iii) high oxygen surface exchange rate iv) compatibility with other cell materials. CeO_2 is a mixed conductor in a reducing atmosphere and its ionic conductivity can be controlled by adding a divalent or trivalent oxide such as CaO, Y_2O_3, Gd_2O_3 and Sm_2O_3 [29, 30]. It was also observed that $CeO_{1.9}$ has the electronic conductivity of 1S/cm at 900°C and the oxygen partial pressure of 10^{-18} atm.[31,32] S. Park *et al.*[33] reported that the direct oxidation of various hydrocarbon-containing fuels such as methane, ethane, 1-butane, n-butane and toluene can be accomplished with the composite anode of Cu and CeO_2 fabricated by wet impregnation.

Doped-CeO_2 has also been investigated as anode materials for promoting the cell performance. It was found that adding an interlayer of YDC (Y_2O_3 doped CeO_2) in between the Ni-YSZ anode and the electrolyte lowered the interfacial resistance measured in 97%H_2 + 3%H_2O. The direct oxidation of CH_4 without carbon deposition was also successfully demonstrated by applying the porous YDC layer of 0.5μm thickness on the both side of the electrolyte with the Ni-YSZ anode of 2μm thickness as a current collector.[34] This experiment showed that the doped-CeO_2 can solely have the catalytic effect for the direct oxidation of hydrocarbons. However, S. McIntosh *et al.*[35] reported that SDC (Sm_2O_3 doped CeO_2) slightly reduced the cell performance and the catalytic activity in comparison with undoped-CeO_2 when butane was used, in spite of the increased ionic conductivity.

2.5.3. Catalytic Effect of Noble Metals and PdCu alloy

Another approach to enhance the catalytic effect for the direct oxidation of hydrocarbon fuels is adding a noble metal such as Ru, Pt, Pd, Rh and Ir. Noble metals promote the catalytic behavior of the dissociation of hydrogen or the reformation of hydrocarbons at the anode. In spite of the high cost, noble metals have been used for promoting the performance because of the remarkable catalytic effect, carefully considering the amount of noble metals and the recycling.

The addition of Rh to SDC showed that the performance can be catalytically enhanced when CH_4 is used. But, slight improvement was found, when hydrogen was used, indicating that Rh can be only a catalyst for the hydrocarbon oxidation.[36] It was

also found that Pt, Rh or Ni added doped-CeO_2 can catalyze the reformation of iso-octane in the temperature range of 500 - 800°C, producing H_2, CO, CO_2 and CH_4.[37] The reduction of the anode polarization by the catalytic activity of the small amount of Ru, Rh, Ir or Pt dispersed onto SDC particles was observed when hydrogen is used.[38] It was also demonstrated that Ru-SDC anode can oxidize CH_4 at intermediate temperatures[39]. Z. Zhan *et al.*[40] applied a thin Ru-CeO_2 catalyst layer on the top of a Ni-YSZ anode and confirmed the partial oxidation of propane without carbon deposition at above 500°C. Recently, the Ru-CeO_2 catalyst layer was added on Ni-YSZ anode and Ni-GDC respectively and the direct oxidation of iso-octane using the layer was reported.[41] This experiment showed that Ni could be used without severe degradation if the pre-reforming of iso-octane in a SOFC is achieved through the catalyst layer. However, the drawbacks of this configuration were also described by the authors such as the decrease of the power density aroused from the lowered diffusion rate of the fuel through the catalyst layer and the difficulty of the current collection from the anode due to the poor electrical conduction of the catalyst layer. F. Chen *et al.*[42] also introduced the combination of a catalytic chamber and a fuel cell expecting the pre-reforming of propane. In the experiment, it was confirmed that the pre-reforming of propane producing H_2, CH_4, CO and CO_2 is possible with the addition of 1wt% Pt into the porous GDC. A power density of 247 mW/cm^2 was measured using the noble metal dispersed anode when propane was used. Pd is not only a good catalyst for the direct oxidation of hydrocarbons but also a remarkable absorbent of hydrogen. Several results have been reported that the addition of Pd can significantly increase the power density of the cell and the direct hydrocarbon

oxidation.[43] T. Hibino showed that Pd dispersed Ni-GDC anode can catalyze the partial oxidation of CH_4 in a single-chamber SOFC.[52]

Recently, PdCu alloy has received attention due to the potential possibility to be used as a new membrane material for hydrogen purification from mixed gases. In spite the alloy of Pd and Cu, the hydrogen permeability of the alloy was observed similar with that of pure Pd.[45-47] It was also reported that this alloy can maintain its hydrogen permeability even in H_2S gas which severely poisons anode materials and degrades the electrochemical performance at few tenths of ppm level concentration.[48] Besides, PdCu alloy can reduce the cost which is the major barrier to Pd use. The catalytic activity of PdCu alloy for hydrocarbon fuels in a SOFC has not been deeply studied, whereas Pd has been well known as a catalytic material for the direct oxidation of hydrocarbons. Therefore, PdCu needs to be studied because it could be a catalyst for promoting the reformation of hydrocarbons and the dissociation of hydrogen produced from hydrocarbon fuels in a SOFC.

2.6. References

1. B.C.H. Steele, K.M. Hori, and S. Uchino, Solid State Ionics, **135**, 445 (2000).

2. D. R. Peterson, and J. Winnick, J. Electrochem. Soc. **145 (5)**, 1449-1454 (1998).

3. D. Weaver, and J. Winnick, J. Electrochem. Soc. **136 (6)**, 1679-1686 (1989).

4. Y.M. Choi, et al., Chem. Phys. Lett. **421**, 179-183 (2006).

5. E. Ramirez-Cabrera, A. Atkinson, and D. Chadwick, Appl. Cataly., **B47,** 127 (2004).

6. S.P. Jiang, and S.H. Chan, J. Materials Science, **39,** 4405 (2004).

7. D.W Dees, U. Balachandran, S.E. Dorris, J.J. Heiberger, C.C. McPheeters, and J.J. Picciolo, *Proceedings of the First International Symposium on Solid Oxide Fuel Cells*, **89-11**, 317 (1989).

8. J. Geyer, H. Kohlmuller, H. Landes, and R. Stubner, *Proceedings of the 5th International Symposium on Solid Oxide Fuel Cells*, **97-18,** 585 (1997).

9. Y. Matsuzaki, and I. Yasuda, 2004 Office of Fossil Energy Fuel Cell Program Annual Report, 90 (2004).

10. K. Sasaki, K Susuki, A. Iyoshi, M. Uchimura, N. Imamura, H. Kasaba, Y. Teraoka, H. Fuchino, K. Tsujimoto, Y. Uchida, and N. Jingo, *Proceedings of the 9th International Symposium on Solid Oxide Fuel Cells*, **2005-7,** 1267 (2005).

11. S.J. Xia, and V.I. Birss, *Proceedings of the 9th International Symposium on Solid Oxide Fuel Cells*, **2005-07**, 1275 (2005).

12. R.J. Gorte, S. Park, J.M. Vohs, and C. Wang, Adv. Mater., **19**, 1465 (2000).

13. H. He, R.J. Gorte, and J.M. Vohs, Electrochemical and Solid-State Letters, **8(6),** A279 (2005).

14. H. Kim, J.M. Vohs, and R.J. Gorte, Chemcomm 2334 (2001).

15. R. J. Gorte, J.M. Vohs and S. McIntosh, Solid State Ionics, **175**, 1 (2004).

16. S. Zha, A. Moore, H. Abernathy, and M. Liu, J. Electrochem. Soc., **151**, A1128 (2004).

17. C. Lu, W.L. Worrell, J.M. Vohs, and R.J. Gorte, J. Electrochem. Soc., **150**, 1357 (2003).

18. M. Liu, G. Wei, J. Luo, A.R. Sanger, and K.T. Chuang, J. Electrochem. Soc., **150(8),** A1025 (2003).

19. C. Yates, and J. Winnick, J. Electrochem. Soc., **146,** 2841 (1999).

20. M. Smith, and A.J. McEvoy, *Proceedings of the 9th International Symposium on Solid Oxide Fuel Cells*, **2005-07**, 1437 (2005).

21. R. Mukundan, E.L. Brosha, and F.H.Garzon, Electrochemical and Solid-State Letters, **7(1)**, A5 (2004).

22. S. Tao, and J.T.S. Irvine, Nature Letters, **2**, 320 (2003).

23. S. Zha, P. Tsan, Z. Cheng, and M. Liu, J. Solid State Chemistry, **178,** 1844 (2005).

24. L. Auilar, S. Zha, S. Li, J. Winnick, and M. Liu, Electrochemical and Solid-State Letters, **7**, A324 (2004).

25. S. Tao, and J.T.S Irvine, The Royal Society of Chemistry, **178,** 1844 (2005).

26. C.M. Reich, A. Kaiser, and J.T.S. Irvine, Fuel Cells-from Fundamentals to Systems, **1**, 249 (2001).

27. A. Lashtabeg, J.T.S. Irvine, and A. Feighery, Ionics, **9**, 22 (2003).

28. B.C.H. Steele, P.H. Middleton, and R.A. Rudkin, Solid State Ionics, **40,** 388 (1990).

29. H. Yokokawa, T. Horita, N. Sakai, K. Yamaji, M.E. Brito, Y.P. Xiong, and H. Kishimoto, Solid State Ionics, **174,** 205 (2004).

30. B.C.H. Steele, Solid State Ionics, **129**, 95 (2000).

31. H. L. Tuller, and A.S. Nowik, J. Electrochem. Soc., **126**, 209 (1979).

32. S. Park, J. M. Vohs, and R.J. Gorte, Nature, **404,** 265 (2000).

33. T. Suzuki, I. Kosacki, and H.U. Anderson, Solid State Ionics, **151**, 111 (2002).

34. E.P. Murray, T. Tsai, and S. A. Barnett, Nature, **400**, 649 (1999).

35. S. McIntosh, J.M. Vohs, and R.J. Gorte, Electrochimica. Acta., **47**, 3815 (2002).

36. E.S. Putna, J. Stubenrauch, J.M. Vohs, and R.J. Gorte, Langmuir, **11**, 4832 (1995).

37. M. Krumpelt, T. Krause, J. Kopasz, D. Carter, and S. Ahmed, Unpublished, Prepared for presentation at the 2002 Spring Meeting, New Orleans, LA, March, 2002.

38. M. Watanabe, H. Uchida, U. Shibata, M. Mochizuki, and K. Amikura, J. Electrochem. Soc., **141,** 342 (1994).

39. H. Uchida, H. Suzuki, and M. Watanabe, J. Electrochem. Soc., **145**, 615 (1998).

40. Z. Zhan, J. Liu, and S.A. Barnett, Appl. Cataly., **A262,** 255 (2004).

41. Z. Zhan, and S.A. Barnett, Science, **308**, 844 (2005).

42. F. Chen, S. Zha, J. Dong, and M. Liu, Solid State Ionics, **166**, 269 (2004).

43. S. McIntosh, J.M. Vohs, and R.J. Gote, Electrochem. solid-state lett., **6 (11),** A240 (2003).

44. T. Hibino, A. Hashimoto, M. Yano, M Suzuki, S. Yoshida, and M. Sano, J. Electrochem. Soc., **149**, A133 (2002).

45. P. Kamakoti, B.D. Morreale, M.V. Ciocco, B.H. Howard, R.P. Killmeyer, A.V. Cugini, and D.S. Sholl, Science **569**, (2005).

46. F. Roa, and D. Ways, Ind. Eng. Chem. Res., **42**, 5827 (2003).

47. B.H. Howard, R.P. Killneyer, K.S. Rothenberger. A.V. Cugin, B.D. Morreale, R.M.Enick, and F. Bustamante, J. Mem. Xci., **241,** 207 (2004).

48. B.D. Morreale, M.V. Ciocco, B.H. Howard, R.P. Killmeyer, A.V. Cugini, and R. M. Enick, J. Mem. Sci., **241**, 219 (2004).

CHAPTER 3

EXPERIMENTAL

3.1. Cell design for surface modification

Because of the excellent conductivity, thermal and mechanical stability, and compatibility of Ni-YSZ anode with YSZ electrolyte, it is desirable to modify the surface of Ni-YSZ rather than to replace it altogether.

Thus, the modification of Ni-YSZ surface with an additive or protective layer was studied in order to improve the tolerance to sulfur and coking, while retaining the other desirable properties of Ni-YSZ cermet.

As schematically shown in Figure 3.1 (a), however, a mixed ionic-electronic conductor would be an ideal case; it is hard to find a material that will meet all requirements for anode in addition to sulfur tolerance as described above. The schematics shown in Figure 3.1 (b) and (c) are relatively simple to achieve because a conventional Ni-YSZ can be used as the backbone while the surface is modified for sulfur tolerance. However, the surface modification should offer adequate catalytic property for fuel oxidation as well.

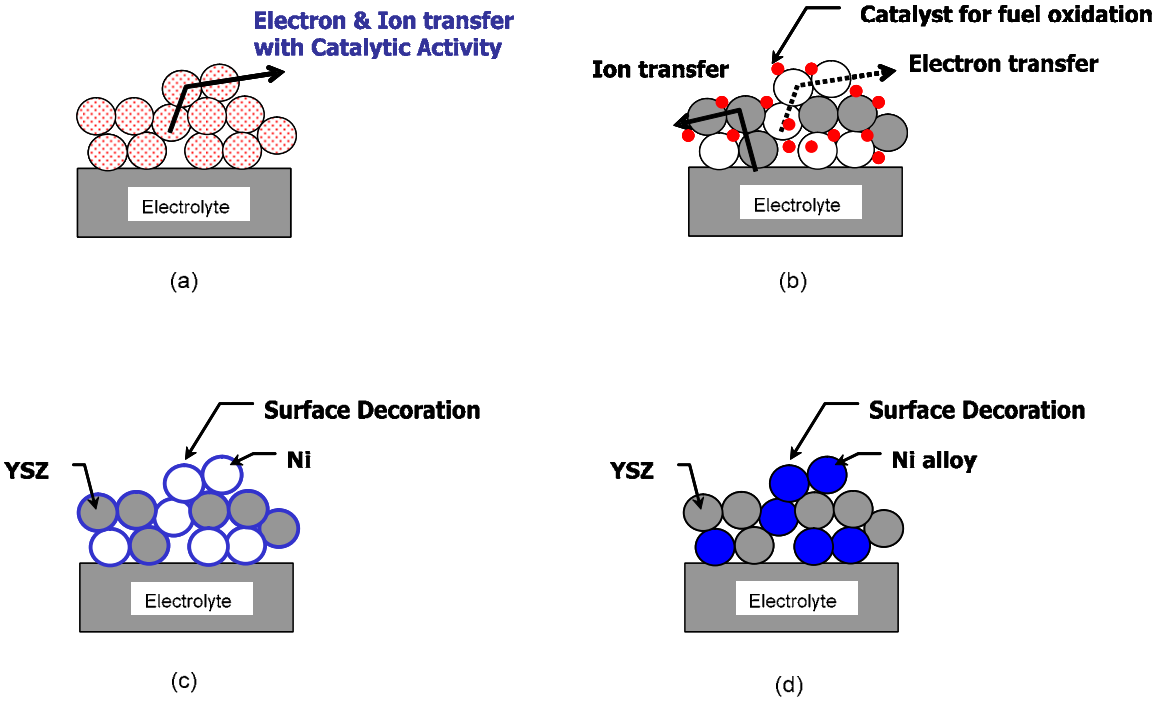

Figure 3. 1. Various anode designs for sulfur tolerant materials

Schematically shown in Figure 3.1 (d) is another alternative approach; alloying of Ni with some transition metals such as Mo to improve sulfur tolerance. This method may be suitable for materials that will react with Ni to form alloys under operating or processing conditions.

The materials to be used for surface modification should be active to electro-oxidation of H_2 and resistant to surface poisoning and carbon deposition and should have reasonable electrical conductivity, chemical stability and compatibility to Ni-YSZ-based anode. These requirements are used as criteria for screening suitable materials for surface modification.

In this research, the focus was mainly on transition metals and their oxides with high electrical conductivity and resistance to sulfidation, and carbon formation such as niobium oxide, cerium oxide, and molybdenum.

Shown in Figure 3.2 (a) and (b) are the schematics of two cell structures used in this research for evaluation of tolerance to sulfur and carbon. For example, the cell configuration shown in Figure 3.2 (a) was used for Nb_2O_5-coated dense Ni-YSZ whereas that shown in Figure 3.2 (b) was for CeO_2 impregnated Mo-Ni/YSZ anode, respectively.

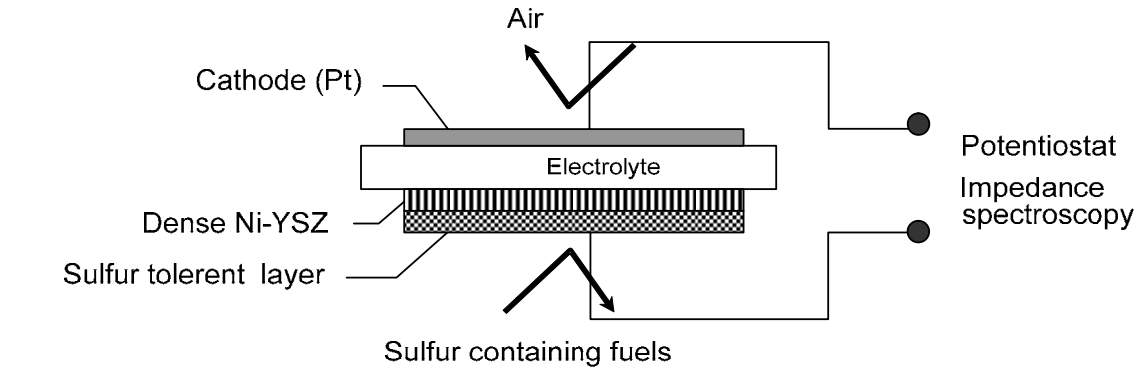

(a)

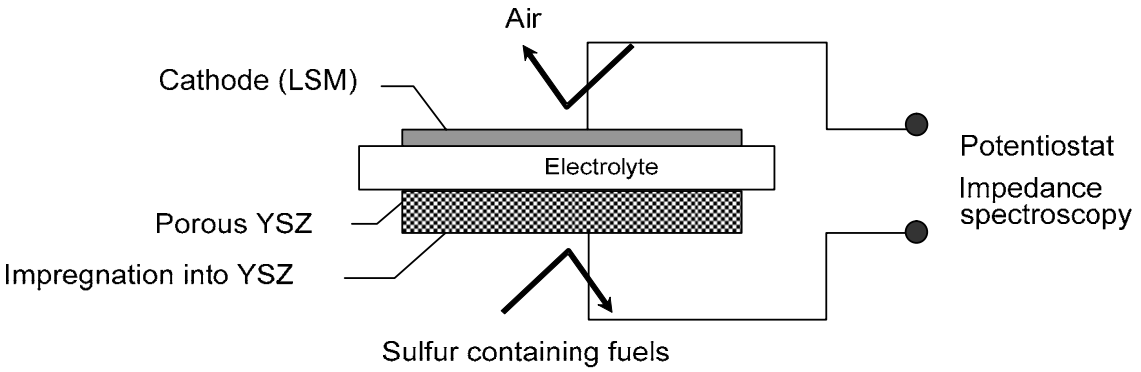

(b)

Figure 3. 2. (a) Surface modification of Ni-YSZ and (b) Ni alloying using impregnation method

3.2. Fabrication of cells, electrodes, and surface modification

3.2.1. Dense Ni-YSZ anode with surface modification (Nb_2O_5)

To minimize the uncertainties associated with a porous structure, dense Ni-YSZ was used as the substrate to evaluate the effectiveness of the coating materials. The advantages of a dense anode structure can be summarized as follows.

(1) The cell degradation due to Ni agglomeration as a function of time can be suppressed.

(2) The uniform coating of a candidate material can be achieved on the surface of a dense Ni-YSZ so that experimental errors can be minimized due to imperfect coating.

(3) Direct surface analysis is possible because the active sites for electrochemical reactions are on the surface, while the active area is close to the vicinity of the electrolyte and the anode in porous structures.

Shown in Figures 3.3 are the cross sectional views of a dense Ni-YSZ that were fabricated using a co-pressing and co-firing in 4% H_2 at 1400ºC for 3 h. As shown in (b), Ni particles are constrained by dense YSZ matrix.

For the dense Ni-YSZ, 20 wt% of metal Ni (Alfa asear, 3~5 um) was used to avoid significant distortion of the cells due to mismatch in shrinkage and the coefficient of thermal expansion. The surface of dense Ni-YSZ was confirmed conductive using an ohmmeter due to well-distributed Ni network in the dense structure. A Pt cathode was formed using a brush-painting method on the electrolyte.

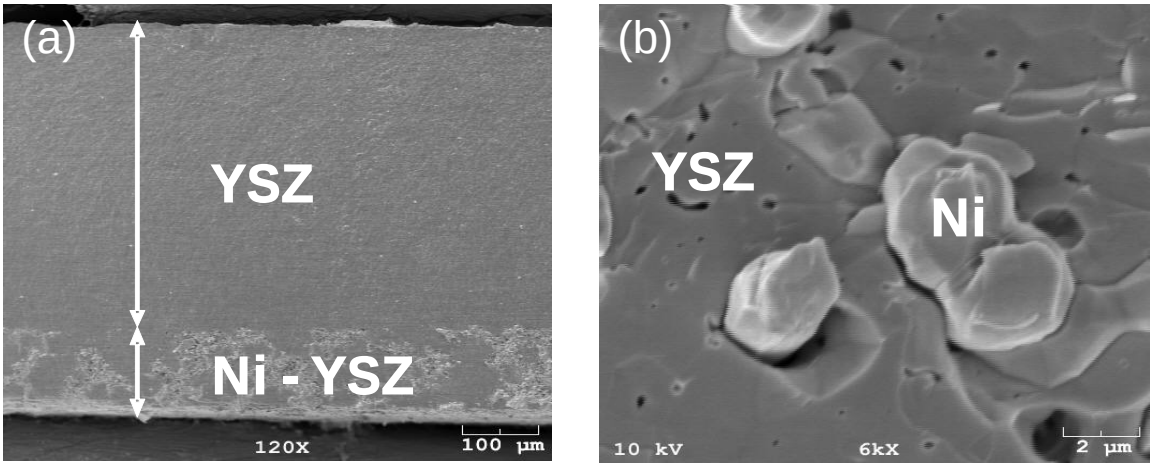

Figure 3. 3. SEM pictures of dense Ni-YSZ. (a) Cross section of the entire cell and (b) fractured cross section of dense Ni-YSZ anode

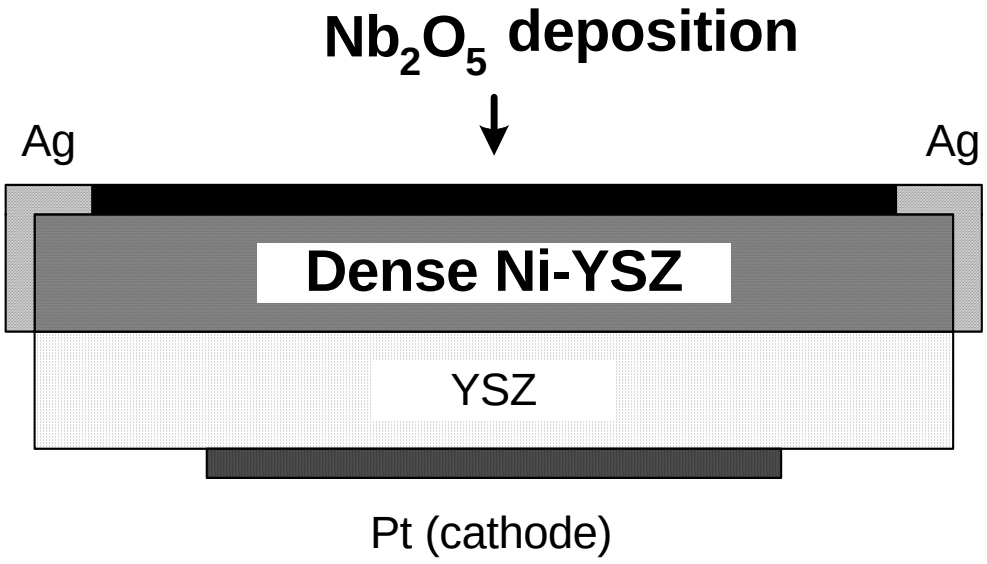

Figure 3. 4. Schematic of dense Ni-YSZ structure with Nb_2O_5 coating for sulfur tolerance test

On the dense Ni-YSZ surface, Nb_2O_5 was deposited using reactive sputtering method with a Nb target in the thickness of 300 ~ 500 nm, approximately, after the small area of the edge was masked for current collection described in Figure 3.4. Ag current collector was used and directly contacted with Ni-YSZ through the masked area in order to reduce any contribution between the current collector and the modified surface with Nb_2O_5 coating.

3.2.2. Ni modification using impregnation method

To prepare wet-impregnated anode samples, bi-layer YSZ (Daiichi Kogensu, $(ZrO_2)_{0.92}(Y_2O_3)_{0.08}$) substrates consisting of dense and porous structures were prepared by tape casting. YSZ powder (50g) was added to an ethanol-xylenes solvent mixture (50:50 ratio) along with 2g menhaden fish oil dispersant. The slurry was milled for 4hrs before adding polyalkylene glycol (type I plasticizer, butyl benzyl phthalate (type II plasticizer) and polyvinyl butyral (binder) and milling again for 24 hours. The slurry was then cast on a heated (27ºC) bed and allowed to dry overnight. Porous YSZ tape was also prepared by adding carbon pore former (15g) to YSZ powder (35g) and repeating the aforementioned organic addition and milling schedule. Circular 1.3cm disks were punched from each of the tapes and then were stacked together and uniaxially pressed together before sintering at 1400ºC in air. The thicknesses of the resulting dense and porous YSZ layers were approximately 100 and 200 μm, respectively. The porous YSZ layer had about 33% open porosity as determined by Archimedes method.

For Ni-Mo wet-impregnated samples, we used aqueous solutions of $Ni(NO_3)_2$ $6H_2O$ (Alfa Aesar, Ni 19.8%) and $(NH_4)_6Mo_7O_{24}$ $4H_2O$ (Sigma-Adrich, 99.98%) with 50:50 wt % of metals. YSZ samples impregnated with the metal salt solution were dried in air at 70°C for 1 hr and then calcinated at 500°C for 1 hr. The process was repeated until loading levels of Mo-Ni reached 20 wt. %. To prepare Ni-Mo/CeO_2 samples, we first wet-impregnated CeO_2 using aqueous solutions of $Ce(NO)_3$ $6H_2O$ (Aldrich, 99%) into the YSZ substrates with loading levels of 15 wt. %. Then, Ni-Mo was wet-impregnated as described above. Finally a cathode was painted on the YSZ electrolyte using a slurry containing equal parts $La_{0.85}Sr_{0.15}MnO_3$ (LSM, Rhodia) and YSZ (Tosoh, $(ZrO_2)_{0.92}(Y_2O_3)_{0.08}$) was brush-painted on the dense YSZ side and fired in air at 1150^{o}C for 3 hrs.

3.3. Electrochemical testing

Functional cells for electrochemical testing were fabricated as shown in Figure 3.2 (a,b) and mounted on alumina tubes using Ag, Pt or ceramic paste, and placed in a furnace to control the operating temperature. The schematic of a test cell is represented in Figure 3.5.

3.3.1. Electrochemical characterization in sulfur-containing fuel

As shown in Figure 3.6, dry H_2 was introduced to the anode side after mixing with humidified H_2 (3 vol. % H_2O) through a water bubbler, while the cathode side was exposed to air. For sulfur tolerance tests, after dry H_2 was shut off, 100 ppm H_2S balanced by H_2 was introduced with the humidified H_2 in order to obtain the gas mixture of 50 ppm H_2S containing H_2. The H_2S balanced by H_2 was not fed directly through the water bubbler because H_2S is easily dissolved in water. The total gas flow rate to the anode side was kept at 40 ml/min with mass flow controllers.

The electrochemical behavior of functional cells was recorded by measuring the current-voltage characteristics and impedance spectra. The impedance was typically measured in the frequency range from 1 MHz to 0.01 Hz using a lock-in amplifier (Princeton Applied Research) and a potentiostat/galvanostat (EG&G, 273A) interfaced with a computer. The fuel cell performance was acquired using a CorrWare software. For sulfur poisoning tests, 50 ppm H_2S balanced with H_2 was introduced to the anode as sulfur-containing fuel and the experimental apparatus as shown in Figure 3.6.[1] The sulfur tolerance was monitored in a potentiostatic mode while the fuel was switched from clean H_2 to 50ppm H_2S containing fuel or vice versa. Every cell was typically stabilized in H_2 at 750 ^oC for several days before small amount of H_2S was introduced.

In this way, the sulfur-poisoning behaviors of the Ni-YSZ coated with a decorative layer (Nb_2O_5) and the infiltrated anodes (CeO_2-Ni/Mo) before and after H_2S exposure were electrochemically analyzed.

3.3.2. Electrochemical characterizations in hydrocarbon fuels

Hydrocarbon fuels, such as CH_4 and C_3H_8, were also used to verify the possibility of direct utilization of hydrocarbon fuels. The oxidation and reformation of hydrocarbon fuels in the proposed structure was confirmed by measuring the power density and the anode polarization using impedance spectroscopy at various temperatures. The electrochemical performances and the stabilities of the functional cells in humidified CH_4 and C_3H_8 were characterized using a potentiostat/galvanostat (EG&G, Model 273). The electrochemical stability in hydrocarbon fuels were analyzed by monitoring current density changes in the fuels at a cell voltage of 0.5 volt.

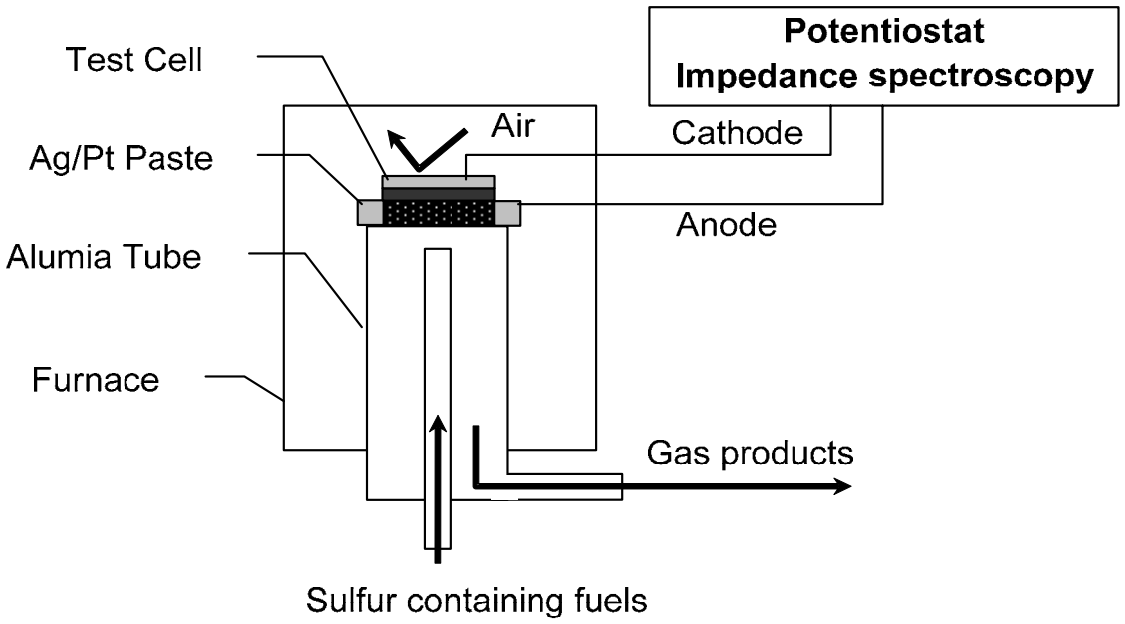

Figure 3. 5. Schematic of cell performance evaluation

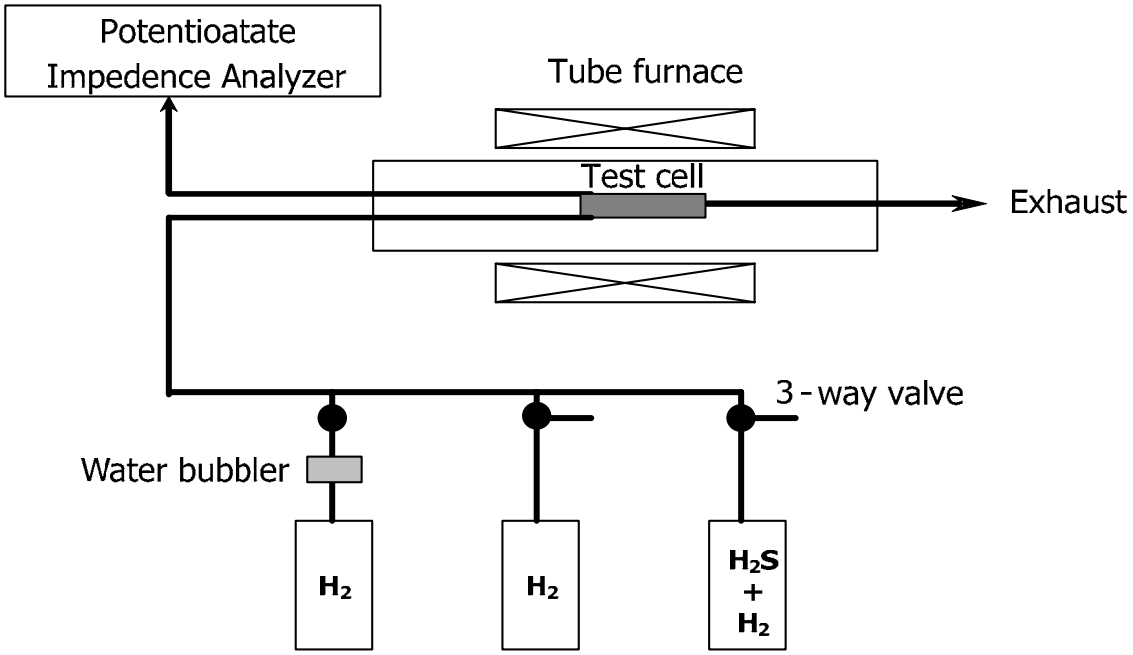

Figure 3. 6. Schematic of experimental set-up for sulfur tolerance test

3. 4. Characterization of structure, phase and microstructure of electrode materials

3.4.1. Phase analysis and electrical property of reduced Nb_2O_5

To investigate the phase stability of Nb_2O_5 under the operating conditions for fuel cells, the prepared Nb_2O_5 powder was reduced in H_2 at 800 ^oC for 24 h. The resulting phase was then analyzed using XRD (Philips, PW-1800). The electrical conductivity of the reduced phase was measured using impedance spectroscopy in the temperature range from 600 to 850 ^oC with 50 ^oC increments in H_2 after a Nb_2O_5 pallet sintered at 1250 ^oC for 5 h was reduced under the same conditions.

3.4.2. Surface analysis of Nb_2O_5-coated Ni-YSZ

To investigate the surface change in a H_2S containing fuel, fine Nb_2O_5 powder with large surface area was prepared by evaporating the solution of $Nb(HC_2O_4)_4 \cdot 6H_2O$ at 150 ^oC. The collected powder was calcinated at 500 ^oC for 5h and reduced in dry H_2 at 800 ^oC for 24 h. Then, the powder was exposed to 100 ppm H_2S balanced with H_2 at 700 ^oC for 15 h. The reaction chamber was cooled down in Ar instead of 100 ppm H_2S to avoid further reaction of the powder with H_2S at lower temperature. Raman spectroscopy was carried out for the powder after reduction, after exposure to 100 ppm H_2S and after regeneration in H_2. XRD analysis was also implemented to support the Raman spectra after 100 ppm H_2S exposure.

3.4.3. Surface analysis of carbon formation in hydrocarbon fuels

To compare the extent of carbon formation on the surfaces of Ni-YSZ and Nb_2O_5-coated Ni-YSZ, the pellets were exposed to humidified CH_4 (3% H_2O) at 850°C for 12 h. The surface carbon was detected using a Renishaw RM 1000 microscope with a 25mW 514nm Argon ion laser source (Melles Griot). Each spectrum shown here is a sum of 10-second measurements. Surface morphology changes near the boundaries of Ni and YSZ after wet CH_4 exposure were also investigated using SEM (LEO, 1530).

3.5. Computational details

First-principles calculations were carried out using the VASP (Vienna ab initio simulation package) software.[2,3,4] Generalized gradient approximation (GGA) using the Perdew-Wang (PW91) functional[5,6] with the projector-augmented wave method (PAW)[7,8] was utilized to describe the exchange and correlation energies. Brillouin-zone integrations were carried out with the Monkhorst-Pack method[9] for the bulk and slab models. Total energies were converged to 1.0 meV using the parameters for the cut-off energy and **k** points. All of optimized crystal structures were compared with experimental data to validate our computational methodology. For adsorption-energy predictions using the slab model, a vacuum space greater than ~15 Å was used to avoid interactions between slabs. In addition, density of state (DOS) calculations was performed to examine electronic structures of the systems in more detail.

3.5.1. Phase diagram construction and phonon mode analyses

To simulate SOFC conditions, the Gibbs free energy G(T,p) of the whole system was calculated as a function of temperature and pressure using DFT (density functional theory) results, as described elsewhere.[10-14] The Gibbs free energy for a solid phase was approximated by the DFT computed energy, $G_{surface}(T,p) \approx E^{DFT}_{surface}$ because of the relatively small variation, <10 meV, in a wide range of temperature (<1500 K) and pressure (<100 atm).[10,14] The Gibbs free energy of the gas phase O_2 was obtained by adding the thermodynamic corrections from the database[15] to DFT values: $G_{O_2}(T,p) =$

$E_{O_2}^{DFT} + \Delta H_{O_2}(T,p^0) + RT \cdot \ln(p_{O2}/p^o)$, where H_{O_2} is the standard enthalpy of O_2 and R is the gas constant. This thermodynamic correction was applied to NbO and carbon-NbO_2 systems. Furthermore, in order to interpret measured Raman data, phonon mode calculations were carried out by applying the finite displacement approach.[16,17] The inter-atomic force-constant matrix (Hessian matrix) was derived from a set of calculations on a periodically repeated super cell that contains several unit cells. At the starting point, all atoms were put at the equilibrium position. Then, each atom was slightly displaced and the forces on all atoms were calculated. These computed forces were proportional to the inter-atomic force constants times the displacement.

3.5.2. Surface modification of Ni with transition metals

We computationally modified Ni surfaces with various transition metals (3d or 4d) to predict sulfur tolerance and catalytic activity for fuel oxidation on the basis of adsorption-energy calculations. Our calculations of the bulk structure of the Ni surfaces predicted a lattice constant of 3.53 Å, which agrees well with the experimental value of 3.52 Å.[19] As shown in Figure 3.7, we first constructed a three-layer p(2×2) Ni(111) surface, which is the most densely packed. Three atoms of each transition metal (3d or 4d) were randomly placed on the optimized Ni(111) surface and fully optimized. Mittendorfer and Hafner[18,19] demonstrated that the magnetic effect for Ni(111) is insignificant using spin-polarization calculations in terms of adsorption energies and geometries. Thus, in this study all calculations were carried out using non-spin-polarization methods. To examine sulfur tolerance for modified Ni surfaces, an H_2S

molecule with the most stable configuration (parallel to the surface)[20] was located at one of deposited transition metals (M1, M2, or M3. see Figure 3.7 b), and the initial geometries were fully optimized to predict adsorption energies (see Figure 3.7 b) according to ΔE = E[slab + adsorbate] – E[slab] – E[adsorbate], where, E[slab + adsorbate], E[slab], and E[adsorbate] are the calculated electronic energies of adsorbed species on a modified metal surface, a bare modified surface, and a gas-phase H_2S molecule, respectively. Similar to sulfur tolerance, we also calculated dissociative adsorption energies of H_2 on modified Ni surfaces by placing an H atom on the deposited atom on Ni. The dissociative adsorption energies of H_2 were computed as E[slab + adsorbate] – E[slab] – E[H], which corresponds to catalytic activity for H_2 fuel oxidation. To interpret sulfur tolerance and catalytic activity of modified Ni anodes, we estimated averaged adsorption energies by placing H_2S (or H) on M1, M2, or M3.

3.6 Screening test of candidate materials

Based on the property requirements for anode materials, some candidate materials for sulfur / carbon tolerant anodes were chosen as listed in Table 3.1. Shown in Table 3.2 are the results of screening test for selected candidate materials. Among these materials, Ni-Mo/CeO_2 and Nb_2O_5 which satisfied the preliminary screening criteria (conductivity, compatibility, catalytic activity, and sulfur tolerance) were chosen for further studies of sulfur tolerance and carbon deposition.

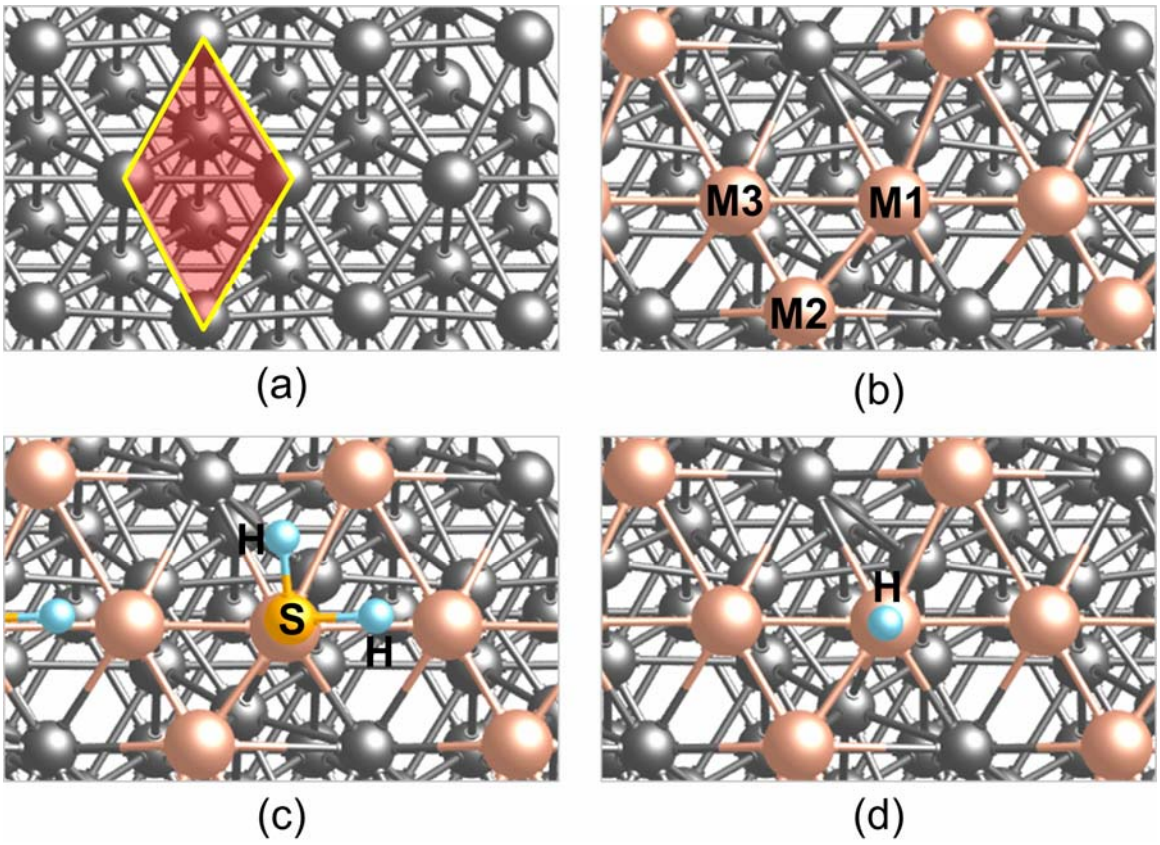

Figure 3. 7. Top views of (a) pure Ni(111) before modification, (b) modified Ni(111) with transition metals (Ni-M), (c) an adsorbed H_2S species on Ni-M surfaces, and (d) an adsorbed hydrogen species on Ni-M surfaces. A parallelogram represents a supercell (collaborated with Dr. Y. Choi)

Table 3.1. Material systems studied

	Materials	Expected advantages for sulfur / carbon tolerant anode
Metal alloys	Ag (Cu)	High electronic conductivity (metal-based materials) Low sulfidation compared to other transition metals Simple replacement or modification of the conventional Ni
	W-Ni	
	Mo-Ni/CeO_2	
Double perovskite oxides	$La_{1.8}Ce_{0.2}Mo_2O_7$	Resistance to sulfidation (oxide-based materials) Mixed ionic-electronic conductivity
	La_2MoCrO_7	
Carbides	WC	Inertness to carbon formation and sulfidation
Reducible oxides	Nb_2TiO_7	High electronic conductivity in reduced phases (reducible oxides) Resistance to sulfidation (oxide-based materials) Possibility of carbon / sulfur oxidation due to redoxability
	V_2O_5	
	CeO_2	
	Nb_2O_5	

Table 3.2. Experimental results from screening test

	Materials	Experimental results (sulfur tolerance)	Tested structure
Metal alloys	Ag (Cu)	Cell degradation due to Ag migration	Porous, impregnated
	W-Ni	Performance degradation due to surface oxidation	Porous, sintered
	Mo-Ni/CeO_2	Sulfur tolerant (slow recovery in second stage)	Porous, impregnated
Double perovskite oxides	$La_{1.8}Ce_{0.2}Mo_2O_7$	Hard to make porous structure (m.p. ~900ºC)	Porous, sintered
	La_2MoCrO_7	Thermal mismatch, low cell performance	Porous, sintered
Carbides	WC	Decomposition of WC to W with electrical polarization	Film on dense Ni-YSZ
Reducible oxides	Nb_2TiO_7	Low performance with thermal mismatch	Porous, sintered
	V_2O_5	Sulfur poisoned	Film on dense Ni-YSZ
	CeO_2	Sulfur tolerant (no second stage poisoning)	Film on dense Ni-YSZ
	Nb_2O_5	Sulfur tolerant (no poisoning)	Film on dense Ni YSZ

3.7. References

1. S. Zha, Z. Cheng, and M. Liu, J. Electrochem. Soc., **154**, B201 (2007).

2. G. Kresse and J. Furthmüller, Comp. Mater. Sci., **6**, 15 (1996).

3. G. Kresse and J. Furthmüller, Phys. Rev., B **54**, 11169 (1996).

4. G. Kresse and J. Hafner, Phys. Rev., B **47**, 558 (1993).

5. C. Lee, W. Yang, and R. G. Parr, Phys. Rev., B **37**, 785 (1988).

6. J. P. Perdew and Y. Wang, J. Chem. Phys., **45**, 13244 (1992).

7. P. E. Blöchl, Phys. Rev., B **50**, 17953 (1994).

8. G. Kresse and D. Joubert, Phys. Rev., B **59**, 1758 (1999).

9. H. J. Monkhorst and J. D. Pack, Phys. Rev., B **13**, 5188 (1976).

10. J. Xie, S. d. Gironcoli, S. Baroni, and M. Scheffler, Phys. Rev., B **59**, 970 (1999).

11. S. Cristol, J. F. Paul, E. Payen, D. Bougeard, S. Clemendot, and F. Hutschka, J. Phys. Chem., B **106**, 5659 (2002).

12. W.-X. Li, C. Stampfl, and M. Scheffler, Phys. Rev., B **68**, 165412 (2003).

13. A. Michaelides, M.-L. Bocquet, P. Sautet, A. Alavi, and D. A. King, Chem. Phys. Lett., **367**, 344 (2003).

14. K. Reuter and M. Scheffler, Phys. Rev., B **65**, 35406 (2001).

15. http://webbook.nist.gov/. (Apr. 2007)

16. X. Gonze, Phys. Rev., B **55**, 10337 (1997).

17. G. Kresse, J. Furthmuller, and J. Hafner, Europhy. Lett., **32**, 729 (1995).

18. Kresse, G.; Hafner, J. *Surf. Sci.* 459, 287. (2000)

19 Mittendorfer, F.; Hafner, J. *Surf. Sci.* **472**, 133. (2001)

20. Choi, Y. M.; Compson, C.; Lin, M. C.; Liu, M. L. *Chem. Phys. Lett.* **421**, 179. (2006)

CHAPTER 4

SURFACE MODIFICATION OF NI-YSZ USING NIOBIUM OXIDE FOR SULFUR TOLERANCE

Abstract

The surface of a dense Ni-YSZ anode was modified with niobium oxide (Nb_2O_5) in order to achieve sulfur tolerance. Results suggest that the niobium oxide was reduced to NbO_2 under operating conditions, which has high electrical conductivity. The NbO_x coated dense Ni-YSZ showed sulfur tolerance when exposed to 50 ppm H_2S at 700°C over 12 h. Raman spectroscopy and XRD analysis suggest that different phases of NbS_x can be formed on the surface. Further, the DOS (density of state) analysis of NbO_2, NbS, and NbS_2 indicate that niobium sulfides can be considered as active surface phases in the H_2S containing fuels.

4. 1. Introduction

The advantages of solid oxide fuel cells (SOFCs) over other types of fuel cells include high energy efficiency and excellent fuel flexibility.[1,2] In particular, the possibility of direct utilization of fossil fuels and renewable fuels (e.g., bio-fuels) may significantly reduce the cost of SOFC technologies. However, it is known that these types of fuels contain many contaminants that may be detrimental to SOFC performance. For example, sulfur could deteriorate the functionality of Ni-based anodes under SOFC operating conditions.[3] Even though the desulphurization of fuels for the removal of sulfur species in some levels is available, the process becomes another source of high cost and system complexity in order to achieve low concentration of sulfur species. Thus, the design of sulfur tolerant anode materials is essential to durability and commercialization of SOFCs.

Investigations into the mechanism of sulfur poisoning suggest [4,5,6] that the performance degradation of the Ni-Y_2O_3 stabilized ZrO_2 (YSZ) based anodes can be attributed to sulfur adsorption on active surface sites and subsequent formation of nickel sulfides upon exposure to H_2S. The degree of the degradation of the anode varies with operating conditions such as temperatures, concentration of H_2S, and current density passing through the cell.[7] While several alternative anode materials such as $La_{1-x}Sr_xVO_3$ (LSV),[8] $La_{1-x}Sr_xTiO_3$ (LST),[9] Y-doped $SrTiO_3$ (SYTO),[10] and CeO_2 based anodes[11,12] have showed some sulfur tolerance, other difficulties are yet to be addressed for practical SOFC applications. Recently, we have studied the effect of surface modification of Ni-YSZ anodes on sulfur tolerance.

In this chapter, we report our findings in surface modification of Ni-YSZ using niobium oxide for sulfur tolerance. In order to minimize experimental uncertainty in porous anodes, a dense Ni-YSZ anode was used for this study. Sulfur tolerance of Ni-YSZ coated with a thin film of niobium oxide was investigated experimentally and computationally in order to understand the mechanism of sulfur tolerance.

4.2. Results and Discussion

4.2.1. Phase analysis of Nb_2O_5 under reducing conditions

As shown in Figure 4.1, Nb_2O_5 was reduced to NbO_2 after being immersed in dry H_2 at 750 ^oC for 1 day. Thus, Nb_2O_5 is not stable under fuel cell operating conditions and the actual phase will be either Nb_2O_5 or NbO_2, depending on the partial pressure of oxygen. It is known that the reduced phases of Nb_2O_5 have high electronic conductivities while their ionic conductivities are negligible.[13,14]

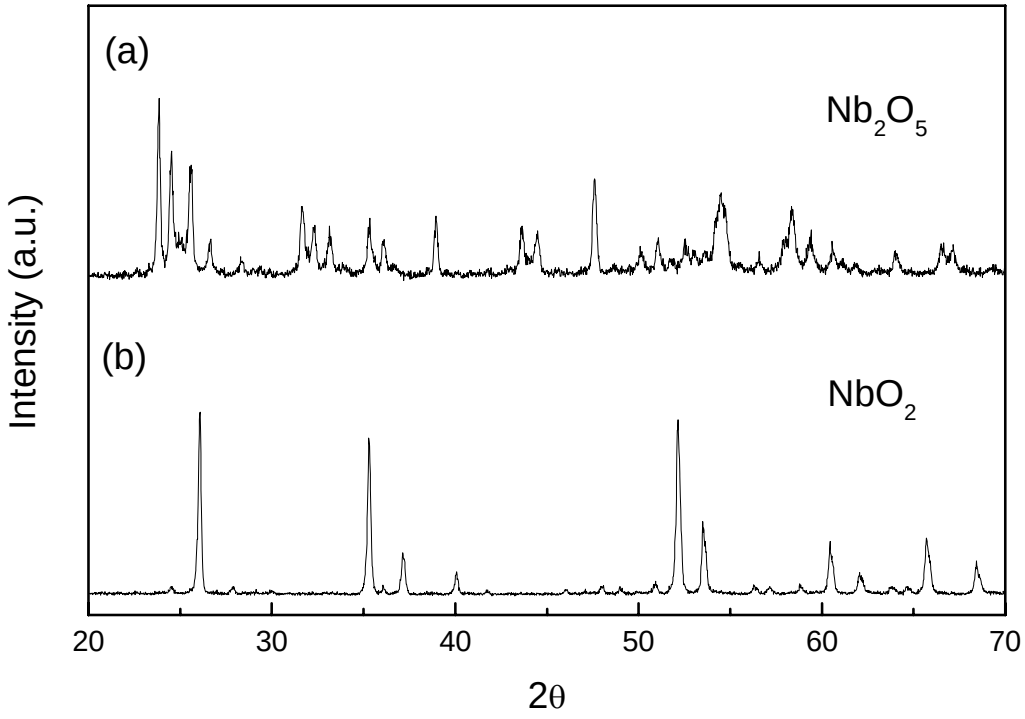

Figure 4. 1. XRD spectra of Nb_2O_5 power (a) before and (b) after reduction in dry H_2 at 750 °C for 24 h

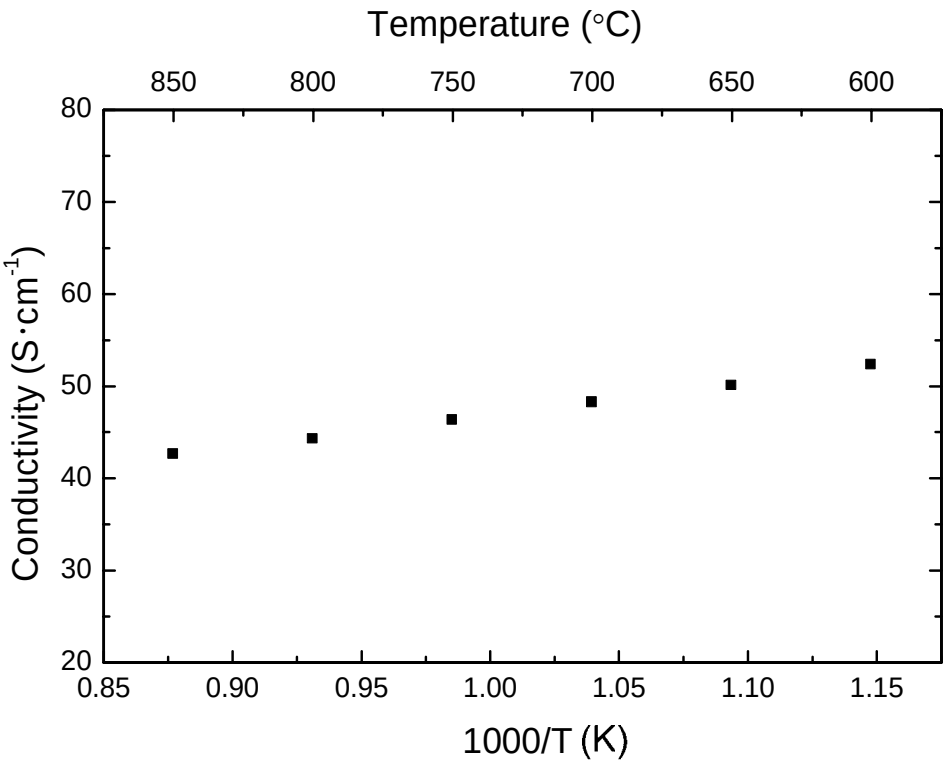

Figure 4. 2. Conductivity of NbO_2 reduced from Nb_2O_5 as function of temperature in dry H_2 measured by two-electrode AC measurement.

To determine the temperature dependence of electrical property of NbO_2, we measured the electrical conductivity of NbO_2 in pure H_2. As shown in Figure 4.2, NbO_2 displayed typical metallic behaviors.

The result of NbO_2 formation was also confirmed with the predicted phase diagram from Gibbs free energy calculations, as shown in Figures 4.3. The oxygen-rich oxides appear in the higher oxygen partial pressures. The oxidized phases are more stable at low temperatures since the oxidation processes are all exothermic: $Nb + ½\ O_2 \rightarrow NbO$ $\Delta E = -4.26$ eV; $NbO + ½\ O_2 \rightarrow NbO_2$ $\Delta E = -3.74$ eV; and $NbO_2 + ½\ O_2 \rightarrow ½\ Nb_2O_5$ ΔE

= -1.70 eV. Under the experimental condition at 750 ^{o}C, the Nb_2O_5 will reduce to NbO_2 when p_{O_2} is less than 10^{-22} atm at thermo-equilibrium. In addition, the observed electrical behavior of NbO_2 is consistent with the prediction from the DOS analysis; as shown in Figure 4.4, only Nb_2O_5 in the Nb-O systems has a wide band gap around the Fermi level.

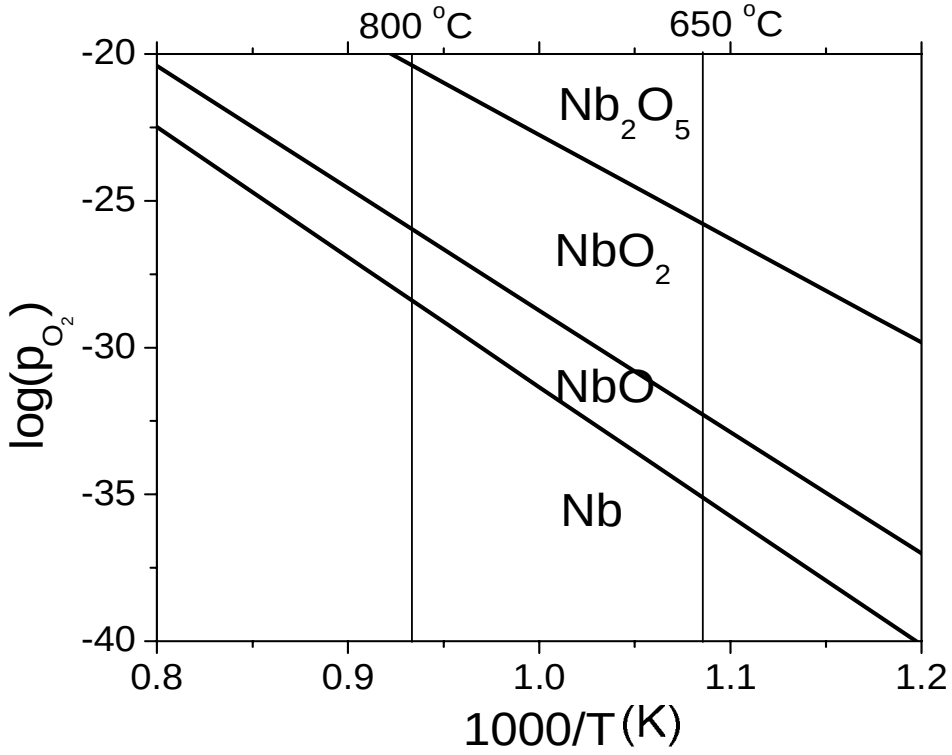

Figure 4. 3. Phase diagram of Nb-O system (collaborated with Dr. J.H. Wang)

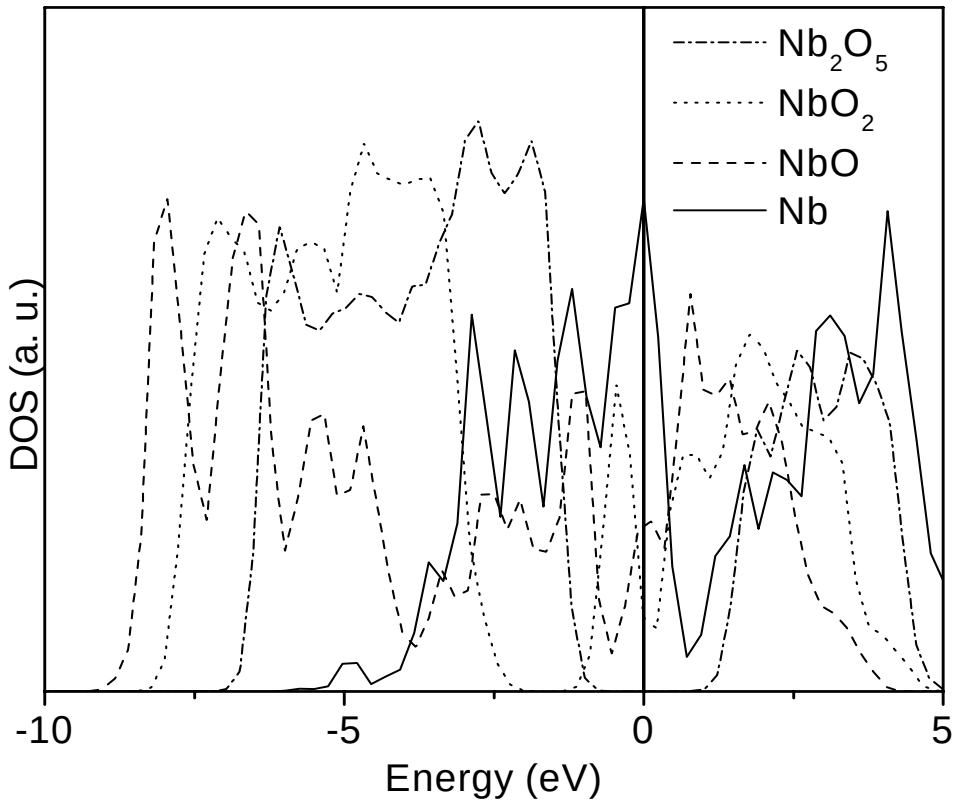

Figure 4. 4. Total DOS of Nb_2O_5, NbO_2, NbO and Nb (collaborated with J.H Wang)

4.2.2. The effect of Nb_2O_5 coating on electrochemical performances

Shown in Figure 4. 5 (a) are the power densities as a function of current density for cells of Pt/YSZ/dense Ni-YSZ with and without Nb_2O_5 coating in dry H_2 at 700 ºC. The peak power density was ~23 mW/cm^2 for the cell without Nb_2O_5 coating and ~49 mW/cm^2 for the cell with Nb_2O_5 coating on the dense Ni-YSZ anode.

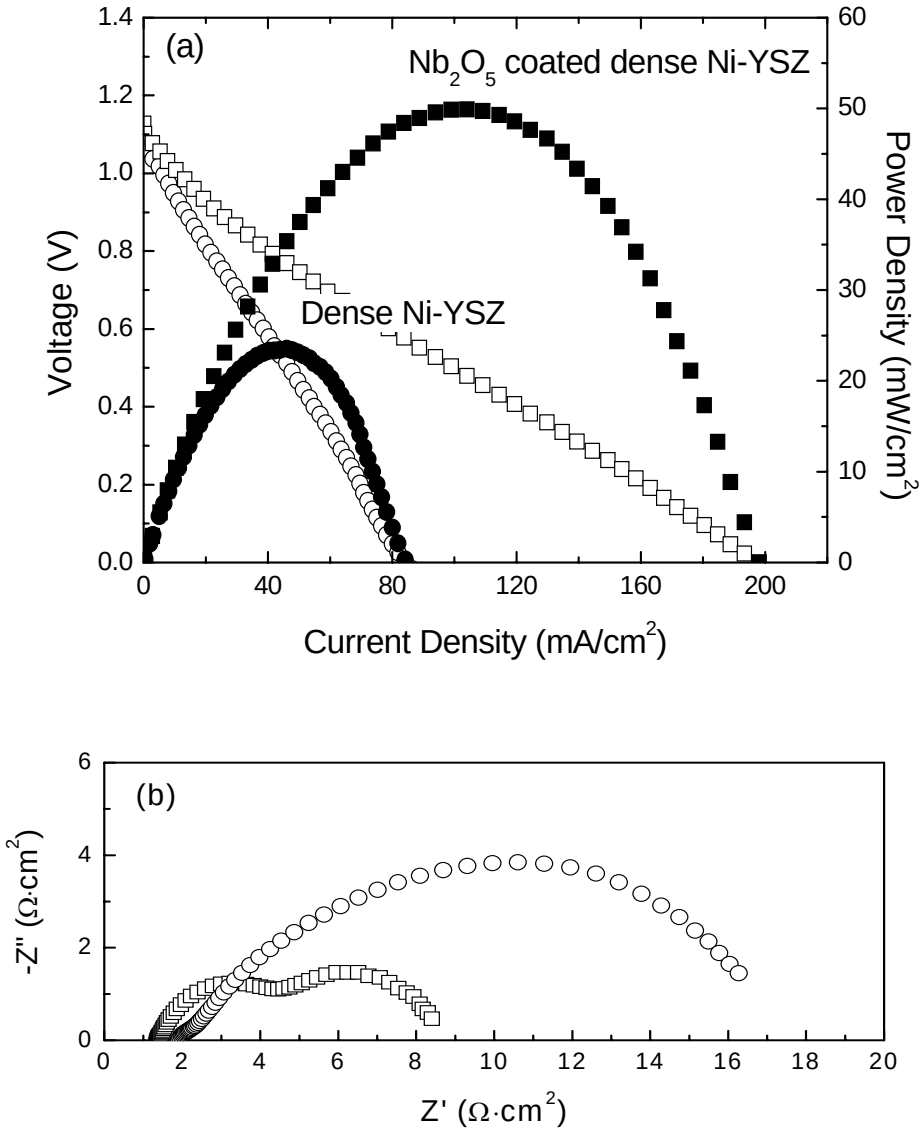

Figure 4. 5. Comparison of (a) power densities as function of current densities and (b) impedance spectra of Pt/YSZ/dense Ni-YSZ with (squares) and without (circles) Nb_2O_5 coating in dry H_2 at 700 °C

This enhancement in power output resulted from the reduced NbO_2 with high electrical conductivity under operating conditions; the conductive NbO_2 coatings may create additional triple phase boundaries for the electrochemical reactions. In addition, the good catalytic activity of niobium oxides for H_2 dissociative adsorption claimed by previous studies[14,15,16] may also attribute to the enhanced power density of Nb_2O_5 modified Ni-YSZ anode.

Shown in Figure 4. 5 (b) are the impedance spectra of the two cells, under fuel cell operating conditions. The observed increase in power density was due mainly to the decrease in the interfacial resistance from about 15 to 7 $\Omega \cdot cm^2$ because of the Nb_2O_5 coating. A small change in the bulk resistance is within the experimental variation. Thus, the conductive phases of NbO_2 are effectively contributing to the addition of triple phase boundaries to the dense Ni-YSZ anode and increase the power density.

4.2.3. Sulfur tolerance test

As the reference data for sulfur poisoning behavior of dense Ni-YSZ anode, the anode side was exposed to 50ppm H_2S without Nb_2O_5 coating. After the performance in H_2 at 700 ºC was stabilized, H_2 was switched to 50ppm H_2S as shown in Figure 4.6. As the dense Ni-YSZ was exposed to H_2S, fast degradation was observed showing ~7 % performance loss. Interestingly, the second degradation which is usually followed by the first sharp degradation in porous Ni-YSZ anode was not clearly confirmed within 36h. This may indicate that the second degradation in porous Ni-YSZ is mainly caused by structural degradation, or the degree of degradation in dense structure is limited due to small active area, compared to that of porous structure.

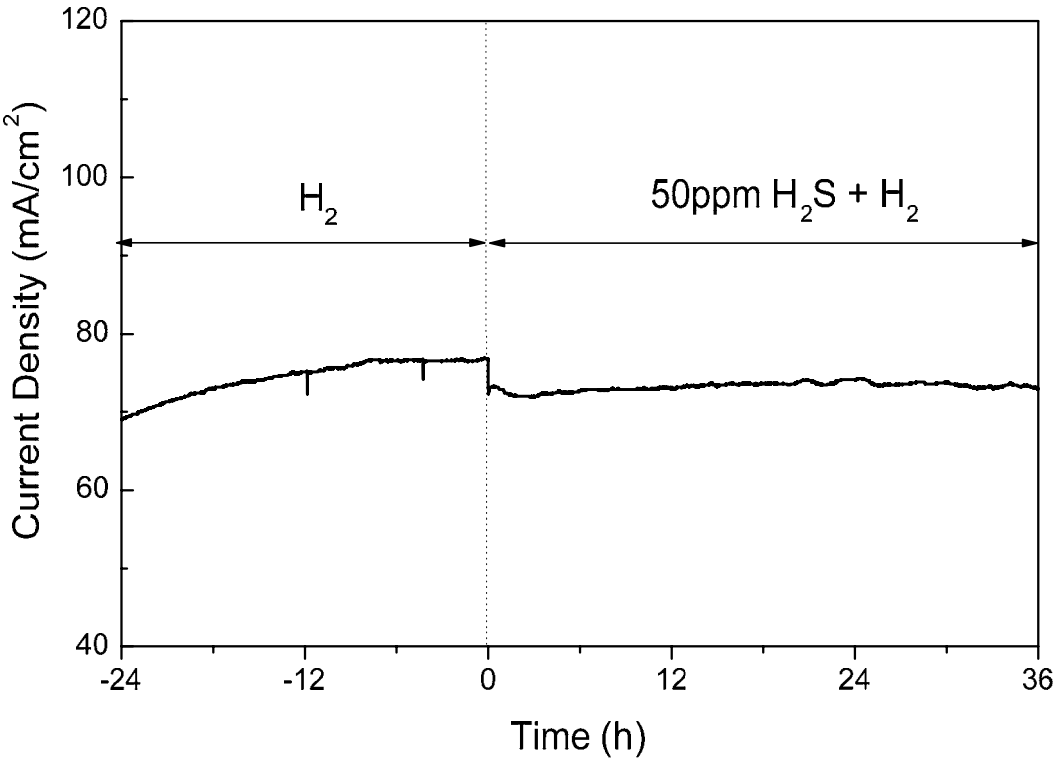

Figure 4. 6. Change of current density as a function of time of Pt/YSZ/dense Ni-YSZ without coating in dry H_2 and 50 ppm H_2S balanced with H_2 at 700 ºC after 0.5 V is applied.

Shown in Figure 4.7 is the sulfur tolerance test of Pt/YSZ/dense Ni-YSZ with Nb_2O_5 coating. The Nb_2O_5-coated Ni-YSZ anode was exposed to 50 ppm H_2S after the cell performance was stabilized in H_2 at 700 °C. The operating temperature was kept at 700 ^oC to observe significant sulfur poisoning effect[2]. The change of current density as a function of time by switching the fuel from H_2 to 50 ppm H_2S balanced with H_2 shows a slight, quick drop when H_2S was introduced, but, immediately, the current density increased slightly above the initial current density in H_2 during the exposure in 50 ppm H_2S, followed by stable performance over 12 h. There is a slight increase of current

density in 50ppm H_2S and it is achieved over about 3 h. This behavior is not well explained with given data. However, the result shows that the modified anode surface has excellent sulfur tolerance, which might correspond to the good catalytic activity for H_2S and H_2 oxidation of the surface sulfides formed on the surface of NbO_2 in low concentration of H_2S. It is apparent that the gain of current density in H_2S is attributed to the chemical surface change of NbO_2 because it is not shown in Ni-YSZ anode without surface modification. The initial slight drop of the current density as H_2S is introduced may be affected by the sulfur adsorption on active sites composed of Ni and YSZ.

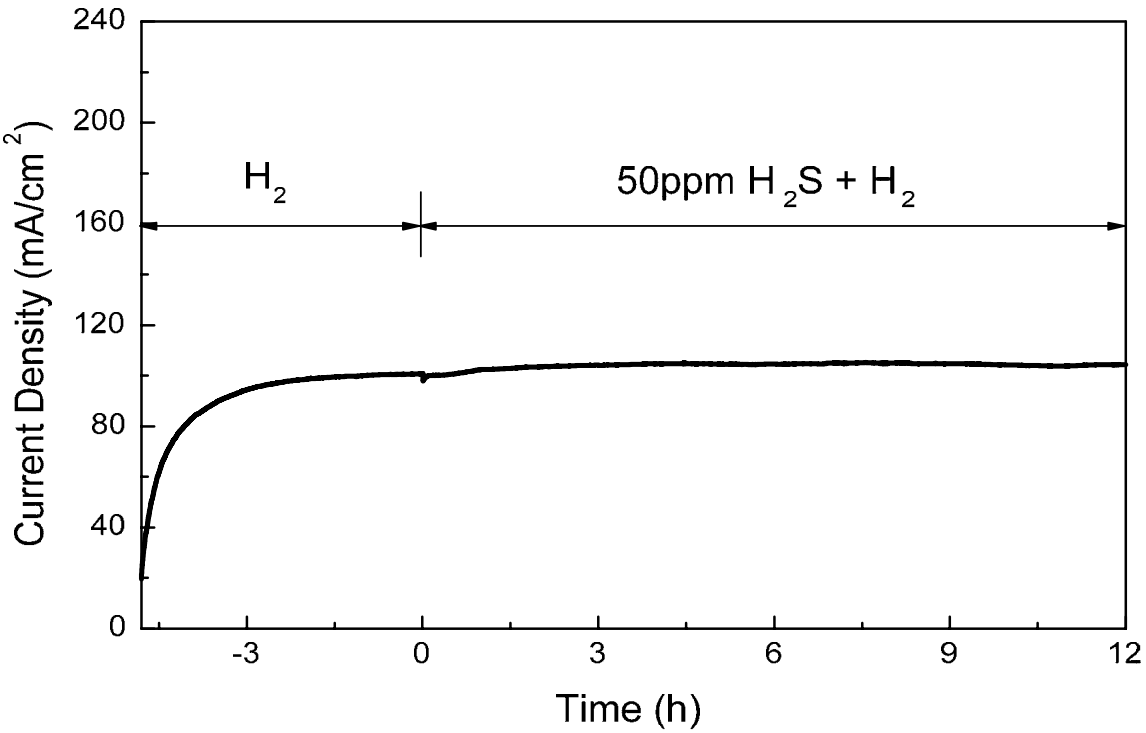

Figure 4. 7. Change of current density as a function of time of Pt/YSZ/dense Ni-YSZ with Nb_2O_5 coating in dry H_2 and 50 ppm H_2S balanced with H_2 at 700 °C after 0.5 V is applied.

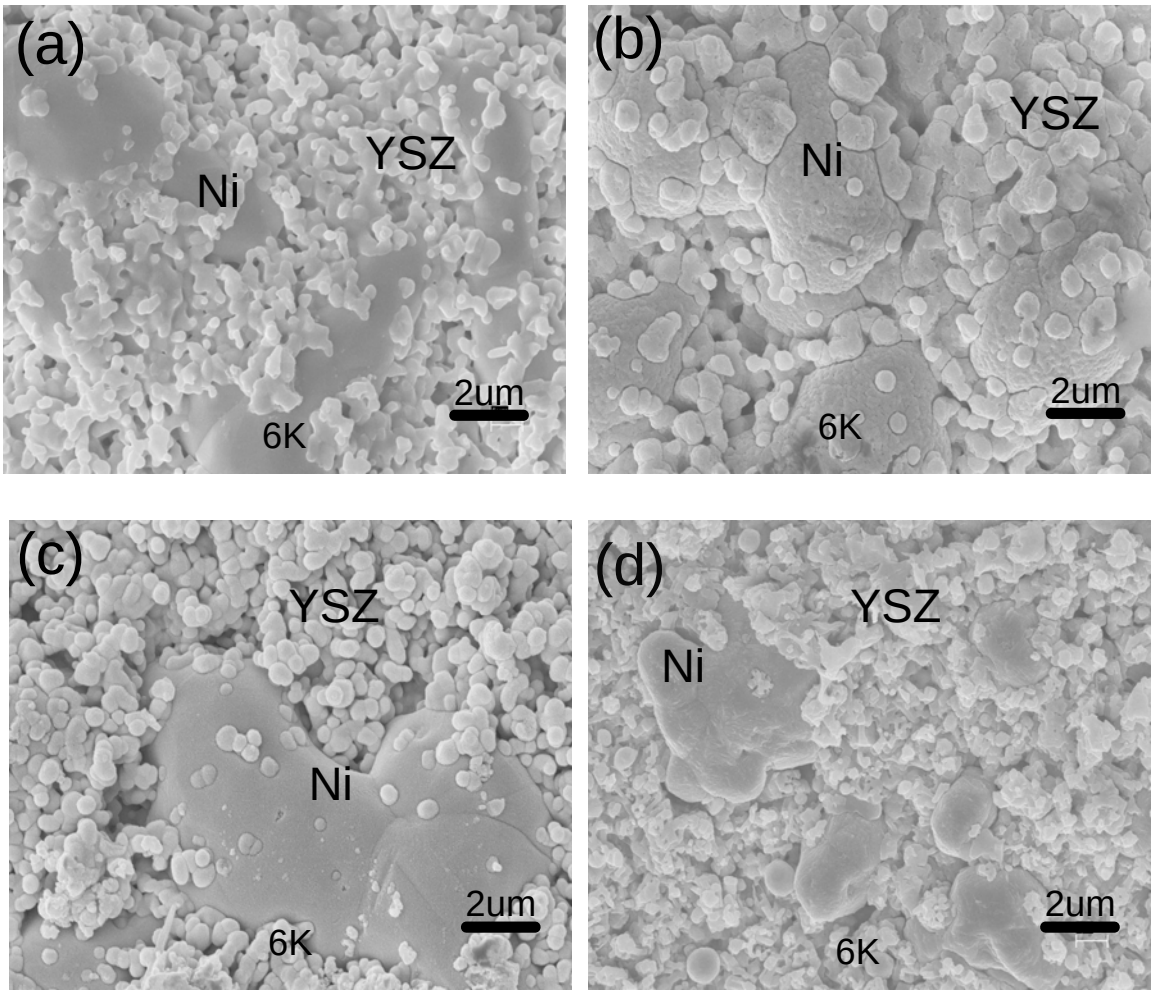

Figure 4. 8. SEM analysis of dense Ni-YSZ surfaces (a) before and (b) after Nb_2O_5 coating, and of Nb_2O_5 coated Ni-YSZ (c) after annealing in H_2 at 700ºC and (d) after sulfur tolerance tests in 50ppm H_2S balanced with H_2 at 700ºC over 15 h, respectively.

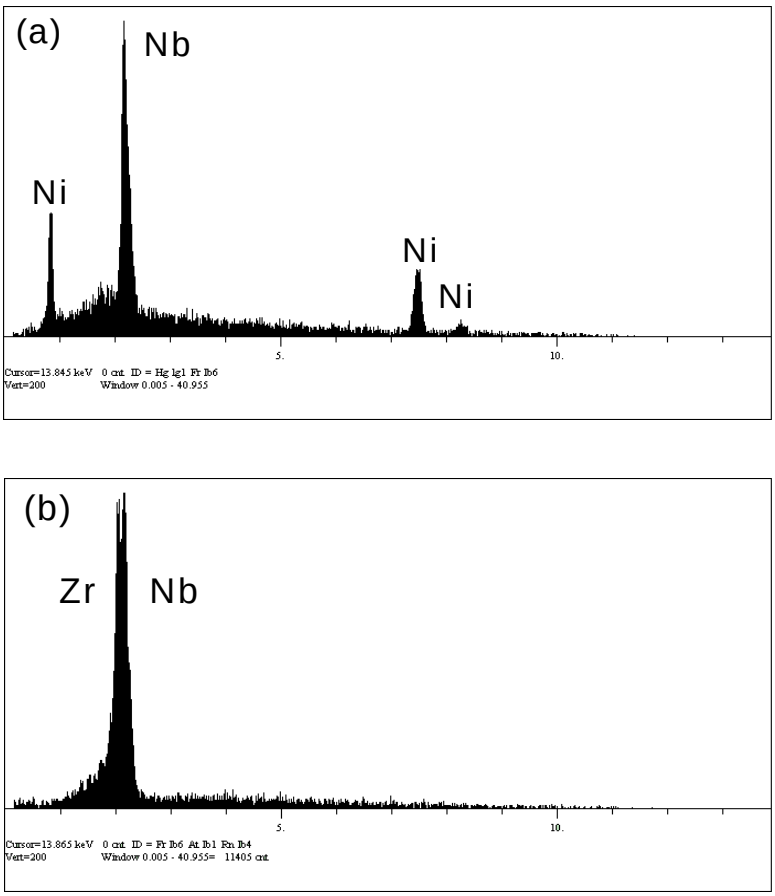

Figure 4. 9. EDS spectra from (a) Ni surface and (b)YSZ surface of dense Ni-YSZ coated with Nb_2O_5 after sulfur tolerance test in 50 ppm H_2S balanced with H_2 at 700 ^oC over 15 h

4.2.4. SEM and EDS analysis

After the anode with Nb_2O_5 coating was exposed to 50 ppm H_2S, the surface morphology and the chemical composition of the anode surfaces were investigated using SEM and EDS as shown in Figure 4.8 and 4.9, respectively. For comparison, the surfaces with Nb_2O_5 coating with (c) and without (b) annealing in H_2 were also shown in Figure 4.8. It is seen that the surface was covered with Nb_2O_5 coating in Figure 4.8 (c) and it seems that the coating layer became thin and dense after annealing in H_2, expecting the reduction of Nb_2O_5 to NbO_2. The surface morphology appeared to change after sulfur tolerance tests shown in Figure 4.8 (d) comparing with the surface before the deposition shown in Figure 4.8 (a) and (c). From EDS analysis of the surface after sulfur poisoning test, as shown in Figure 4.9, Nb was detected on the both of Ni and YSZ surfaces, indicating that the whole surface was modified, and Ni surface modification with Nb_2O_5 was maintained. However, no second phase was found after the sulfur tolerance test from XRD analysis and sulfur element which was expected after H_2S exposure was not detected using EDS as well.

4.2.5. Surface analysis

For further study on the surface change of the anode with H_2S exposure, surfaces of NbO_2 powder before, after the exposure to100ppm H_2S balanced with H_2 at 700 °C for 15 h, and after regeneration in H_2 were analyzed. Shown in Figure 4.10 is the Raman spectra, which showed that several sharp peaks indicated by * in (b) appeared after being

exposed to 100 ppm H_2S compared with the spectrum of NbO_2 in (a). These new Raman peaks, assigned from the DFT calculation and compared with previous works[17,18,19] in Table 4.1, result from the 3*R*-NbS_2 formation. The high-frequency vibration at 463 cm^{-1} and the low-frequency vibrations at 187 and 155 cm^{-1} can be attributed to NbS_2 formation as compared in the table. On the other hand, the peaks at 393 and 347 cm^{-1}, for A_1 and E vibrational modes, respectively, may be identified as the 3*R*-NbS_2 crystal phonons but they are not certain due to the duplication of peaks of NbO_2 (403, 333 cm^{-1}). Interestingly, the new peaks disappeared after exposing the powder in H_2 for 12 h indicating that the new phase was decomposed as shown in Figure 4.10 (c).

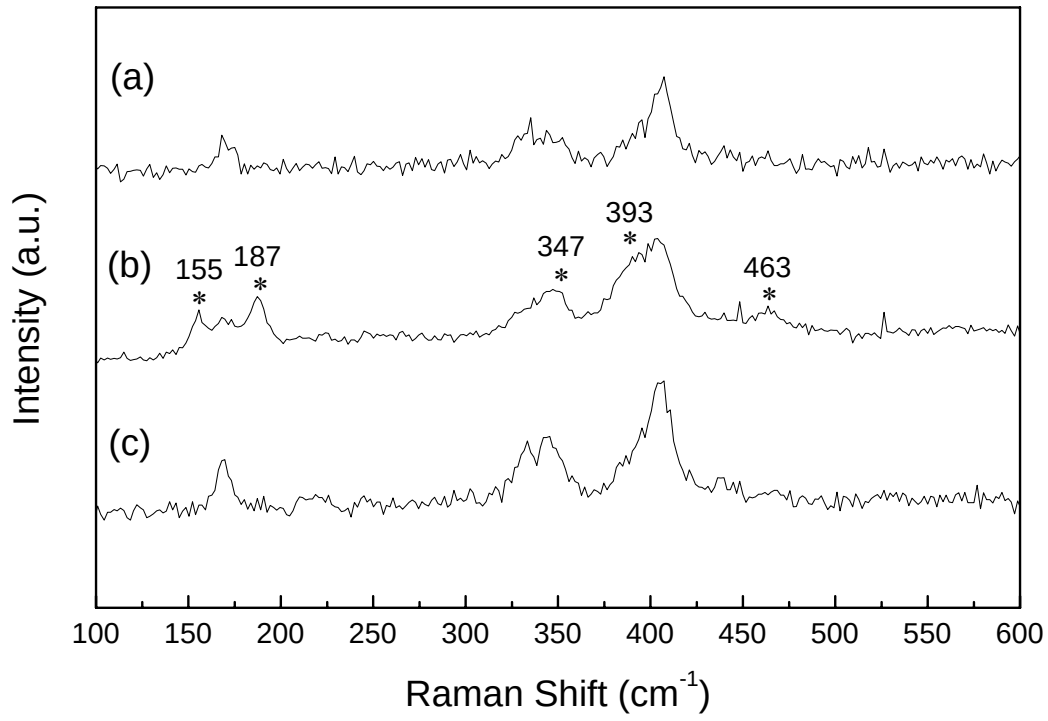

Figure 4. 10. Raman spectra of (a) NbO_2 powder after reduction in H_2 at 800 ^oC for 24 h, (b) NbO_2 powder after being exposed to 100 ppm H_2S balanced with H_2 at 700 ^oC for 15 h, and (c) Nb_2O_5 powder after regeneration in H_2 at 700 ^oC for 15 h

Table 4. 1. Experimentally observed and computed Raman frequencies of NbS_2

	Modes	Experimental	Calculation	Ref.
NbS_2		467		458,[18] 462[19]
	A_1	403	394	382,[17] 386[18,19]
	E	347	349	329,[17] 330,[18] 322[19]
		187		191[19]
		155		150,[17] 158[18]

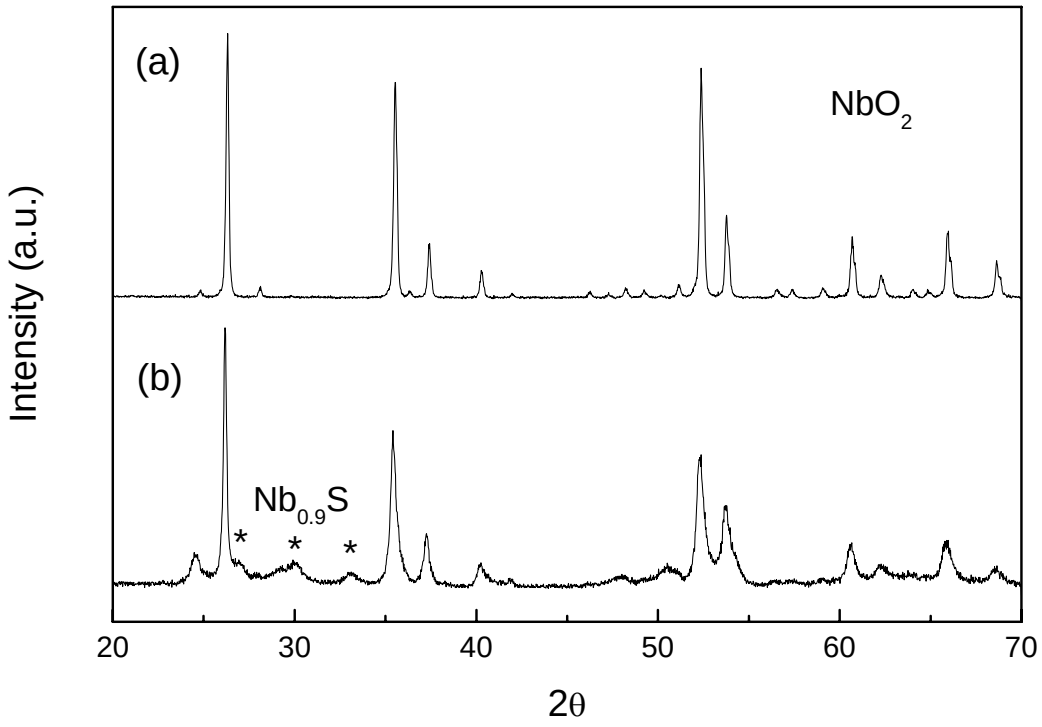

Figure 4. 11. XRD spectra of (a) NbO_2 powder after reduction in H_2 at 800 ^oC for 24 h and (b) NbO_2 powder after being exposed to 100 ppm H_2S balanced with H_2 at 700 ^oC for 15 h

Furthermore, the sulfide phase formed in 100 ppm H_2S exposure was also analyzed by the XRD, as shown in Figure 4.11. Several new peaks were found and identified as $Nb_{0.9}S$ after the exposure. In addition, some nonstoichiometric phases could be expected due to the broadness of peaks.

The different phases observed from Raman (NbS_2) and XRD ($Nb_{0.9}S$) can be attributed to the detection limits between them. Raman spectroscopy is more sensitive to the surface phases because of the limited penetration depth of visible light while XRD has much greater penetration depth, probing the bulk properties. As a result, the sulfur-rich compound (NbS_2), detected from Raman spectroscopy, is expected to appear in the top layers when H_2S directly react with the surface. The deeper layers, detected by XRD, have a Nb-rich stoichiometry because the formation depends on the bulk diffusion of sulfur atoms. In both cases, niobium sulfides were formed by the reaction of NbO_2 with H_2S on the surface. However, in the functional cell tests, no evidence of sulfide formation was identified from the modified anode surface after exposure to 50ppm H_2S, due probably to the oxidative environment in the presence of water and oxygen ions transferred from the electrolyte in a functional cell.

4.2.6. DOS analysis

The degradation of electrochemical performance corresponds to the changes of conductivity and catalytic ability of the anode materials when sulfides are formed in sulfur poisoning process. The conductivity can be attributed to the band gap calculations and the catalytic ability of H_2 oxidation corresponds to the band structure of the materials.

These intrinsic properties can be understood from the electronic structure (DOS) analysis. Shown in Figure 4.12 is the the DOS analysis of the NbO_2 (before H_2S exposure) and the possible sulfides, NbS and NbS_2, (after H_2S exposure). The results show that no obvious band gaps were found around Fermi level in the sulfides, indicating that the sulfide-covered anode is still conductive for the electrochemical reactions. In addition, comparing the DOS of the phases without (NbO_2) and with sulfur exposure (NbS and NbS_2), all of them have similar DOS distribution, indicating that the catalytic activity of the sulfides is as good as NbO_2. Thus, the DOS analysis predicts that both NbO_2 and niobium sulfides (NbS or NbS_2) should have sulfur tolerance.

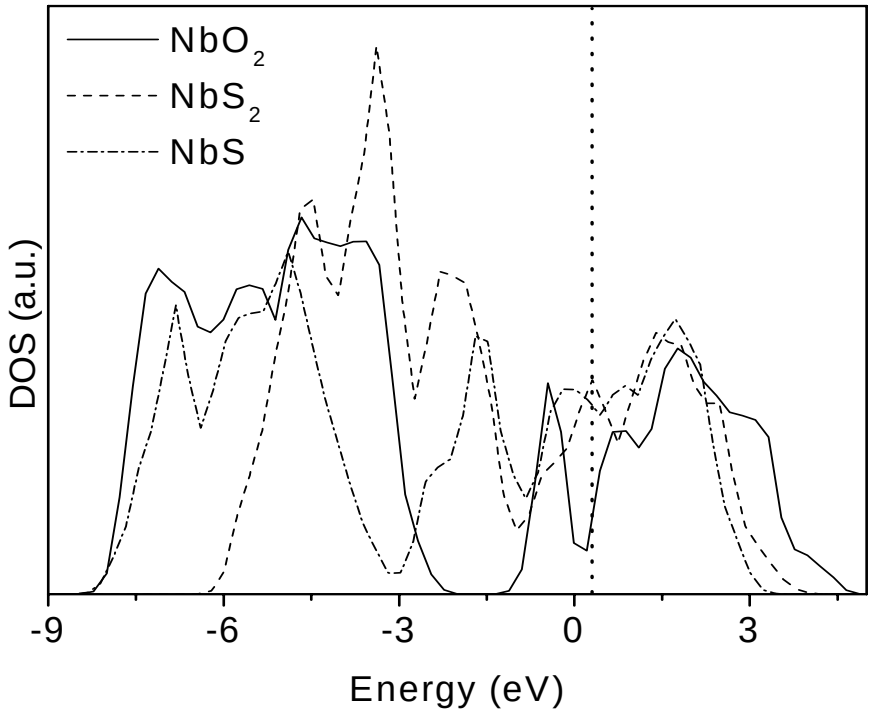

Figure 4. 12. DOS analysis of before (NbO_2) and after (NbS_2) sulfur exposure (collaborated with Dr. J.H. Wang)

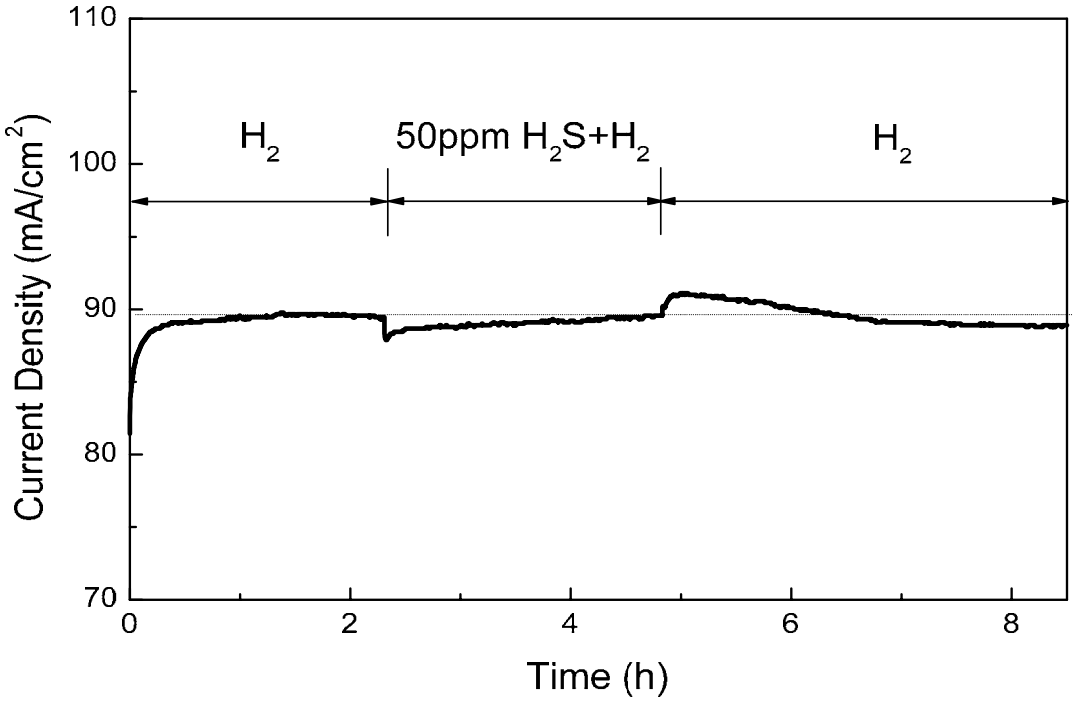

Figure 4. 13. Variation of current density depending on fuels of of Pt/YSZ/dense Ni-YSZ with Nb_2O_5 coating in dry H_2 and 50 ppm H_2S balanced with H_2 at 700 ºC after 0.5 V is applied

4.2.7. Surface regeneration

To investigate the regeneration process on the modified anode with Nb_2O_5, the current density was monitored in a short-term based test carried out at 700 ^oC with fuel transitions, from H_2 to 50 ppmH_2S with H_2 and vice versa, as shown in Figure 4.13. After the sulfur tolerance test with 50 ppm H_2S, the fuel was switched back to pure H_2 and the

current density returned to the initial value in the measurement. Similar to the result in sulfur tolerance test in Figure 4.7, the current density in Figure 4.13 shows a quick drop when H_2S is introduced and slowly increased in the following 3 h. Furthermore, in the regeneration process when 50ppm H_2S was switched to pure H_2, the current density increased abruptly and started to decrease slowly, followed by stable current density. As the assumption of the initial drop in H_2S originated from the sulfur adsorption of Ni-YSZ in the poisoning process, the abrupt increase with H_2 reintroduction in the regeneration process could be considered as the desorption of the adsorbed sulfur in the reverse reaction. The slow increase of current density in 50 ppm H_2S and slow decrease in pure H_2 can be explained by the surface changes, the formation of niobium sulfides, of NbO_2 on Ni-YSZ by the interaction with H_2S, as identified in Raman spectroscopy and XRD. The formation and decomposition of niobium sulfides can be taken into account for the slow changes. This behavior is not seen in the conventional Ni-YSZ anode, indicating that the changes of current density in H_2S can attribute to the surface modification with Nb_2O_5.

4.3. Conclusions

In this study, we demonstrated the possibility of surface modification for sulfur tolerance using dense Ni-YSZ anode coated with niobium oxide. Further, theoretical calculations were used to aid the interpretation of experimental results.

The increase in peak power density of a cell with surface modified dense Ni-YSZ was mainly originated from the decrease of the interfacial resistance after the surface modification with niobium oxide. It was also found that Nb_2O_5 was reduced to NbO_2 under upon exposure to H_2 as predicted phase diagram from Gibbs free energy calculations. The metallic behavior of NbO_2 was confirmed by conductivity measurement. These results indicate that NbO_2, the conductive phase, is further promoting the electrochemical reaction of H_2 oxidation.

In sulfur tolerance test, the current density as a function of time was stable during the exposure in 50 ppm H_2S over 12 h without showing performance degradation. The excellent sulfur tolerance of the modified anode surface can be explained by the good catalytic activity for H_2 oxidation of the surface sulfides, formed on the NbO_2 surface in low concentration of H_2S. In the DOS analysis of the NbO_2 and the possible sulfides, NbS and NbS_2, no obvious band gaps around Fermi level in the sulfides and similar DOS distribution were found, indicating that the sulfide-covered anode is still conductive for the electrochemical reactions and the catalytic ability of the sulfur-exposed anodes is as good as that of NbO_2. Thus, the sulfur tolerant behavior of Nb_2O_5 coated Ni-YSZ anode, when niobium sulfides are formed on the surface, was explained by the DOS analysis.

From the behavior of current density in fuels from H_2 to 50 ppm H_2S containing H_2 and vice versa, the slow increase of current density in 50 ppm H_2S and slow decrease in pure H_2 can be explained by the surface changes of NbO_2 on Ni-YSZ, as identified in Raman spectroscopy and XRD analyses. The formation and decomposition of niobium sulfides can be taken into account for the slow changes, and are corresponding to the Raman spectrum change before and after H_2S exposure, respectively. However, in the functional cell tests, no indication of sulfide formation was revealed from the anode surface after the exposure to 50 ppm H_2S, probably, due to limited sulfide layer in several atomic layers in more oxidative environment.

4.4. References

1. B. C. H. Steeele and A. Heinzel, Nature, **414**, 345 (2001).

2. A. Atkinson, S. Barnett, R. J. Gorte, J. T. S. Irivine, A. J. McEvoy, M. Morgensen, S. C. Singhal, and J. Vohs, Nature materials, **3**, 17 (2004).

3. M. Gong, X. Liu, J. Trembly, and C. Johnson, J. of power sources, **168**, 289 (2007).

4. S. Zha, Z. Cheng, and M. Liu, J. Electrochem. Soc., **154**, B201 (2007).

5. D. Weaver and J. Winnick, J. Electrochem. Soc., **136 (6)**, 1679 (1989).

6. Y. M. Choi, C. Compson, M. C. Lin, and M. Liu, Chem. Phys. Lett., **421**, 179 (2006).

7. Y. Matsuzaki and I. Yasuda, Solid State Ionics, **132**, 261 (2000).

8. L. Aguilar, S. Zha, Z. Cheng, J. Winnick, and M. Liu, J. of Power Sources, **135**, 17 (2004).

9. R. Mukundan, E. L. Brosha, and F. H. Garzon, Electrochem. Solid-State Lett. **7** (1), A5 (2004).

10. H. Kurokawa, L. Yang, C. P. Jacobson, L. C. D. Jonghe, and S. J. Visco, J. of power sources, **164**, 510 (2007).

11. H. Kim, J. M. Vohs, and R. J. Gorte, Chem. Commun., 2334 (2001).

12. H. He, R. J. Gorte, and J. M. Vohs, Electrochem. Solid-State Lett., **8**, A279-A280 (2005).

13. R. Elo, R. A. Swalin, and W. K. Chen, J. Phys. chem. Solids, **28**, 1625 (1967).

14. C. M. Reich, A. Kaiser, and J. T. S. Irvine, Fuel Cells, **1** (2001).

15. A. Borgschulte, J. H. Rector, B. Dam, R. Griessen, and A. Zuttel, J. of Catalysis, **235** (2), 353 (2005).

16. G. Barkhordarian, T. Klassen, and R. Bormann, Scripta Materialia, **49**, 213 (2003).

17. M. Hangyo, K. Kisoda, S. Nakashima, A. Meerschaut, and J. Rouxel, Phys. B, **219&220**, 481 (1996).

18. W. G. McMullan and J. C. Irwin, Solid State Comm., **45**, 557 (1983).

19. C. J. Carmalt, E. S. Peters, I. P. Parkin, T. D. Manning, and A. L. Hector, Eur. J. Inorg. Chem., 4470 (2004).

CHAPTER 5

SUPPRESSION OF CARBON FORMATION ON ANODE FOR DIRECT HYDROCARBON

Abstract

It is demonstrated that carbon formation can be suppressed with niobium oxide coating on dense Ni-YSZ in humidified CH_4 (3% H_2O) at 850ºC. Raman spectroscopy indicates that carbon was not formed on the surface of an anode under active operation due probably to rapid electrochemical oxidation of carbon. In addition, stable performance of functional cells consisting of Pt/YSZ/Nb_2O_5 coated dense Ni-YSZ in the fuel was achieved; performance degradation due to carbon formation was not observed. The results suggest that the catalytic cracking of CH_4 is not enhanced by a niobium oxide coating and carbon formed on the surface can be electrochemically oxidized on niobium oxide coated Ni-YSZ. However, when humidified C_3H_8 was used as the fuel, fuel cell performance decreased gradually with exposure time due to carbon deposition.

5.1. Introduction

One of the unique advantages of SOFCs over other types of fuel cells is the possibility of direct utilization of hydrocarbon fuels (e.g., methane, propane, and butane) through internal reforming in SOFCs.[1,2] Hydrocarbon fuels are already used for vehicles and for heating homes, so the existing production and distribution system can be more readily expanded for SOFC use also.[3]

However, one critical challenge to overcome is carbon deposition on the anode in order to be successful in direct utilization of hydrocarbon fuels.[4] Currently, a Ni-YSZ cermet is the most commonly used anode material.[5] While Ni has good catalytic activity for hydrogen oxidation, it also acts as a catalyst for carbon formation upon exposure to hydrocarbon fuels.[6,7,8] The carbon formation on Ni will not only degrades the performance of the cell by covering the electrochemically active sites at the anode but also lead to metal dusting, a catastrophic destruction to the anode. Therefore, the prevention of carbon deposition represents a vital challenge for the direct use of hydrocarbon fuels in a SOFC.[9]

To date, two approaches have been introduced to solve the problem of carbon deposition. One is the introduction of a new material which is inactive to carbon formation in the presence of hydrocarbon fuels. Recently, it has been demonstrated that Cu could be a potential alternative to Ni in the anode by suppressing carbon deposition when various hydrocarbon fuels are used.[10] The other solution is to achieve the pre-reformation of a hydrocarbon fuel by introducing an additional pre-reforming layer using highly catalytic materials[11] or the dispersion of a reforming catalyst in the anode.[12,13,14]

In this chapter, the results on carbon-tolerant materials are reported. Dense Ni-YSZ electrodes coated with a thin layer of Nb_2O_5 were prepared and studied in humidified CH_4 and C_3H_8. A dense structure was used to minimize experimental uncertainties; a modified porous anode with irregular coating would be difficult to characterize. In order to quantify the effect of carbon suppression by Nb_2O_5 coating on Ni-YSZ, the electrode surfaces after chemical exposures and electrochemical tests were analyzed using Raman spectroscopy and SEM. Electrochemical characterizations of Nb_2O_5 coated Ni-YSZ anode was also carried out in CH_4 and C_3H_8.

5.2. Results and Discussion

5.2.1. Carbon formation during chemical exposure to wet CH_4

It is known that the carbon formation on Ni, a good catalyst for cracking hydrocarbons such as CH_4,[15] involves the following reactions :

$$CH_4 = C + 2H_2 \quad \text{or}$$

$$CH_4 + H_2O = CO + 3H_2 , \qquad 2CO = C + CO_2$$

Shown in Figure 5.1 are the surface views of Ni anodes before and after exposure to humidified CH_4 at 850ºC for 12h. A thick fibrous layer of carbon was formed on Ni surface.

However, no carbon was detected by XRD analysis. Shown in Figures 5.2 (a) and (b) are the Raman spectra collected from the Ni-YSZ surfaces before and after exposure to humidified CH_4, respectively. The strong Raman peaks near 1350 cm^{-1} and 1605 cm^{-1} are indicative of the 'D' and 'G' bands of an amorphous or highly defective carbon. The high relative intensity of the D-band peak with respect to the G-band peak reflects the amorphous nature of the deposited carbon, and explains why it was not detectable by XRD. Thus, a Ni-YSZ anode is expected to be poisoned by carbon formation in CH_4 containing low concentration of H_2O (3 vol%) at 850°C.

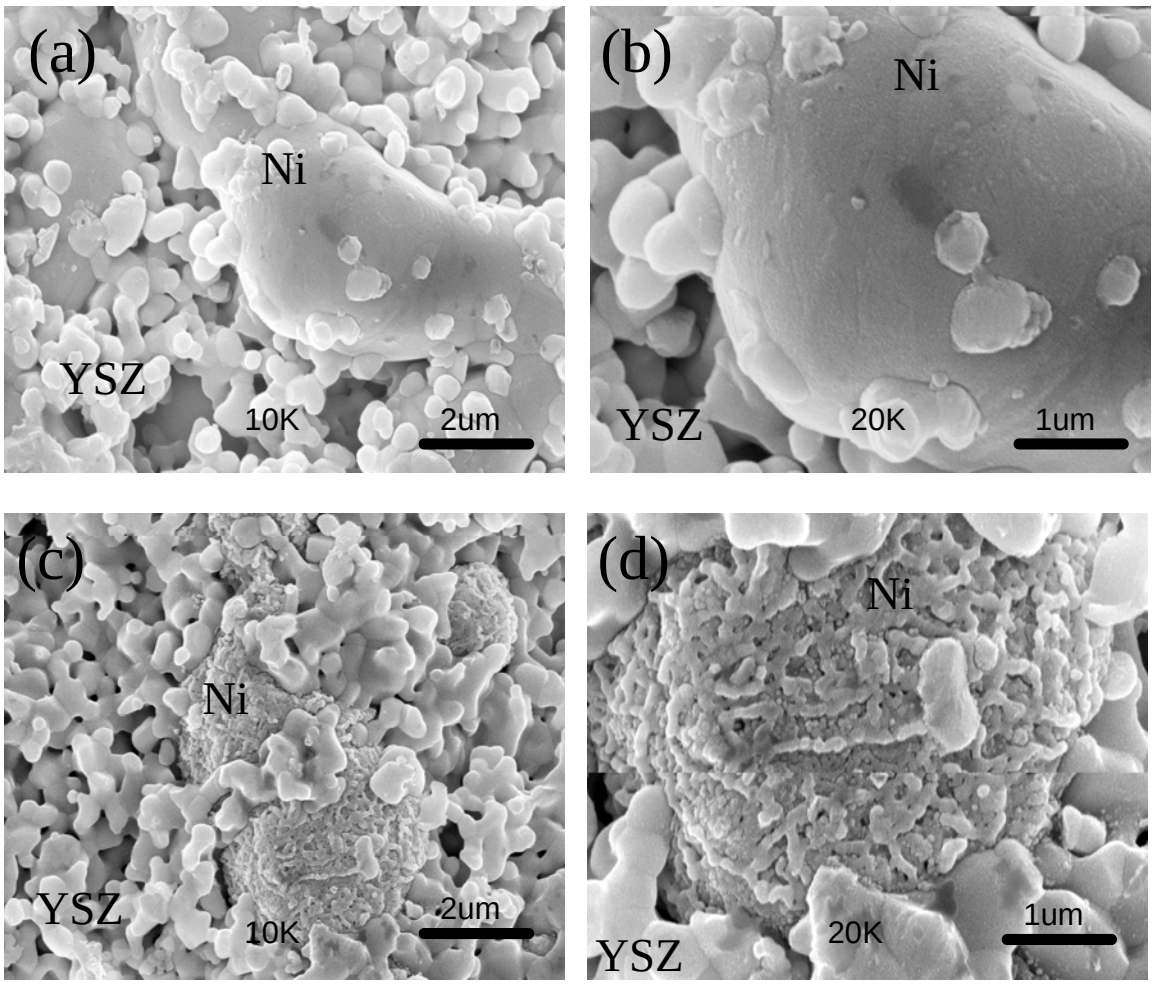

Figure 5. 1. SEM images of Ni-YSZ surfaces (a ,b) before and (c, d) after exposure to CH_4 (3% H_2O) at 850°C for 12h without electrical polarization.

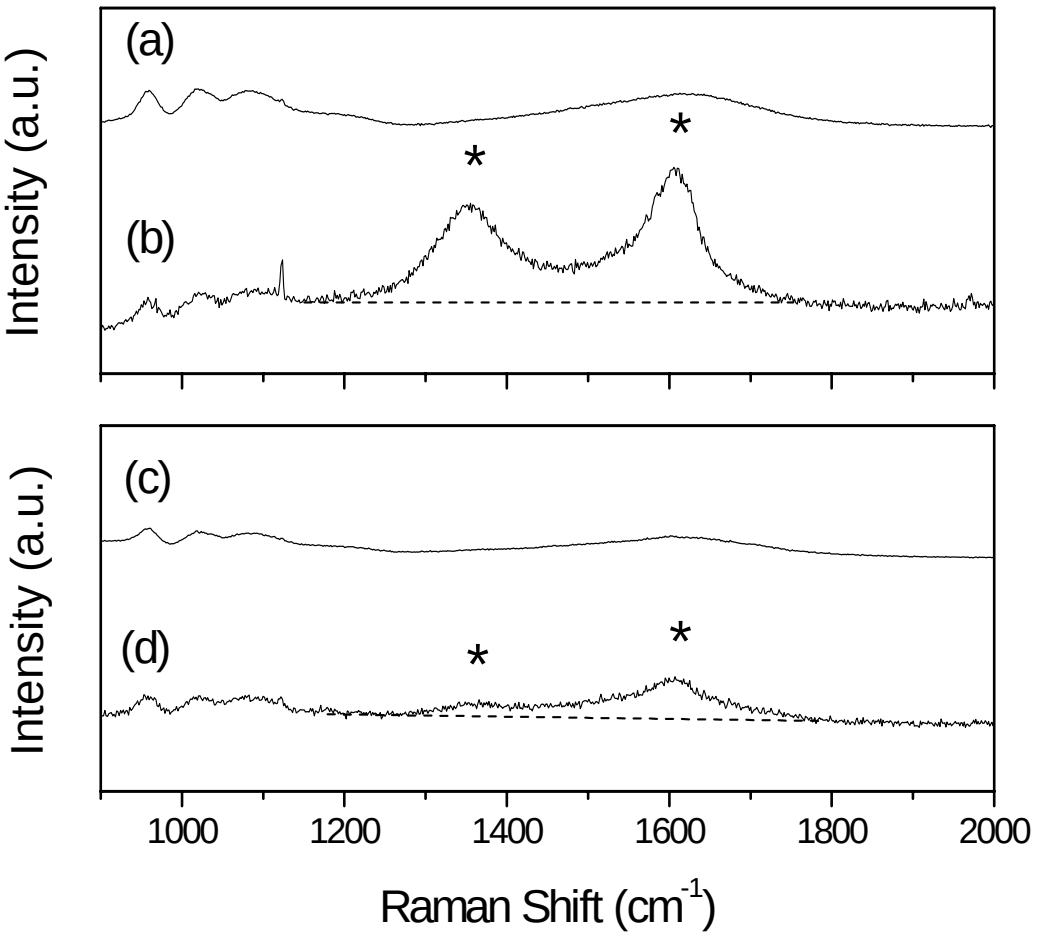

Figure 5. 2. Typical Raman spectra of Ni-YSZ surfaces (a,b) and of Nb_2O_5 coated Ni-YSZ surfaces (c,d) before [(a) and (c)] and after [(b) and (d)] exposure to CH_4 (3% H_2O) at 850°C for 12h without electrical polarization.

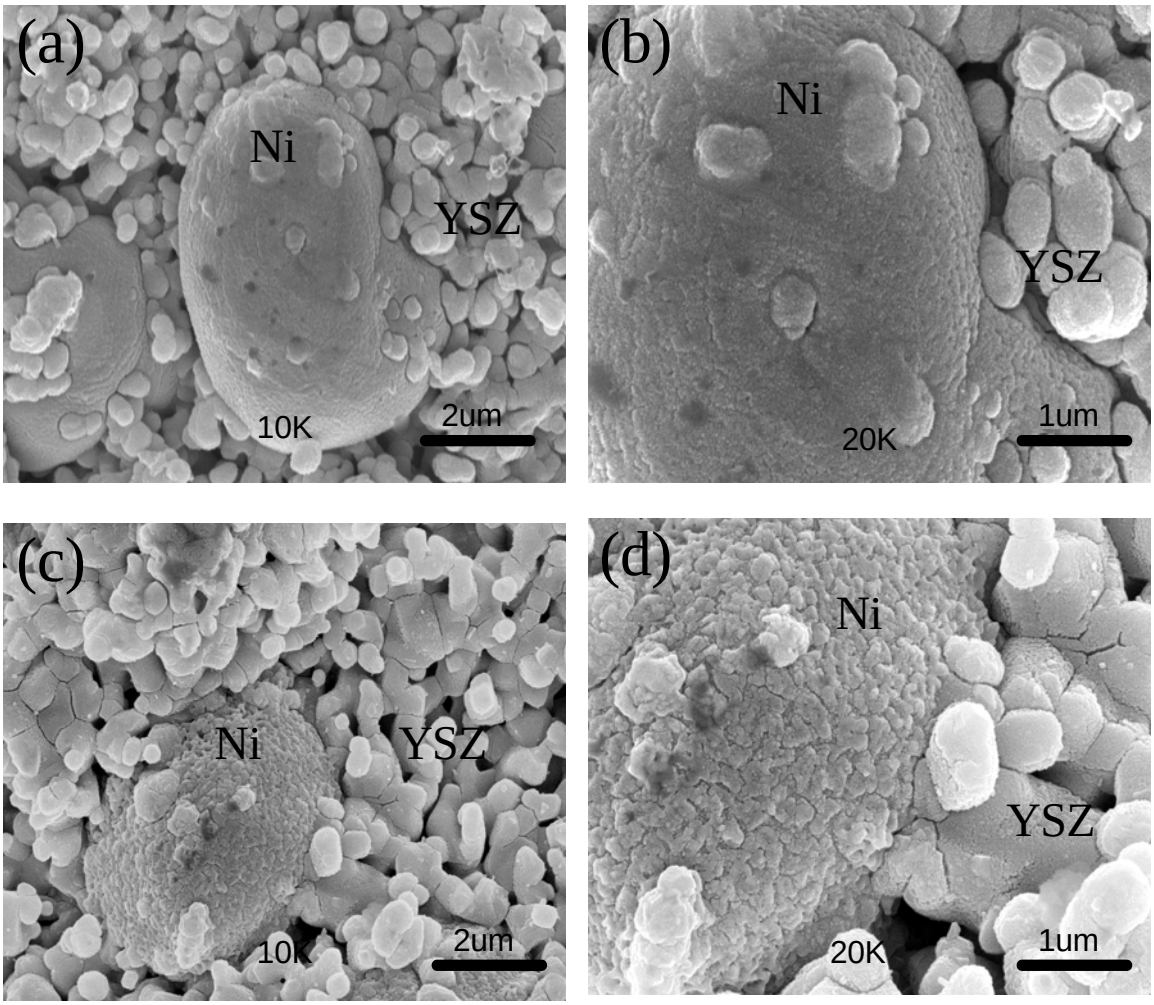

Figure 5. 3. SEM images of Nb_2O_5 coated Ni-YSZ surfaces (a, b) before and (c, d) after exposure to CH_4 (3% H_2O) at 850°C for 12h without electrical polarization.

To investigate any possible suppression of carbon formation using surface modification of Ni-YSZ with niobium oxide, the morphology changes of the coated Ni surfaces were also compared after exposure to humidified CH_4.

Figures 5.3 (a) and (b) show the surface views of a Nb_2O_5-coated Ni-YSZ anode annealed at 850°C in 4%H_2. The whole Ni-YSZ surface was coated by niobium oxide, compared with the clean Ni-YSZ surface in Figures 5.1 (a) and (b). After exposure to wet CH_4 the surface shown in Figures 5.3 (c) and (d) appeared rougher, and the grains on the Ni surface coarsened. Unlike the pictures for the Ni-YSZ surface exposed to humidified CH_4 (Figures 5.1 (c) and (d)), the modified Ni surface does not have fibrous morphology. Incidentally, the intensities of the Raman peaks near 1350 cm^{-1} and 1605 cm^{-1} shown in Figure 5.2 (d) were dramatically reduced for the Nb_2O_5-coated sample, a quantitative indication that carbon deposition was decreased by the niobium oxide coating. While carbon formation was suppressed, it was not eliminated.

Therefore, the probability of CH_4 cracking was significantly reduced by the niobium oxide. The small carbon peaks observed in the Raman spectrum of niobium oxide coated Ni-YSZ, as shown in Figure 5.2 (d), however indicate that some carbon formation was still there due probably to thermal decomposition of hydrocarbons (CH_4).

5.2.2. Electrochemical characterizations in CH_4

Current-voltage relationships for functional cells consisting of Pt/YSZ/Nb_2O_5-coated Ni-YSZ were measured in dry H_2 and humidified CH_4 at 800°C and 850°C, respectively, as shown in Figures 5.4 (a) and (b). The cells were initially tested in dry H_2.

Upon exposure to H_2, Nb_2O_5 was fully reduced to NbO_2 or NbO, the actual active phases under the operating conditions areas described in chapter 4.[16]

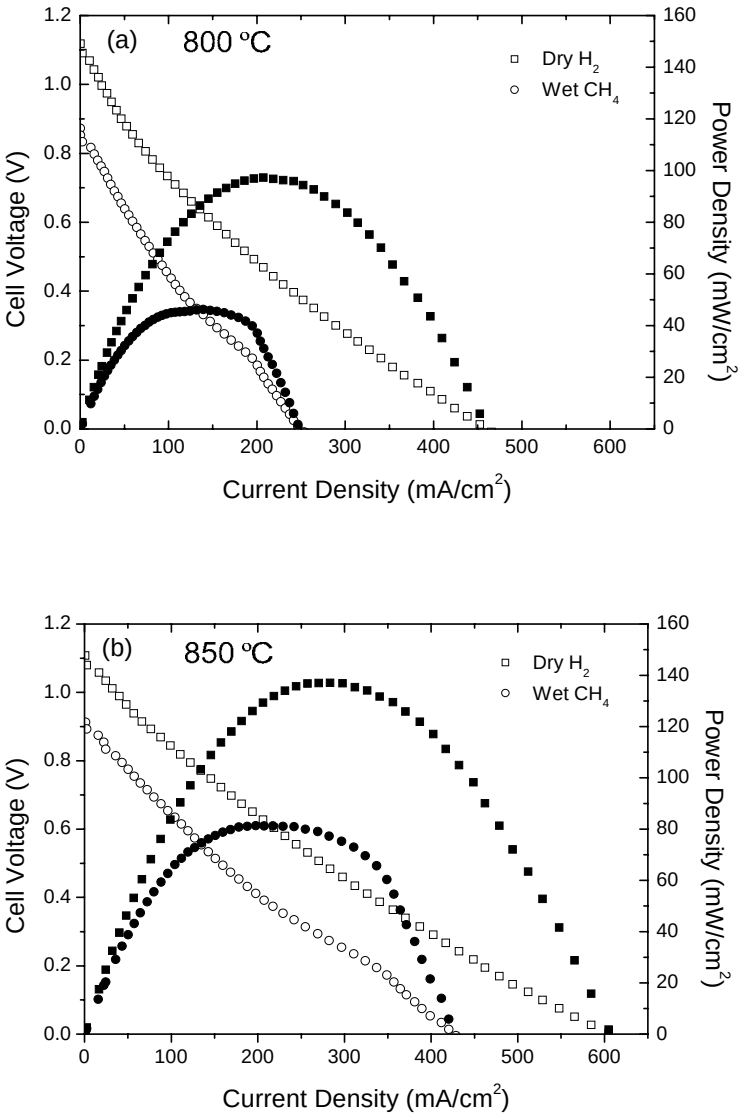

Figure 5. 4. Cell voltage and power density as a function of current density of Pt/YSZ/Nb_2O_5 coated Ni-YSZ cells measured in dry H_2 and CH_4 (3% H_2O) at (a) 800°C and (b) 850°C.

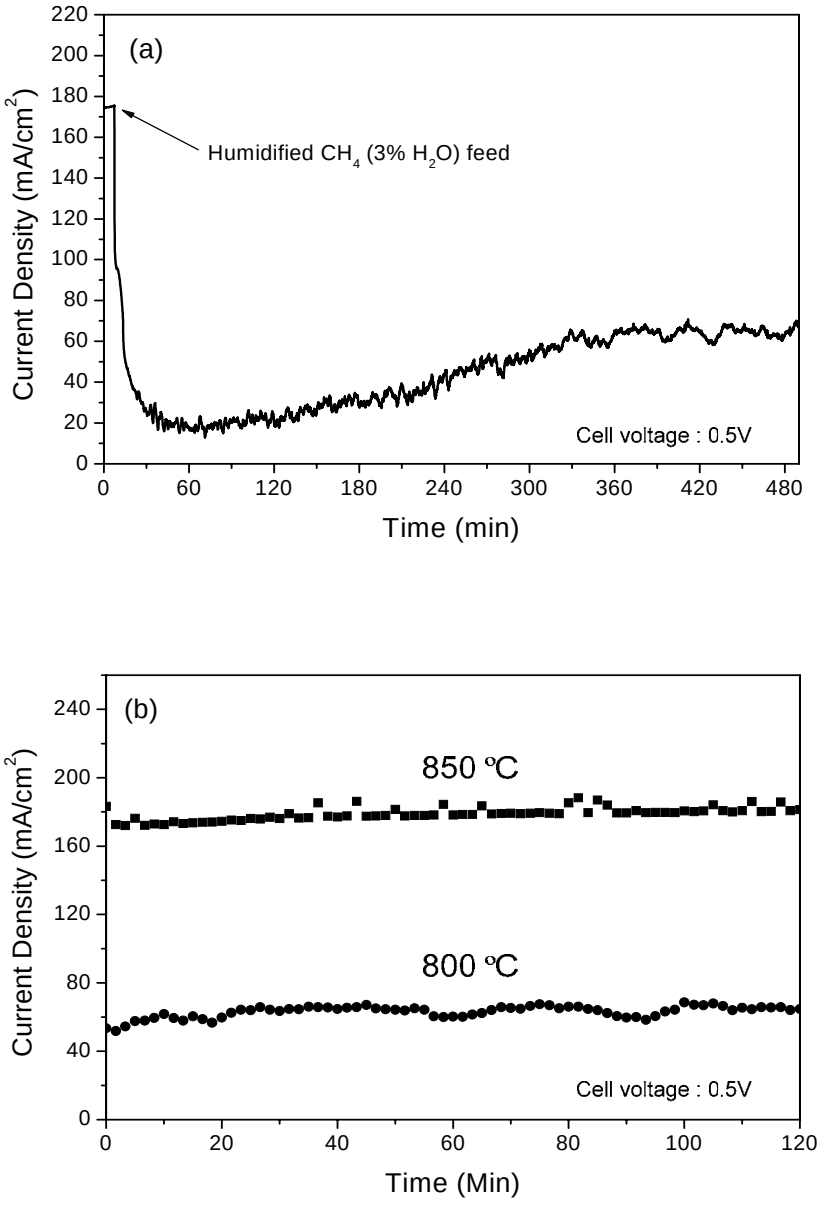

Figure 5. 5. (a) Variation of current density for a cell of Pt/YSZ/Nb_2O_5 coated Ni-YSZ after the fuel was switched from dry H_2 to CH_4 (3%H_2O) at 800ºC and (b) the stability of current densities in CH_4 at a cell voltage of 0.5V

As the fuel was switched from H_2 to CH_4, the peak power densities of the cells were lowered to ~46mW/cm^2 and ~81mW/cm^2 at 800ºC and 850ºC, respectively. The open circuit voltages(OCV) were 0.87V and 0.91V at 800°C and 850ºC, respectively, indicating that oxygen partial pressure was increased by cracking products and small amount of steam reforming of humidified CH_4 such as CO, CO_2 or H_2O. The steam reforming involves the following reaction:

$$CH_4 + H_2O = CO + 3H_2$$

The relatively low OCV also suggest that the direct oxidation of CH_4 on niobium oxide coated Ni-YSZ doesn't seem significant under the testing conditions.[17]

Shown in Figure 5.5 (a) is the change in current density of a cell with a cell voltage of 0.5V. The current density decreased dramatically as the fuel was switched from H_2 to humidified CH_4 stabilized after about 1 h exposure. As shown in Figure 5.5 (b), current densities stabilized over a longer exposure time to CH_4 at 800ºC and 850ºC, indicating that performance degradation due to severe carbon formation can be managed by the niobium oxide coating. In contrast, in the case of Ni-YSZ anode without Nb_2O_5 coating, the current density went to zero within an hour of fuel cell operation, indicating that the active sites severely poisoned by carbon deposition.

Figure 5.6 shows an image of the surface after an electrochemical test in humidified CH_4. The surface appears rough but similar to the surface morphologies seen in Figures 5.3 (a) and (b).

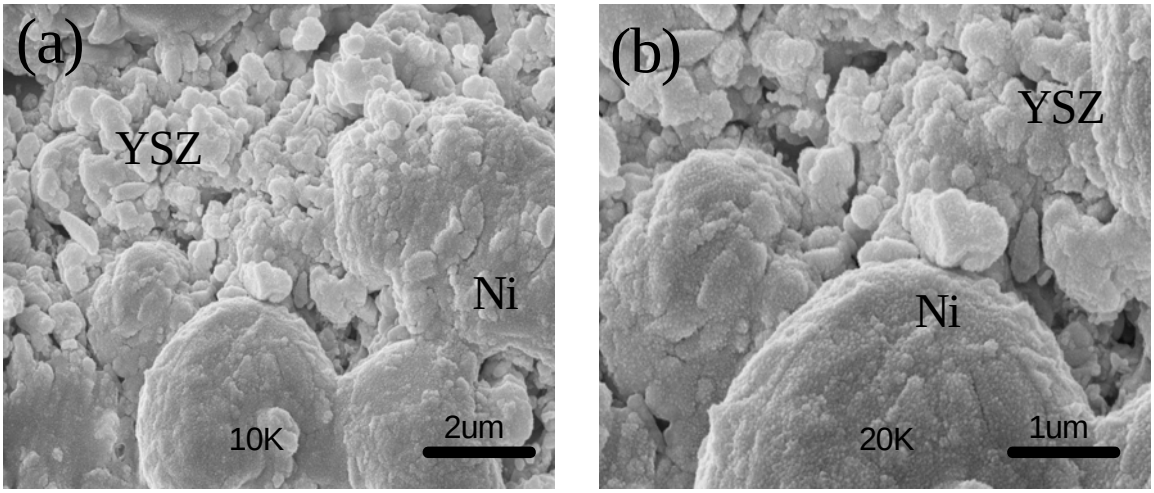

Figure 5. 6. SEM image of Nb_2O_5 coated Ni-YSZ surface after electrochemical tests in CH_4 (3% H_2O) at 850°C over 12 h

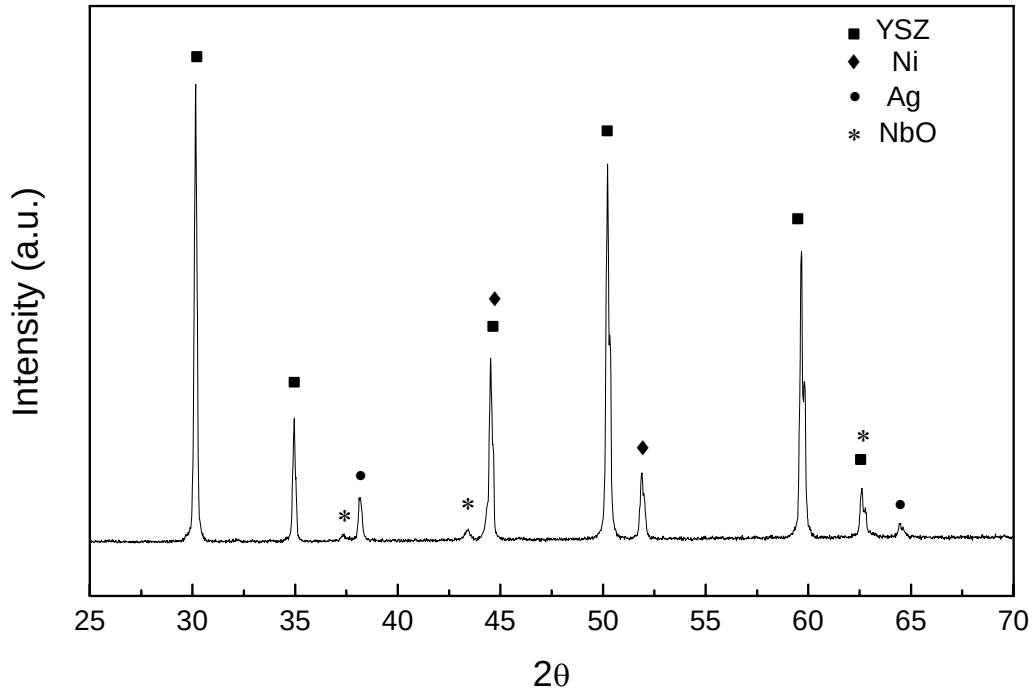

Figure 5. 7. XRD analysis of Nb_2O_5 coated Ni-YSZ surface after electrochemical tests in CH_4 (3% H_2O) at 850°C over 12 h

XRD peaks from NbO are observable in Figure 5.7, indicating that Nb_2O_5 was reduced by dry H_2 at 850ºC. The typical peaks from Ni and YSZ were also seen in the XRD pattern. The Ag in the pattern was from some residue of the current collector. There was no indication of niobium carbide formation[18,19] from the XRD result, indicating that niobium carbide did not form under the operating conditions, probably due to slight oxygen partial pressure in the humidified CH_4. In addition, no crystalline carbon such as graphite was observed as the one chemically exposed to humidified CH_4.

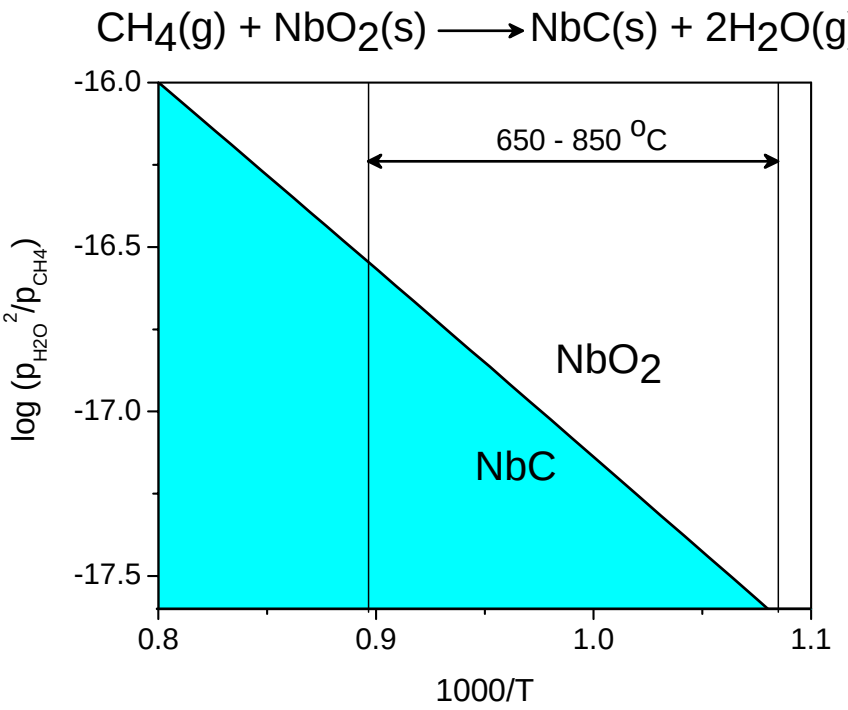

Figure 5. 8. Phase diagram of NbO_2 –NbC (collaborated with Dr. J.H. Wang)

Even though small peaks corresponding to NbO were observable from the XRD analysis, dominating phase of niobium oxide is NbO_2, considering thermodynamic calculations of Nb-O phase diagram described in the previous work[16] in the oxygen partial pressure under the operating conditions. Thus the possibility of NbC formation under the operating conditions is also verified from the computational predictions based on the reaction of surface NbO_2 with CH_4. Shown in the Figure 5.8 is the predicted phase diagram of NbC-NbO_2 systems from Gibbs free energy calculations.

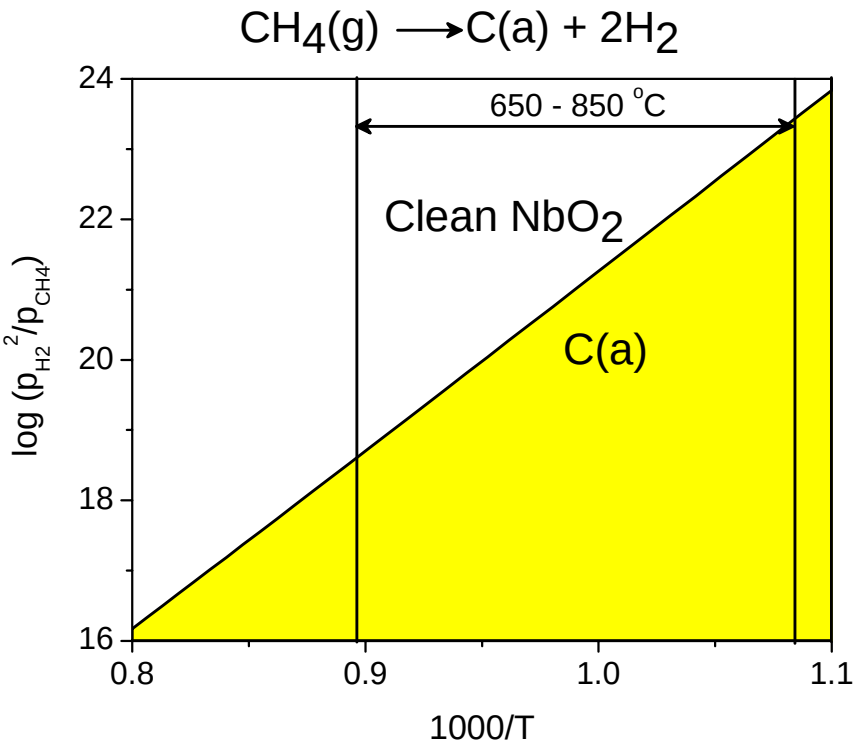

Figure 5. 9. Phase diagram of NbO_2-C (collaborated with Dr. J.H. Wang)

For temperature effect, NbO_2 phase will transform to NbC phase as temperature increases since the reaction of $CH_4(g) + NbO_2(s) \rightarrow NbC(s) + 2H_2O$ is exothermic. For

the pressure effect, lower pressure ratio of (p_{H2O}/p_{CH4}) with more carbon sources will induce more NbC formation. Under the current experimental conditions at 850 ^{o}C with 3 vol% H_2O, which is in further up of the predicted phase diagram, the NbO_2 surface will remain the same phase and seems intact when exposed to methane fuel.

In addition, the C(a) adsorption phase was also considered in this system, as shown in the Figure 5.9. The most stable NbO_2(010) surface is modeled and the most stable C(a) adsorption on surface Nb site is considered in the phase diagram calculation. Since the adsorption process, CH_4(g) + NbO_2(010) → C-NbO_2(010) + 2 H_2(g), is an exsothermic process, C(a) adsorption phase is easier to form at lower temperature.

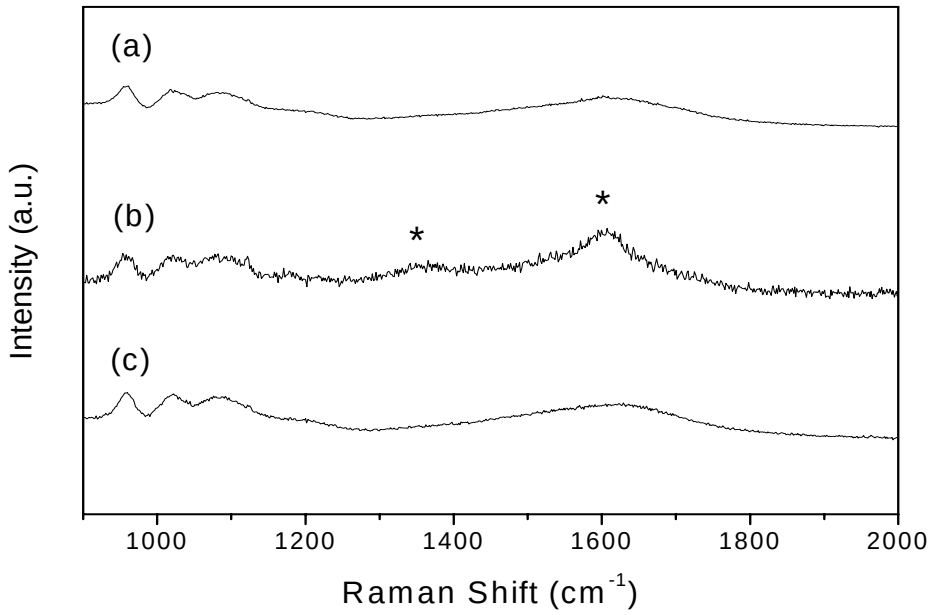

Figure 5. 10. Comparison of Raman spectrum of Nb_2O_5 coated Ni-YSZ surfaces (a) before and (b) after chemical exposure to CH_4 (3%H_2O) at 800°C for 12h without electrical polarization, and (c) after electrochemical tests in CH_4 at 850°C over 12h

The surfaces after electrochemical tests were analyzed using Raman spectroscopy as shown in Figure 5.10. The broad peak around 1630 cm^{-1} originates from YSZ. As compared with the surface exposed to humidified CH_4 without electrical polarization indicated by (b), the carbon peaks around 1350 cm^{-1} and 1605 cm^{-1} were not detected after electrochemical tests. The Raman spectrum (c) matches that of the unexposed niobium oxide-coated Ni-YSZ surface. No detectable amount of carbon was formed on the surface during electrochemical operation of the cell exposed to CH_4. Thus, these results suggest that not only the carbon formation due to catalytic cracking of CH_4 is suppressed by the niobium oxide coating but also the small amount of carbon formed on the surface can be electrochemically oxidized during normal SOFC operation.

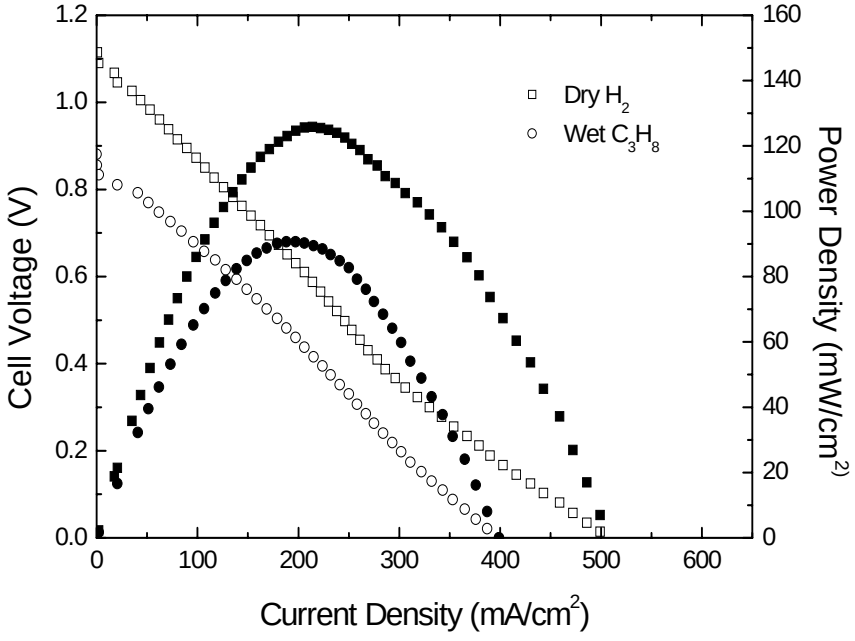

Figure 5. 11. Cell voltage and power density as a function of current density of Pt/YSZ/Nb_2O_5 coated Ni-YSZ cells measured in dry H_2 and C_3H_8 (3% H_2O) at 850°C

5.2.3. Electrochemical characterization in C_3H_8

The Nb_2O_5-coated Ni-YSZ was also exposed to C_3H_8, which has a higher carbon-to hydrogen ratio. Shown in Figure 5.11 is the cell voltage and power density as a function of current density of a functional cell when dry H_2 and wet C_3H_8 (3%H_2O) were used as the fuel at 850ºC. The peak power density in C_3H_8 was ~90 mW/cm^2, showing smaller drop of performance by switching fuel from H_2 to C_3H_8 at 850 ºC, compared to the performance change in CH_4 shown in Figure 5.4. This indicates that H_2 generation from C_3H_8 is easier because the higher hydrocarbons tend to crack at lower operating temperatures.[17]

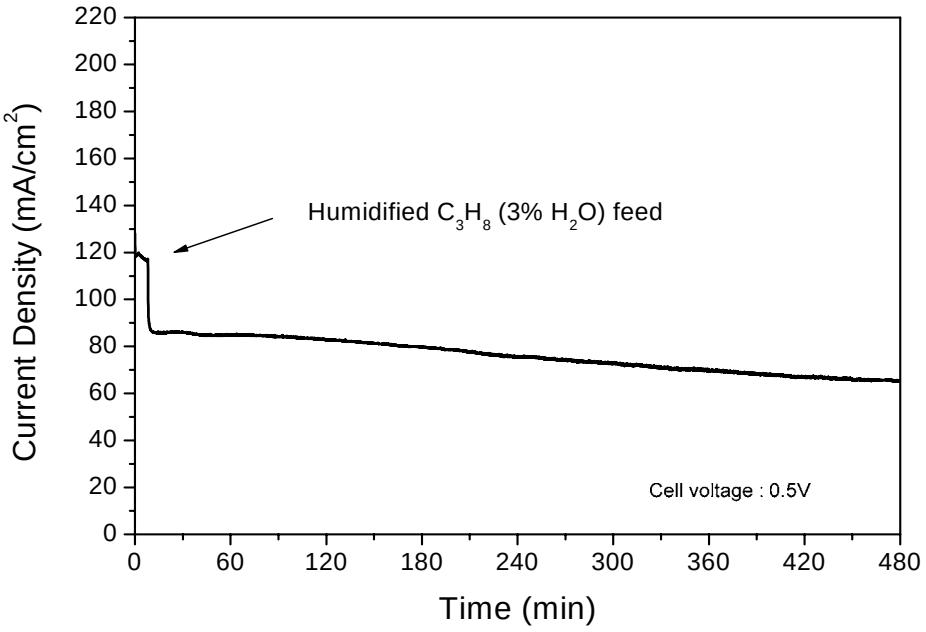

Figure 5. 12. (a) Variation of current density of a cell with configuration of Pt/YSZ/Nb_2O_5 coated Ni-YSZ as the fuel was switched from dry H_2 to C_3H_8 (3%H_2O) at 800ºC

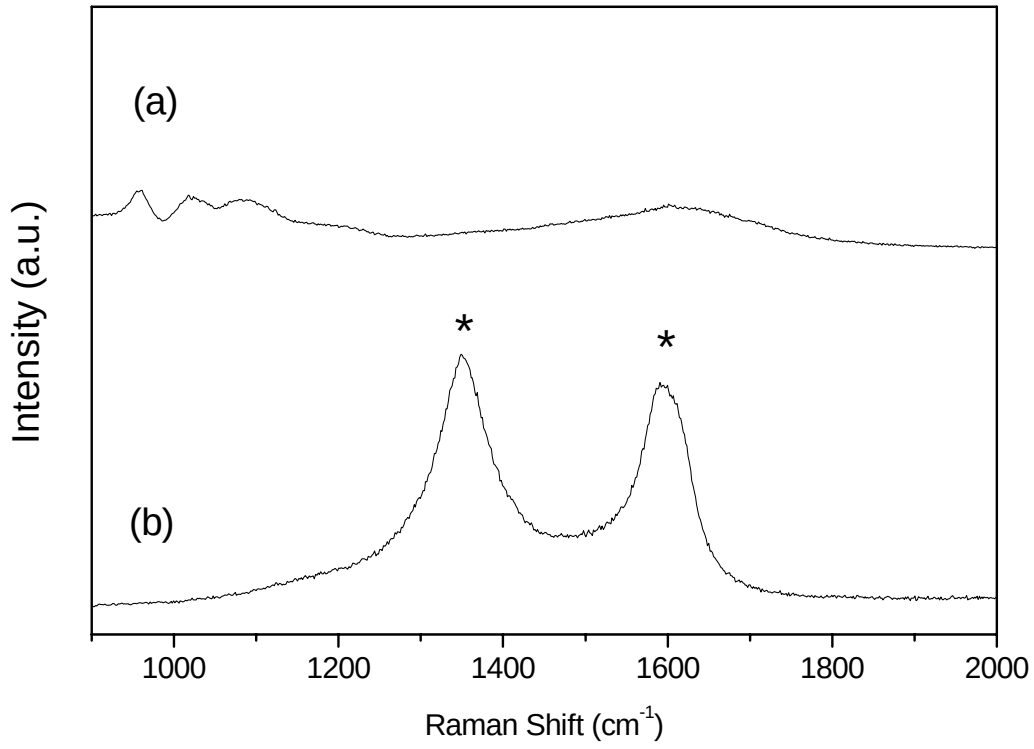

Figure 5. 13. Comparison of Raman spectra of Nb_2O_5 coated Ni-YSZ surfaces (a) before and (b) after electrochemical tests in C_3H_8 at 850°C over 12h

The electrochemical stability of the cell in C_3H_8 at 800ºC was monitored as shown in Figure 5.12. As the fuel was switched from H_2 to humidified C_3H_8, the performance dropped quickly, followed by gradual degradation. This gradual degradation can be attributed to the accumulation of carbon on the anode surface. The presence of carbon was confirmed by the Raman spectrum shown in Figure 5.13. The typical YSZ signals observed between 950 and 1200cm^{-1} (see spectrum Figure 5.13 (a)) are not detected in the sample exposed to C_3H_8. The carbon layer was probably thicker than the penetration depth of the laser. As shown in Figure 5.14, the whole surface exposed to C_3H_8 during

the electrochemical testing was covered by carbon. This result indicates that thick carbon layer was deposited and the electrochemical reaction can not sufficiently oxidize the carbon formed on the surface during C_3H_8 exposure. Thus, in higher hydrocarbons, it seems that carbon formation still cannot be avoided by coating the Ni-YSZ surface with Nb_2O_5. Further modification of the surface or other mitigative procedures must be implemented to minimize the carbon deposition problem, such as internal reforming or intermittent oxidation of surface carbon by air.

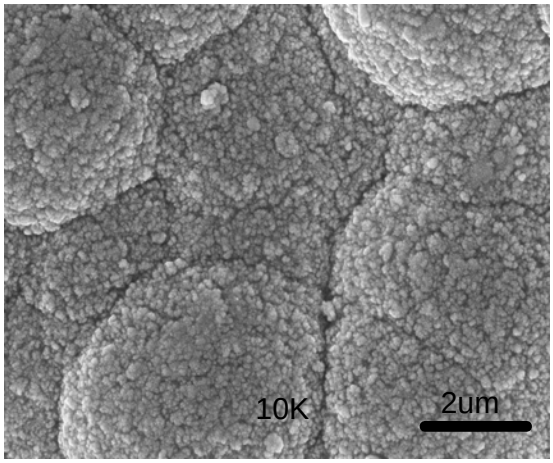

Figure 5. 14. SEM image of Nb_2O_5 coated Ni-YSZ surface after electrochemical tests in C_3H_8 (3% H_2O) at 850°C over 12 h

5.3. Conclusion

In this work, we have demonstrated that carbon formation can be suppressed with a niobium oxide coating in humidified CH_4 (3% H_2O) at 850ºC. Raman spectroscopy can be used to detect carbon formation under fuel cell operating conditions.

Under active fuel cell operation, no surface carbon deposits were detected on niobium oxide coated Ni-YSZ exposed to humidified CH_4 due to electrochemical oxidation of carbon. In addition, stable performance of functional cells consisting of Pt/YSZ/Nb_2O_5-coated dense Ni-YSZ in CH_4 was achieved. In contrast, a conventional Ni-YSZ anode displayed significant performance degradation due to carbon formation and the cell failed shortly after exposure to CH_4 under SOFC operating conditions.

However, when humidified C_3H_8 was used as the fuel, the electrochemical performance decreased gradually with exposure time because of severe carbon formation on the surface of niobium oxide-coated Ni-YSZ.

5.4. References

1. N. Q. Minh and T. Takahashi, *Science and Technology of Ceramic Fuel Cells*. (Elsevier, The Netherlands, Amsterdam, (1995).

2. R. M. Ormerod, The royal society of chemistry **32**, 17 (2003).

3. B. C. H. Steele and A.Heinzel, Nature **414**, 345 (2001).

4. B. C. H. Steele, Nature **400**, 619 (1999).

5. M. Ihara, T. Kusan, and C. Yokoyama, J. Electrochem. Soc. **148**, A209 (2001).

6. H. Kim, C. Lu, W. L. Worrell, J. M. Vohs, and R. J. Gorte, J. Electrochem. Soc. **149**, A247 (2002).

7. C. M. Finnerty, N. J. Coe, R. H. Cummingham, and R. M. Ormerod, Catalysis Today **46**, 137 (1998).

8. K. Sasaki and Y. Teraoka, Journal of the electrochemical socieity **150** (7), A878 (2003).

9. R. J. Gorte and J. M. Vohs, Catalysis **216**, 477 (2003).

10. S. Park, R. Cracium, J. M. Vohs, and R. J. Gorte, J. Electrochem. Soc. **146**, 3603 (1999).

11. Z. Shao, S. M. Haile, J. Ahn, P. D. Ronney, Z. Zhan, and S. A. Barnett, Nature **435**, 795 (2005).

12. E. Rmirez-Cabnera, N. Laosiripojana, A. Atkinson, and D. Chadwick, Catalysis Today **78**, 433 (2003).

13. S. P. Yoon, J. Han, S. W. Nam, T. Lim, and S. Hong, J. Power Sources **136**, 30 (2004).

14. G. Finnerty, G. A. Tompsett, K. Kendall, and R. M. Ormerod, J. Power Sources **86**, 459 (2000).

15. H. He and J. M. Hill, Applied Catalysis a-General **317**, 284 (2007).

16. S. Choi, J. Wang, Z. Cheng, and M. Liu, J. Electrochem. submitted (2007).

17. M. Mogensen and K. Kammer, Annu. Rev. Mater. Res. **33**, 321 (2003).

18. V. daSilva, M. Schmal, and S. T. Oyama, J. of Solid State Chemistry **123** (1), 168 (1996).

19. S. Shimada and M. Inagaki, Solid State Ionics **63-65**, 312 (1993).

CHAPTER 6

NI-MO/CEO_2 BASED ANODES FOR SULFUR TOLERENCE

Abstract

First-principles calculations were carried out to predict sulfur tolerance and catalytic activity for fuel oxidation of nickel surfaces modified by various transition metals. Results suggest that, among the metals studied, Mo seems to be a good candidate for Ni surface modification. In order to confirm the prediction, Ni-based anodes were modified with Mo using wet-impregnation techniques, and tested in 50 ppm H_2S-contaminated fuels. We found that the Ni-Mo/CeO_2 anodes have better sulfur tolerance than Ni, showing a current transient with slow recovery rather than slow degradation in 50 ppm H_2S balanced with H_2 at 700°C.

6.1. Introduction

One of the advantages of solid oxide fuel cells (SOFCs) is the potential for the direct utilization of commercially available hydrocarbon fuels,[1] which contain contaminants such as sulfur-containing compounds. Sulfur compounds aren't desired in the fuel stream because they ultimately cause irreversible degradation in fuel cell performance, however they are very difficult to remove economically below ppm levels .[2] Direct utilization of commercial fuels is crucial to reduce fuel processing costs and thus the overall cost of SOFCs and to achieve that we need intelligent design of sulfur-tolerant anodes.[3,4] Much research has been performed to develop sulfur-tolerant anode materials including surface modification, evaluation of new metallic and ceramic phases and even the use of highly conductive oxide based materials. Sasaki and coworkers reported that Ni-SSZ (scandia-stabilized zirconia)[6] cermets show higher sulfur tolerance than Ni-YSZ.[6] Another preliminary study proposed that Ni surfaces modified by transition metals such as Mo or W can reduce fuel-cell degradation from sulfur poisoning.[7,8] To date, as an alternative to Ni-based anodes with respect to sulfur tolerance, a series of extensive experiments have been carried out on Cu/CeO_2/YSZ (yttria-stabilized zirconia; 8 mol % Y_2O_3) fabricated by wet-impregnation techniques,[3,5] exhibiting highly stable performance in sulfur-containing fuels.. Further, researchers have identified various sulfur-tolerant metal oxides, including $La_{0.4}Sr_{0.6}TiO_3$,[9] $La_{0.75}Sr_{0.25}Cr_{1-x}Mn_xO_3$ (x = 0.4, 0.5, and 0.6),[10] $Gd_2Ti_{1.4}Mo_{0.6}O_7$,[11] and $La_{0.7}Sr_{0.3}VO_3$.[12]

Although the development of novel sulfur-tolerant anode materials with high catalytic activity for fuel oxidation is imperative for cost-effective SOFCs, other possible

significant parameters such as thermal match with YSZ electrolytes have to be properly taken into account. Since conventional Ni-YSZ cermets already meet the physical requirements for SOFC anodes, we believed it would be advantageous if sulfur tolerance is improved by modifying the surface with transition metals[7] or metal oxides, similar to Smith and McEvoy.[7,8] However, development of sulfur-tolerant Ni anodes modified with metals or metal oxides is not straightforward due to numerous candidate materials and the complexity of SOFC components and electrochemical systems. Therefore, rather than use trial and error, we used an intelligent design approach where all candidate materials and systems were screened computationally using first-principles calculations before being tested experimentally. Marquez et al.[15] demonstrated that H_2 oxidation kinetics could be prohibited by H_2S addition using cluster-model calculations. Recently, first-principles simulations, using the slab model, suggested a stepwise reaction mechanism for H_2S decomposition on Ni-based anode materials[13] and also proved that Cu is more sulfur-tolerant than Ni by comparing adsorption-energy calculations.[14] In this study, we applied periodic density function theory (DFT) calculations to screen sulfur-tolerant Ni-M alloys (M = 3d or 4d transition metals) and fabricated anodes by means of wet-impregnation methods for electrochemical performance tests.

6.2. Results and Discussion

6.2.1. Screening of Ni-M (M = 3d or 4d transition metals) using first-principles calculations

As shown in Figure 6.1, we predicted the sulfur adsorption energy on transition metal modified Ni surfaces and then normalized those values to that of sulfur adsorption on pure Ni in order to evaluate sulfur tolerance. According to the comparative study, Ag, Cu, Mo, Ru, and Rh metals are significantly more sulfur-tolerant than pure Ni, while Mn, Fe, Nb, and Tc are comparable and Co is slightly worse.

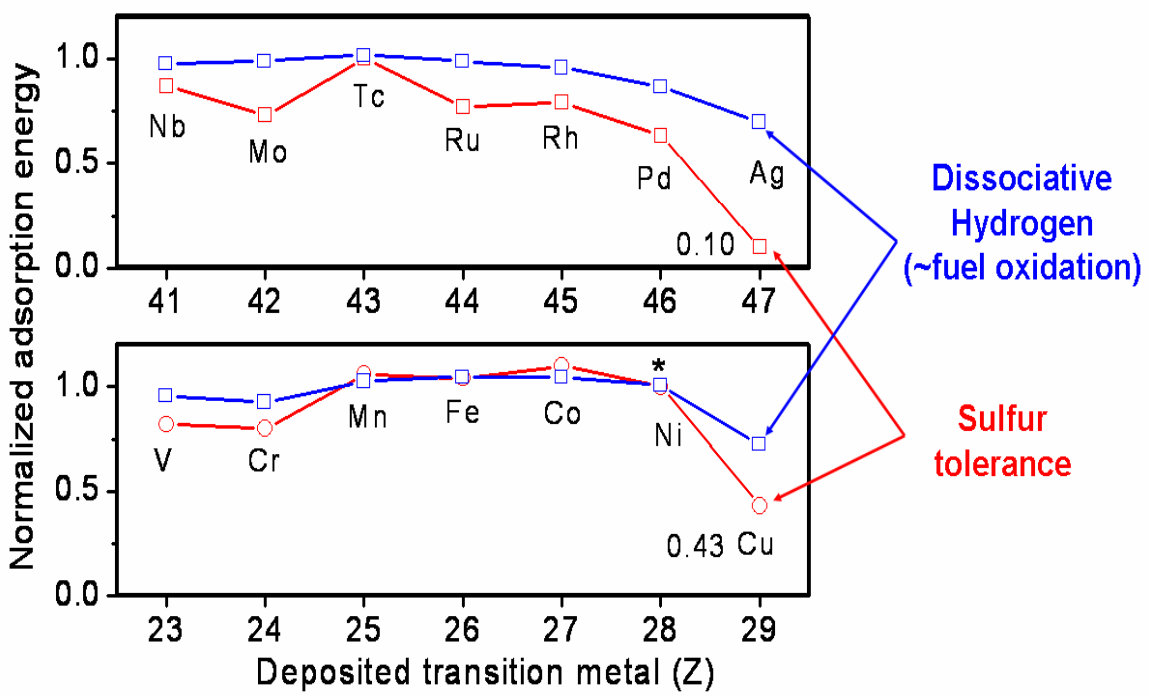

Figure 6. 1. Adsorption energies for sulfur and fuel oxidation on transition metal-modified Ni-surfaces (normalized to that on a pure Ni surface) based on first-principles calculations (collaborated with Dr. Y. Choi)

In addition to the examination of sulfur tolerance for various transition metals, we also predicted the dissociative adsorption energies of H_2, since anode materials must not only have sulfur tolerance but also catalytic activity for fuel oxidation. Interestingly, as displayed in Figure 6.1, Mo, Ru, and Rh have catalytic activities similar to Ni as compared to Ag and Cu, which are much less active. These results highlight the promise of applying first-principles calculations for screening possible sulfur-tolerant catalysts that also have good catalytic activity for fuel oxidation.

6.2.2. Ni-Mo/YSZ anodes

Using computational screening as a benchmark system, we chose to explore Ni-Mo-based materials because Ni-Mo exhibits both sulfur tolerance and good catalytic activity for fuel oxidation. In particular, Mo-based materials have been used for desulfurization processes[16] and it was also found that the oxidation of H_2S was possible with Ni-Mo-S.[17, 18]

Phase analysis and microstructure of Ni-Mo/YSZ anodes: XRD analyses were carried out to verify chemical phases before and after reduction of Ni-Mo fabricated by wet-impregnation methods. Figure 6.2 (a) clearly shows that $NiMoO_4$ was formed after calcination from wet-impregnated Ni-Mo anodes, while as illustrated in Figure 6.2 (b), $NiMoO_4$ was reduced to solid solution phases of metallic Ni-Mo. Three peaks can be assigned to Mo and NiMo with slight shifts. Madeira and coworkers[19] also reported that Mo, Ni_4Mo and NiMo can be formed by reducing $NiMoO_4$. A cross-sectional SEM image of Ni-Mo/YSZ infiltrated anodes is shown in Figure 6.3 (a), which clearly

demonstrates that the wet-impregnated Ni-Mo anodes are well distributed throughout the porous YSZ networks after reduction in H_2.

Electrochemical performances: To examine electrochemical performances of our fuel cells using Ni-Mo/YSZ anodes, we measured power density (mW/cm^2) as a function of current density (mA/cm^2) in pure H_2 and 50 ppm H_2S at 700°C (see Figure 6. 4). The maximum power density in pure H_2 is approximately 63 mW/cm^2, whereas it is reduced to 50 mW/cm^2 in 50 ppm H_2S, indicating that the cell is influenced by sulfur poisoning.

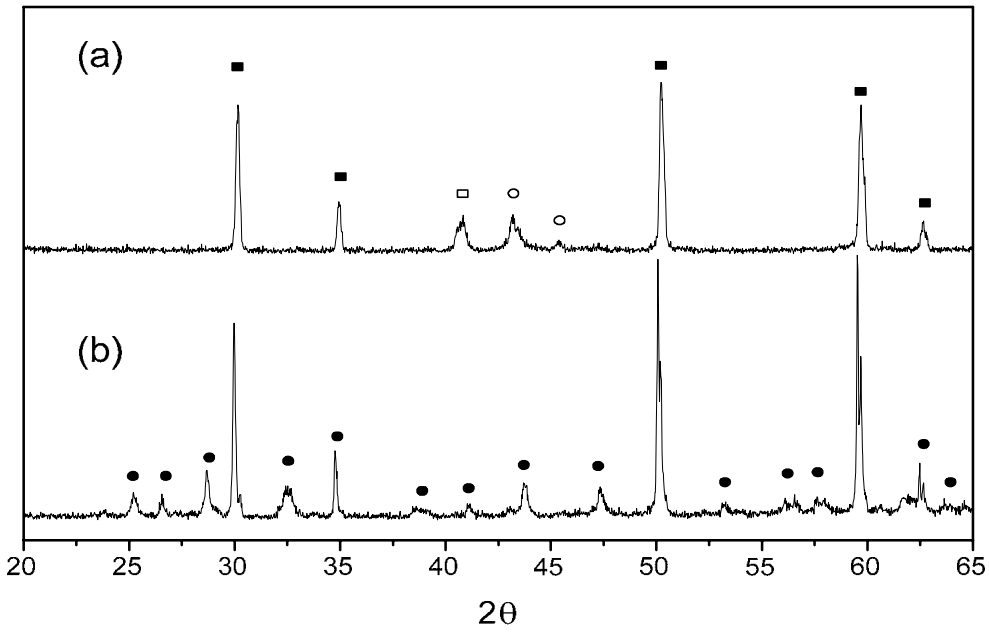

Figure 6. 2. Typical XRD data of Ni-Mo/YSZ anodes fabricated by wet-impregnation methods. (a) After reduction in H_2 at 750 °C. (■), (●), (□), and (○) denote YSZ, $NiMoO_4$, Mo, and NiMo, respectively and (b) before reduction

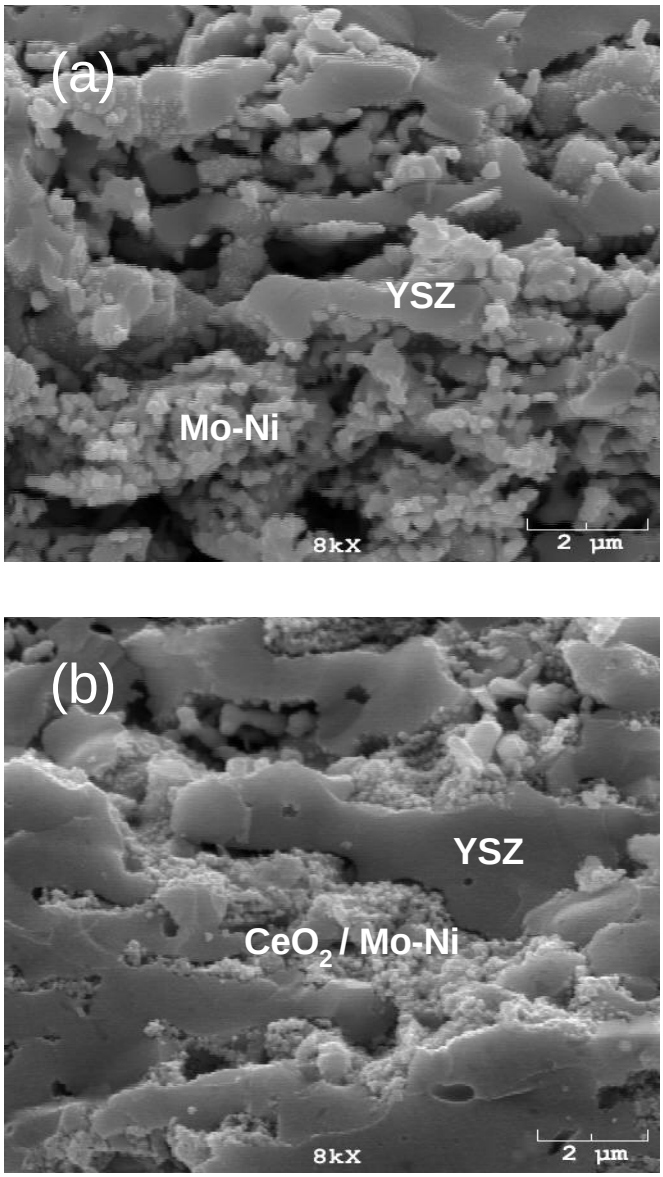

Figure 6. 3. SEM images of (a) Ni-Mo/YSZ and (b)Ni-Mo/CeO_2/YSZ prepared by wet-impregnation methods after electrochemical performance tests

6.2.3. Ni-Mo/CeO_2/YSZ anodes

To improve microstructure and electrochemical performance, CeO_2 was infiltrated into the porous YSZ structure before Ni-Mo. We decided to use CeO_2 because it is a well-known catalyst for fuel oxidation with high sulfur tolerance.[3,5,20,21]

Microstructures and electrochemical performances of Ni-Mo/CeO_2/YSZ anodes : As shown in Figure 6.3, particle sizes of wet-impregnated materials were reduced by adding CeO_2 into porous YSZ networks, leading to more triple-phase boundary (TPBs) between the electronic conductor of Ni-Mo and the ionic conductor of CeO_2 and/or YSZ. In particular, the enhancement of fuel oxidation kinetics is also expected from the CeO_2 addition as described in previous studies.[3,5,20,21]

Figure 6.4 illustrated that the power density for Ni-Mo/CeO_2/YSZ anodes in pure H_2 remarkably increases (~147 mW/cm^2) compared to that for Ni-Mo/YSZ, strongly indicating the significance of TPBs and the catalytic contribution of CeO_2 layers. However, the power density in 50 ppm H_2S was also reduced to ~100mW/cm^2. Similar to Ni-Mo/YSZ, we also observed rapid sulfur poisoning in the contaminated fuel. Even though our computational study and the previous experimental finding[16] suggest the potential sulfur tolerance and catalytic activity of Ni-Mo, Ni-Mo/YSZ anodes exhibit relatively lower cell performance compared to Ni-Mo/CeO_2/YSZ anodes. On the basis of SEM analyses, the lower performance originated from the loss of electrical connectivity by severe agglomeration of reduced metallic phases of Ni-Mo on YSZ surfaces, which is related to interfacial resistance.

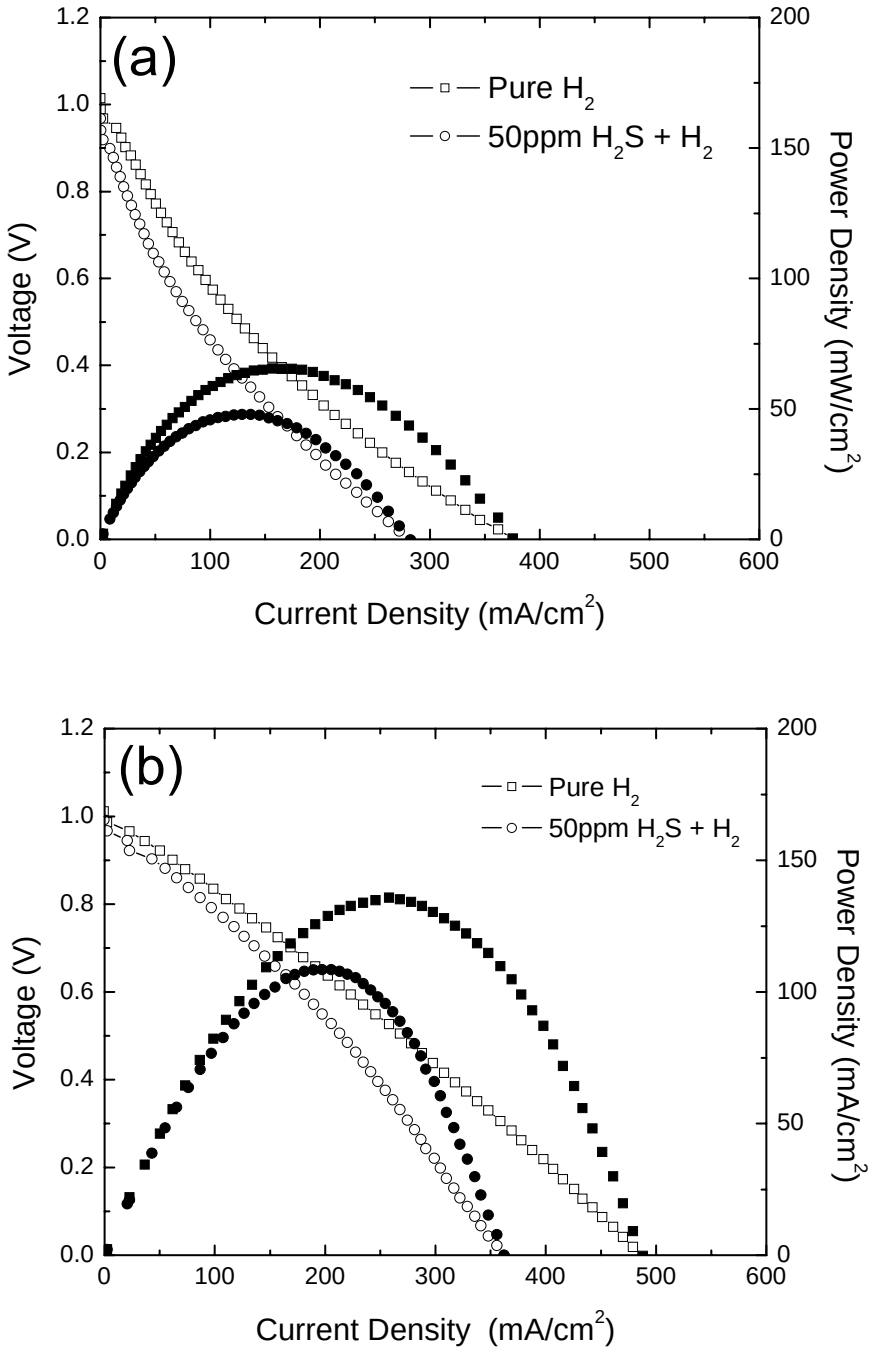

Figure 6. 4. Typical power density (mW/cm^2) as a function of current density (mA/cm^2) for (a) Ni-Mo/YSZ and (b) Ni-Mo/CeO_2/YSZ at 700 °C in pure H_2 and 50 ppm H_2S

Shown in Figure 6.5 is impedance spectra of Ni-Mo/YSZ and Ni-Mo/CeO_2/YSZ anodes, in which ohmic resistance of the cells in pure H_2 at 700°C is approximately 1.0 $\Omega \cdot cm^2$ and 1.1 $\Omega \cdot cm^2$, respectively. For interfacial resistance, Ni-Mo/YSZ does not converge, while Ni-Mo/CeO_2/YSZ in pure H_2 and 50 ppm H_2S are approximately 0.8 $\Omega \cdot cm^2$ and 1.0 $\Omega \cdot cm^2$, respectively. This means that the interfacial resistance is greatly reduced by CeO_2 addition. In addition, the interfacial resistance is increased as much as 25 % in 50 ppm H_2S due to the degradation from sulfur poisoning of the anode.

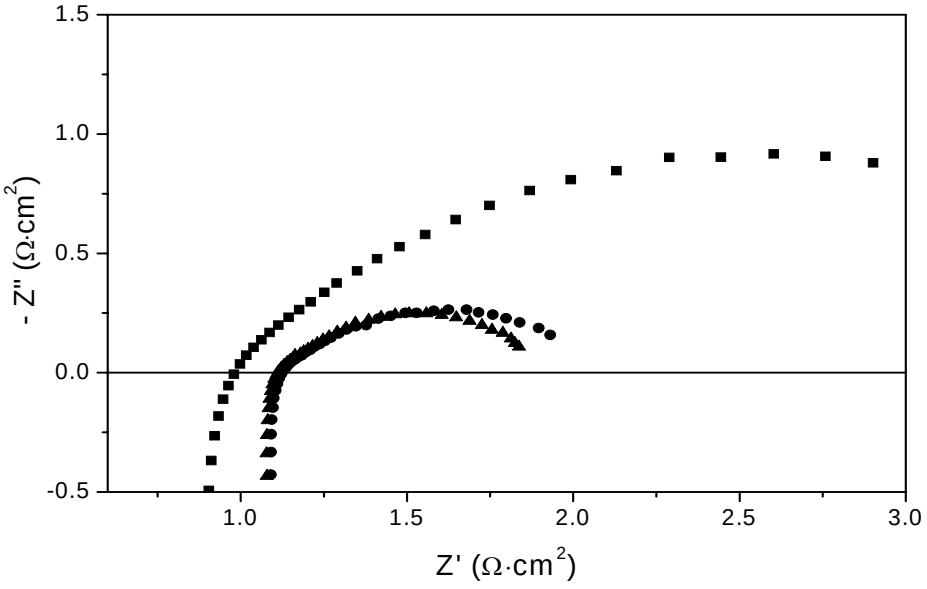

Figure 6. 5. Impedance spectra of fuel cells using Ni-Mo/YSZ anode in pure H_2 (■) and Ni-Mo/CeO_2/YSZ anodes in pure H_2 (▲) and in 50 ppm H_2S (●) at 700 °C

6.2.4. Long-term stability tests of Ni-Mo/CeO_2/YSZ anodes

A previous study[22] demonstrated that an initial sharp degradation is observed using conventional Ni/YSZ anodes upon exposure to H_2S, which is then followed by a slower gradual degradation. To examine the effects of Ni modification, long-term stability tests were carried out on Ni-Mo/CeO_2/YSZ anodes at 700°C for ~5 days. Figure 6.6 shows the change in current density of the fuel cell as a function of time at 700°C and 0.5V DC. Current density was stable in humidified H_2 at 700°C for 24 hrs and then abruptly decreased at 50ppm H_2S was introduced. The significant difference between the response of Ni-Mo/CeO_2/YSZ anodes and that of conventional Ni-YSZ is that after the initial drop, the current density slowly increased rather than decreased,[22] until after 144 hours the current density had recovered back to its initial value. The initial decrease in current is purported to result from fast chemisorption of S species on the Ni surface.

The slow increase in the current density by exposure to H_2S may be rationalized as follows. First, the decomposition rate of H_2S to H_2 and S can be promoted due to the formation of MoS_2,[23] leading to higher concentrations of dissociated hydrogen species. Second, the phase transformation of surface oxides to sulfides such as MoS_2 and Ni-Mo-S can extend electrochemically active sites because MoS_2 formed from the H_2S decomposition reaction has electrical conductivity.[24] As shown in Figure 6.6, after reaching a steady state (~155 h), we re-introduced humidified H_2, resulting in an increase in the current density, indicating that the surface structure was altered by sulfur desorption in such a way that it became more active. Our preliminary reaction mechanism

for the interactions of H_2S on Ni-Mo with and without CeO_2 addition will be verified by first-principles calculations in a future study.

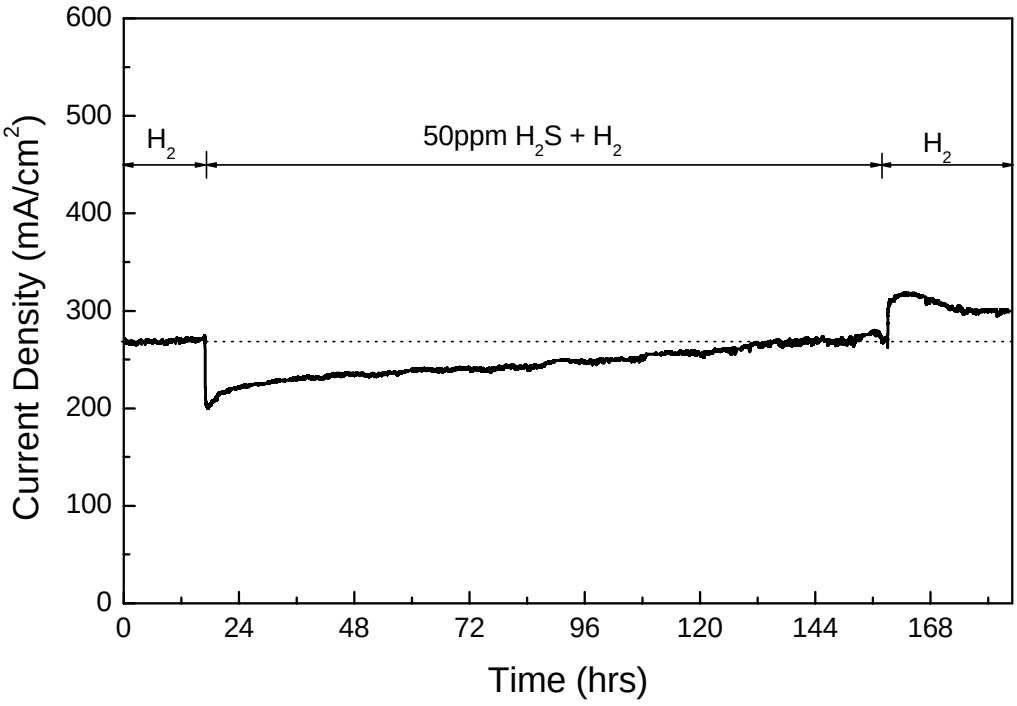

Figure 6. 6. Current density as a function of time for Ni-Mo/CeO_2/YSZ anodes in pure H_2 and in 50 ppm H_2S at 700°C when 0.5 V DC was applied

6.3. Conclusions

First-principles calculations were successfully used to predict the sulfur tolerance of nickel surfaces modified with various transition metals. The calculations suggested that Ni-Mo has better sulfur tolerance and more activity for fuel oxidation then pure Ni under fuel cell operating conditions. To verify our theoretical prediction, we prepared modified nickel-based anodes with Mo using wet-impregnation techniques. We also added CeO_2 to improve the structural stability of Ni-Mo on YSZ and to enhance the electrochemical performance. Even though the initial drop in current density due to sulfur poisoning (followed the introduction of H_2S) could not be avoided, the surface modified nickel anode with CeO_2 addition (Ni-Mo/CeO_2) showed a continuous slow recovery during exposure to hydrogen fuel containing 50 ppm H_2S. Eventually, the current density recovered back to the initial value obtained when using pure humidified H_2 as fuel.

6.4 References

1. Minh, N. Q.; T, T. *Science and Technology of Ceramic Fuel Cells*; Elsevier Science: AmsterdamThe Netherlands, 1995.

2. Matsuzaki, Y.; Yasuda, I. *Solid State Ionics* **132**, 261 (2000).

3. Kim, H.; Vohs, J. M.; Gorte, R. J. *Chem. Commun.* **22**, 2334 (2001).

4. Atkinson, A.; Barnett, S.; Gorte, R. J.; Irvine, J. T. S.; McEvoy, A. J.; Mogensen, M.; Singhal, S. C.; Vohs, J. *Nature Mater.* **3**, 17 (2004)

5. He, H.; Gorte, R. J.; Vohs, J. M. *Electrochem. Solid-State Lett.* (2005).

6. Sasaki, K.; Susuki, K.; Iyoshi, A.; Uchimura, M.; Imamura, N.; Kusaba, H.; Teraoka, Y.; Fuchino, H.; Tsujimoto, K.; Uchida, Y.; Jingo, N. *J. Electrochem. Soc.* **153**, A2023. (2006)

7. Smith, M.; McEvoy, A. J. *Sulfur-Tolerant Cermet Anodes*; The Electrochemical Society: Pennington, NJ, 2005; Vol. 2005-07.

8. Recovery of degraded surfaces may be taken into account during long-term stability tests because the potential interdiffusion between Mo (or W) and Ni due to their miscibility under SOFC operating conditions.

9. Mukundan, R.; Brosha, E. L.; Garzon, F. H. *Electrochem. Solid-State Lett.* **7**, A5. (2004)

10. Zha, S.; Tsang, P.; Cheng, Z.; Liu, M. *J. Solid State Chem.* **178**, 1844 (2005)

11. Zha, S.; Cheng, Z.; Liu, M. *Electrochem. Solid-State Lett.* **8**, A406 (2005)

12. Aguilar, L.; Zha, S.; Cheng, Z.; Winnick, J.; Liu, M. *J. Power Sources* **135**, 17. (2004)

13. Choi, Y. M.; Compson, C.; Lin, M. C.; Liu, M. L. *Chem. Phys. Lett.* **421**, 179. (2006)

14. Choi, Y. M.; Compson, C.; Lin, M. C.; Liu, M. *J. Alloys Comp.* **427**, 25. (2007)

15. Marquez, A. I.; De Abreu, Y.; Botte, G. G. *Electrochem. Solid-State Lett.* **9,** A163. (2006)

16. Brito, J. L.; Barbosa, A. L. *J. Catal.* **171**, 467. (1997)

17. Liu, M.; Wei, G.; Luo, J.; Sanger, A. R.; Chuang, K. T. *J. Electrochem. Soc.* **150,** A1025. (2003)

18. Wei, G.; Luo, J.; Sanger, A. R.; Chuang, K. T. *J. Electrochem. Soc.* **151,** A232. (2004)

19. Madeira, L. M.; Portela, M. F.; Mazzocchia, C.; Kaddouri, A.; Anouchinsky, R. *Catal. Today* **40,** 229. (1998)

20. He, H.; Vohs, J. M.; Gorte, R. J. *J. Electrochem. Soc.* **150**, A1470. (2003)

21. Lee, S.; Vohs, J. M.; Gorte, R. J. *J. Electrochem. Soc.* **151**, A1319. (2004)

22. Zha, S.; Cheng, Z.; Liu, M. *J. Electrochem. Soc.* **154**, B201. (2007)

23. Chivers, T.; Hyne, J. B.; Lau, C. *Int. J. Hydrogen Energy* **5**, 499. (1980)

24. Aoshima, A.; Wise, H. *J. Catal.* **34**, 145. (1974)

CHAPTER 7

CONCLUSIONS AND RECOMMENDATIONS

7.1. Conclusions

In this study, the possibility of surface modification for tolerance to sulfur poisoning and carbon deposition was demonstrated using a dense Ni-YSZ anode coated with niobium oxide. Additionally, nickel-based anodes modified with Mo using a wet-impregnation process were studied for sulfur tolerance. The main conclusions are as follows.

(1) Niobium oxide (Nb_2O_5) coated on Ni-YSZ was reduced to NbO_2 under SOFC operating conditions, which is more conductive and catalytically active toward H_2 oxidation. The increase in peak power density of a cell with NbO_x coated anode was attributed to the decrease in anodic interfacial resistance due to increased catalytic activity toward fuel oxidation.

(2) As the fuel was switched from clean H_2 to 50 ppm H_2S-containing H_2, the performance of a cell with Nb_2O_5-coated Ni-YSZ anode increased slowly accompanied by conversion of surface NbO_2 to niobium sulfides (NbS, NbS_2…). On the other hand, as the fuel was switched back to clean H_2, the cell performance decreased slowly, accompanied by conversion of niobium sulfides back to NbO_2. The phase changes

between niobium oxide (NbO_2) and niobium sulfides (NbS_2, NbS) were confirmed by Raman spectroscopy and XRD analyses.

(3) DOS analysis predicts that there are no obvious band gaps around the Fermi level for niobium sulfides (NbS and NbS_2), similar to the DOS distribution for NbO_2, indicating that the anode exposed to H_2S is still electrically conductive and catalytically active.

(4) It was also found that carbon deposition can be suppressed by a niobium oxide coating in humidified CH_4 at 850ºC. Under SOFC operating conditions, there were no detectable carbon deposits on niobium oxide coated Ni-YSZ exposed to humidified CH_4, as determined using Raman spectroscopy. The results suggest that the niobium oxide not only suppresses the catalytic cracking of CH_4 but also catalytically active toward carbon oxidation under SOFC operating conditions.

(6) The stability and the cell performance of Ni-Mo/YSZ anode were improved by adding CeO_2 using a wet-impregnation process. While the initial drop in current density due to sulfur poisoning was observed as 50ppm H_2S was introduced, the surface modified nickel anode with CeO_2 addition (Ni-Mo/CeO_2) showed a continuous slow recovery during exposure to hydrogen fuel containing 50 ppm H_2S.

7.2. Recommendations

While it has been demonstrated that NbO_x coated dense Ni-YSZ is resistant to sulfur poisoning and carbon deposition under SOFC operating conditions, the dense anode structure limits the cell performance due to limited active area for electrochemical reactions.

Thus, for practical applications, further research of porous Ni-YSZ modified with niobium oxide is recommended. To reduce the experimental uncertainties in the modification of porous Ni-YSZ with thin and uniform coating, a suitable fabrication process for modifying the porous Ni-YSZ structure with niobium oxide should be developed. A solution based impregnation process with surfactants or chemical vapor deposition may be good options.

Once porous Ni-YSZ with proper surface modification is achieved, systematic studies to be performed include (i) the proper ratio of Ni to Niobium oxide for balancing the sulfur tolerance and cell performance, (ii) the dependence of cell performance on concentrations of sulfur contaminants, and (iii) carbon deposition when exposed to different types of hydrocarbon fuels at various operating temperatures.

In addition to niobium oxides, other interesting materials for surface modification include CeO_2, TiO_2, V_2O_5. Similar studies can be performed to evaluate their effects on enhancement of cell performance, structure stability, or direct utilization of longer-chained hydrocarbon fuels such as propane and gasoline.